INFORMATION TO USERS

This manuscript has been reproduced from the microfilm master. UMI films the text directly from the original or copy submitted. Thus, some thesis and dissertation copies are in typewriter face, while others may be from any type of computer printer.

The quality of this reproduction is dependent upon the quality of the copy submitted. Broken or indistinct print, colored or poor quality illustrations and photographs, print bleedthrough, substandard margins, and improper alignment can adversely affect reproduction.

In the unlikely event that the author did not send UMI a complete manuscript and there are missing pages, these will be noted. Also, if unauthorized copyright material had to be removed, a note will indicate the deletion.

Oversize materials (e.g., maps, drawings, charts) are reproduced by sectioning the original, beginning at the upper left-hand corner and continuing from left to right in equal sections with small overlaps.

ProQuest Information and Learning
300 North Zeeb Road, Ann Arbor, MI 48106-1346 USA
800-521-0600

OBJECT-ORIENTED MODELING OF THE DYNAMICS OF SPACE SYSTEMS WITH REACTION WHEELS

Sarthak Misra

Department of Mechanical Engineering
McGill University, Montréal

September 2001

A Thesis submitted to the Faculty of Graduate Studies and Research
in partial fulfilment of the requirements for the degree of
Master of Engineering

ABSTRACT

Analysis of the attitude dynamics of a spacecraft is necessary for its successful operation. Recent research has focussed on the object-oriented analysis and design for generating and solving the complex nonlinear dynamic equations of motion of a multibody space system. In this thesis, an effort has been made to develop objects that can be combined to formulate the complete dynamic equations of a spacecraft containing reaction wheels. In order to generate the mathematical model and dynamical equations of the multibody system, a variation of the Lagrange's method has been used, along with the concept of Natural Orthogonal Complement, in order to eliminate the kinematic constraint force and moments.

The designed objects would be part of a multibody system software package that could simulate the complex dynamics of a spacecraft containing reaction wheels and any arbitrary configuration of connected bodies. The objects have been designed such that the spin rate of the wheels may be specified as a constant nominal rate, or as any function of time, or in the form of a P.I.D. control law, wherein the wheel spin rate is a function of the body quaternion of the motherbody. The accuracy, versatility, and adaptability of the designed objects have been illustrated with numerous examples and compared with results obtained using standard procedure. Maneuvers have also been simulated on the designed model and compared with available spacecraft data in order to substantiate the authenticity of the designed objects.

RÉSUMÉ

Pour mener à bien l'objectif d'un vol spatial, une étude du comportement dynamique du vaisseau est primordiale. La recherche actuelle s'est penchée sur l'analyse et la conception "orientée-objet" pour synthétiser et résoudre de complexes équations dynamiques non-lineaires, des mouvement d'un systeme spatial à plusieurs corps. Dans cette thèse, un effort particulier a été fait pour développer des objets pouvant se combiner afin de formuler des équations dynamiques complètes d'un mobile, embarquant des roues à réactions. Afin de determiner le modèle mathématique et les équations dynamiques du systeme à plusieurs corps, une variante de la méthode de Lagrange, ainsi que le concept de "Natural Orthogonal Complement" ont été appliqués dans le but d'éliminer les forces et moments de contraintes cinématiques.

Les objets conçus feront parti d'un logiciel de systeme à plusieurs corps qui pourrait simuler le dynamique complexe d'un vaisseau possédant des roues à réaction ainsi que de toute configuration arbitraire de corps couplés. Les objets ont été conçus de sorte que le vecteur vitesse angulaire des roues puisse etre defini comme une constante nominale, comme fonction du temps ou encore sous la forme d'une loi de control du type P.I.D., dans laquelle le vecteur vitesse est fonction du vecteur quaternion du mobile-mère. L'efficacité, la polyvalence et l'adaptabilité de ces objets ont été illustrés par de nombreux examples et comparés avec des résultats obtenus par des approches plus classiques. Les fonctionnements ont aussi été simulés sur le modèle

ainsi conçu et comparés avec des données disponibles sur les vaisseaux spatiaux afin de corroborer la légitimité de ces objets.

ACKNOWLEDGEMENTS

I am indebted to Professor A. K. Misra for his continued supervision, guidance, and invaluable support throughout the course of my research. I thankfully acknowledge the excellent facilitation and computing support received from the McGill Centre for Intelligent Machines (McRCIM). Special thanks are due to Mr. Byung No Min for helping me time and again with my queries in ROSE (Real-Time Object Oriented Software Environment).

TABLE OF CONTENTS

LIST OF FIGURES

LIST OF TABLES

NOMENCLATURE

All bold-face, lower-case, Latin and Greek letters used in this thesis denote vectors and all bold-face, upper-case, Latin and Greek letters denote matrices. The term *extended* refers to quantities associated with each body, while the term *generalized* refers to those quantities associated with the overall system. Moreover the terms with a subscript 'B' are associated with the motherbody; the terms with a subscript 'J' are associated with the joint; and the terms with a subscript 'w' are associated with the reaction wheel, unless specified otherwise. Also $(\cdot)_{\ddot{\mathbf{y}}=0}$ stands for the evaluation of a quantity when the generalized acceleration vector ($\ddot{\mathbf{y}}$) of the multibody system is set to zero, whereas the superscript '$\times$' represents the cross product operation.

Latin Symbols

$\mathbf{c}_{o_i}$: Position vector of the center of mass for body i.

$\hat{\mathbf{e}}_i$: Euler axis for body i.

$\mathbf{h}$: Angular momentum of the spacecraft expressed in the inertial coordinate frame.

$\mathbf{I}_{SC}$: Inertia tensor of the spacecraft.

$\mathbf{I}_k$, $k = xx, yy, zz$: Mass moment of inertia of the body around its center of mass.

${}^i\mathbf{J}_J$: Local Jacobian matrix of the joint i.

$\mathbf{K}_k$, $k = 1, 2, 3$: Control gain vectors.

$\mathbf{L}_i$: Matrix transforming the time derivative of the pose $\dot{\mathbf{q}}_i$ to the twist $\mathbf{v}_i$.

m_i: Mass of body i.

$\mathbf{M}_i$: Extended mass matrix of body i.

$\mathbf{M}_{o_i}^{rr}$: Mass moment of inertia of the i^{th} body around its center of mass.

N: Natural Orthogonal Complement matrix.

O: Inertial reference frame for the generic kinematic element.

$\mathbf{O}_B$: Local body frame of the generic rigid link.

$\mathbf{O}_J$: Coordinate frame of the joint before it has undergone motion.

$\mathbf{O}_J^I$: Coordinate frame of the joint after it has undergone motion.

$\mathbf{O}_m$: Local body frame of the generic kinematic element.

$\mathbf{O}_s$: Local body frame of the generic kinematic element after having undergone motion.

$\mathbf{p}_i$: Position vector of the origin of frame (X_i, Y_i, Z_i) with respect to (X_o, Y_o, Z_o).

$\mathbf{p}_m$: Position vector locating the origin of frame $\mathbf{O}_m$ from the inertial reference frame **O**.

$\mathbf{p}_s$: Position vector locating the origin of frame $\mathbf{O}_s$ from the inertial reference frame **O**.

$\hat{\mathbf{q}}_i$: Quaternion of the i^{th} body.

$\mathbf{q}_i$: Pose of body i.

r: Relative displacement from the origin of the original frame to the origin of the new frame, unless stated otherwise.

R: Relative rotation matrix describing the orientation of the new frame with respect to the original frame, unless stated otherwise.

$\mathbf{R}_i$: Rotation Matrix defining the orientation of frame (X_i, Y_i, Z_i) with respect to (X_o, Y_o, Z_o).

$\mathbf{R}_m$: Rotation matrix that represents the orientation of frame $\mathbf{O}_m$ with respect to the inertial reference frame **O**.

$\mathbf{R}_s$: Rotation matrix that represents the orientation of frame $\mathbf{O}_s$ with respect to the inertial reference frame **O**.

RW_k, $k = 1, 2, 3$: Spin rate of the reaction wheels.

t: Time variable.

$\mathbf{T}$: Transformation matrix representing the orientation of the three reaction wheels relative to the body coordinate frame.

T_i: Kinetic energy of body i.

T_{SC}: Kinetic energy of the spacecraft containing the reaction wheel.

$\mathbf{v}_i$: Twist of body i.

${}^{B}\mathbf{v}_w$: Twist of the reaction wheel relative to the motherbody.

$\mathbf{w}_i$: Vector accounting for all the nonconservative wrenches acting on body i.

$\mathbf{w}_i^A$: The algebraic constraint wrench associated with body i.

$\mathbf{w}_i^E$: The external wrench acting on body i.

$\mathbf{w}_i^A$: The kinematic constraint wrench associated with body i.

${}^{i}\mathbf{X}_L^O$: Spatial transformation matrix for the outward link i.

${}^{i}\mathbf{X}_L^I$: Spatial transformation matrix for the inward link i.

${}^{i}\mathbf{X}_J$: Spatial transformation matrix of the joint i.

$\mathbf{y}$: Vector containing the generalized coordinates of the mulitbody system.

$\mathbf{Z}_v$: Joint characteristic matrix for a prismatic joint.

$\mathbf{Z}_\omega$: Joint characteristic matrix for a revolute joint.

(X, Y, Z): Local frame of the motherbody.

(X_i, Y_i, Z_i): Local frame of body i.

(X_o, Y_o, Z_o): Inertial frame of the multibody system located at the base.

Greek Symbols

α, β, γ: Joint angles.

$\mathbf{\Gamma}_i$: Mapping matrix.

θ_i: Euler angle for body i.

$\boldsymbol{\theta}_i$: Joint coordinate vector composed translational displacement and/or rotational angles of the joint i.

$\mathbf{\Lambda}_i$: Matrix transforming the twist $\mathbf{v}_i$ to the time derivative of the pose $\dot{\mathbf{q}}_i$.

τ: Joint torque applied to the arms, unless specified otherwise.

$\mathbf{\Upsilon}_i$: Connectivity matrix.

$\boldsymbol{\phi}_i^E$: Extended external wrench associated with body i.

$\boldsymbol{\phi}_i^K$: Extended kinematic constraint wrench associated with body i.

$\boldsymbol{\phi}_i^S$: Extended system wrench associated with body i.

ω_{wheel}: Spin rate of the reaction wheel.

$\boldsymbol{\omega}$: Relative angular velocity of the new frame with respect to the original frame.

$\boldsymbol{\omega}_i$: Angular velocity of frame (X_i, Y_i, Z_i) with respect to (X_o, Y_o, Z_o).

$\boldsymbol{\omega}_m$: Angular velocity of frame $\mathbf{O}_m$ with respect to the inertial reference frame $\mathbf{O}$.

$\boldsymbol{\omega}_s$: Angular velocity of frame $\mathbf{O}_s$ with respect to the inertial reference frame $\mathbf{O}$.

$\boldsymbol{\omega}_{SC}$: Angular velocity of the spacecraft.

$\boldsymbol{\omega}_k$, $k = x, y, z$: Slew velocity of the spacecraft.

CHAPTER 1

Introduction

1. Multibody Space Systems

The early stages of space exploration saw the spacecraft tending to be small and mechanically simple, in contrast to a modern space vehicle carrying numerous lightweight deployable members, such as solar panels, antennas, and robotic manipulators. This section describes several space systems and illustrates their multibody nature.

FIGURE 1.1. An artist's conception of the International Space Station (courtesy:*NASA Photo gallery*)

The space age truly began with the launch of Sputnik in 1957. Sputnik was a light weight, spherically shaped spacecraft made of aluminum, and had four antennas. The shape and the size of the satellites have changed much since then. From the manned Mercury and Gemini, through Apollo in the sixties, and now the International Space Station (ISS), all represent a wide range of multibody space systems with varying degrees of complexity. The Apollo 11 mission which landed the first men on the Moon consisted of a relatively simple spacecraft with four legs attached to it, and was shaped like a blunt cone. Skylab, Mir, and the ISS, represent a range of complex multibody space systems. The configuration of ISS, shown in figure 1.1, is a set of linear trusses to which pressurized modules, subsystems, and user laboratories are attached. The ISS will be 155 meters in length and 244,055 kilograms in mass after assembly, and would have four large photovoltaic arrays; each array having four modules (**Modi and Ng**, *1990*).

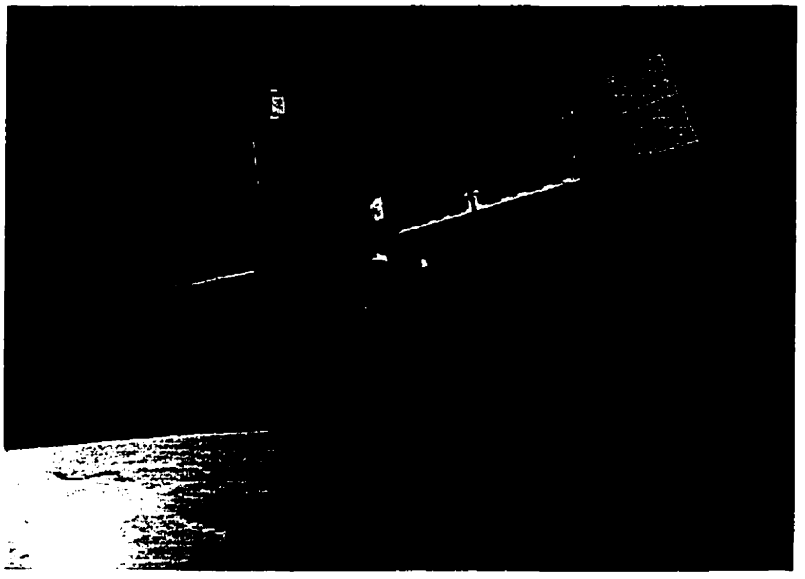

FIGURE 1.2. The Mars Global Surveyor (courtesy:*JPL Photo gallery*)

The path of exploring planets by means of multibody space systems begun with the Pioneers and Voyagers (**Kilston et al.**, *2000*). The Mars Global Surveyor spacecraft, which was launched in 1996, shown in figure 1.2, is an example of one of the

many complex multibody space systems used for planetary exploration. It has four solar panels each of length 12 meters. It also has a high gain antenna mounted on a 2 meters long boom.

The unmanned space observatories also represent multibody space systems that help observe phenomena and objects hard to see from the bottom of our atmosphere. The Hubble Space Telescope, Far Ultraviolet Spectroscopic Explorer, and Chandra X-Ray Telescope, have given us the highest resolution visual images of distant objects, early relics of the Big Bang, and Supernovas, respectively. The Hubble Space Telescope, shown in figure 1.3, is a 13.3 meters long and 4.3 meters wide spacecraft. It has two double roll out solar arrays of dimensions 2.3 meters $\times$ 12 meters.

FIGURE 1.3. The Hubble Space Telescope during the STS 61 flight (courtesy:*NASA Photo gallery*)

The vast range of communication satellites, like SATCOM, INTELSAT, and INMARSAT also belong to the realm of multibody space systems and have led the way for global long distance and maritime communications. The use of large appendages are required for some space systems, for example, the Radio Astronomy

Explorer (RAE) satellite used four 750 feet antennas for detecting low-frequency signals (**Modi**, *1974*). Another example highlighting the complexity of multibody space systems is the Tracking and Data Relay Satellite (TDRS). This satellite has two wing-like solar panels and two high-gain parabolic antennas, that look like giant umbrellas.

Space robotic devices also belong to the category of multibody space systems. Telerobotics can reduce extra-vehicular activity with the associated time overhead and dangers to astronauts. Moreover, the use of automated assembly operations will be advantageous for the in-orbit construction of large space structures (**Mitsushige**, *1997*). To increase the mobility of such space systems, free-flying spacecraft, in which manipulators are mounted on a satellite, are being proposed. The Canadian Remote Manipulator System, better known as the CANADARM, is frequently used in conjunction with the Space Shuttle and is an example of a space robot. A more advanced version of the CANADARM is the Mobile Servicing System (MSS), shown in figure 1.4, part of which was launched in April 2001, is Canada's contribution to the ISS. One of the main components of the MSS is the Special Purpose Dextrous Manipulator (SPDM), which is a highly dextrous robot with two arms that will perform a great many of the tasks in the assembly and maintenance of the ISS. Advanced space manipulators that have currently been developed are the European Hermes Robot Arm (HERA) and the Japanese Experiment Module Remote Manipulator System (JEMRMS). For fine dextrous operations, the functions of future space robots would encompass the servicing of satellites, space debris recovery, and planetary surveys. Such future space robots include the Ranger, Charlotte, and the German built Space Robot Technology Experiment (ROTEX) (**David**, *1995*).

Future space missions, such as Space Technology (2004), Space Terrestrial Planet Finder (2005), Terrestrial Planet Finder (2011), and Life Finder (2016) would consist of highly complex multibody space systems carrying numerous appendages, used for a variety of purposes. Thus, the presence of multiple complex components is evident

in a broad spectrum of space applications. The dynamical analysis of such complex multibody space systems is known to be intricate and demanding. The dynamics and control of multibody space systems are the subjects of discussion in the subsequent sections.

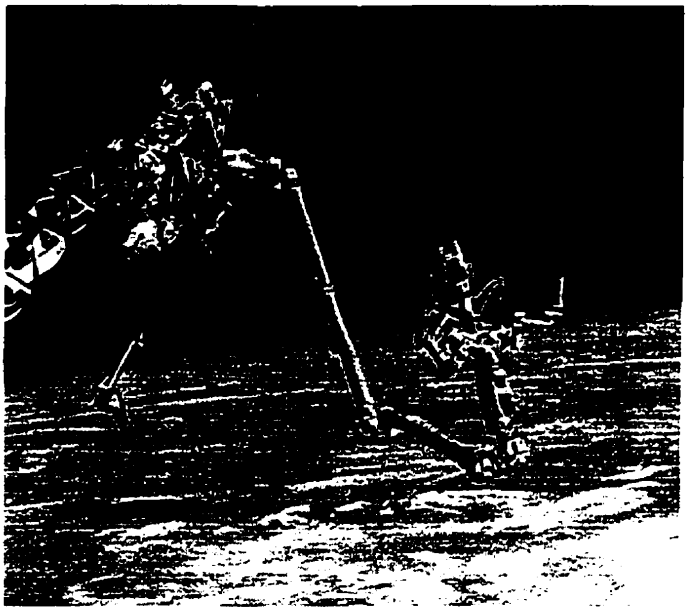

FIGURE 1.4. An artist's conception of the MSS (courtesy:*MacDonald Dettwiler Space and Advanced Robotics*)

2. Dynamics of Multibody Systems

The study of multibody system dynamics dates back to the mid-sixties, when there became an apparent need for designs with higher reliability and faster response. Also, with the advent of the space age, the need to predict the dynamical response of complex satellites in micro-gravity environment became essential. For such and many more applications, the traditional single degree of freedom systems or linear multiple degree of freedom systems were not suitable to meet the ever increasing demands of analytical accuracy. Furthermore, with the advances of digital computers, it was possible to handle millions of floating point operations. Thus, the discipline of multibody dynamics has grown from a small and very specialized subject of classical mechanics to one of the major fields of computational mechanics. Extensive research

has been done, which has led to software simulation tools for modeling mechanical systems with complex geometries.

As mentioned previously, satellites or space systems with connected bodies or appendages belong to the regime of multibody space systems whose dynamics are known to be complex and challenging. The governing equations of motion for the motherbody and the connected bodies can be derived in terms of nonlinear differential equations, by modeling them as a multibody mechanical system. The connected bodies may be in the form of solar panels, booms, antennas, and/or manipulator arms. When bodies are attached to the motherbody, there is an interaction between its dynamics and the dynamics of the motherbody. The motion of the connected bodies produces reaction forces and moments on the satellite through the motherbody base. These forces and moments produce translation of the center of mass of the spacecraft and rotation about its center of mass. Due to such dynamic coupling between the motherbody and the connected bodies, the position and the orientation of the spacecraft are functions of the position and orientation of the connected appendages.

A multibody space system can be modeled for dynamical analysis as a kinematic chain of interconnected rigid bodies (links). This kinematic chain can be simple or complex. The equations of motion for a multibody system can be obtained by using many different formalisms, such as the Newton-Euler method, or the Euler-Lagrange procedure. The first method is based on force and moment equilibrium of component bodies and subsequent elimination of the inter-body forces. The latter method is based on work/energy principles and the system is considered as a whole. To avoid lengthy expressions in the Lagrangian procedure, it is advantageous to derive the equations of motion for component bodies and subsequently eliminate the non-working constraint forces utlitizing the Natural Orthogonal Complement of the velocity constraint matrix (**Cyril et al.**, *1991*). This allows computationally efficient

recursive formulations in which the components are dealt with sequentially, taking advantage of the kinematic and dynamic equations of the previous body (**Woerkom and Misra**, *1996*).

3. Attitude Control of Space Systems

Attitude control is one of the most important problems in spacecraft design, since there are always disturbances due to dynamic interaction, gravitational torques, orbital motion, etc. The basic types of attitude control systems are (**Chobotov**, *1991*):

- Passive Gravity Gradient Control.
- Spin Control.
- Dual-Spin Control.
- Three-Axis Active Control.
- Momentum Bias Control.

The spacecraft attitude stabilization is necessary in order to maintain communication link, generate electrical power from the solar panels, and to comply with the mission objectives of the spacecraft. The dynamic coupling between the attached appendages and the spacecraft poses control problems. In most cases, the position and attitude of the spacecraft are controlled by one of the above stated attitude control methods in conjunction with reaction jets to compensate for the unwanted external torques exerted on the spacecraft. For example, the Mars Global Surveyor, shown in figure 1.2, has three reaction wheels and twelve jet thrusters as its three axis stabilized attitude control system. The utilization of jet thrusters solely as attitude control devices is not prudent as it consumes relatively large amounts of fuel, thus limiting the useful life of the system. Most importantly for intricate motion, thrusters pose the threat of sudden movements/jerks.

Reaction wheels, as shown in figure 1.5, are used in many space applications in order to maintain and/or reorient the attitude of the spacecraft. The wheels are located at a fixed orientation with respect to the spacecraft body axes. The motion of the attached appendages of a multibody space system, causes variation in the attitude of the spacecraft, which in turn causes the angular momentum of the spacecraft to change. The spacecraft attitude is controlled by absorbing the angular impulse from the external torques into the reaction wheels during slew or reorientation maneuvers. The advantages of a three axis stabilized reaction wheel system are:

(i) Capability of continuous high pointing accuracy.
(ii) Large angle slewing maneuvers without fuel consumption.
(iii) Compensation for cyclic torques without fuel consumption.

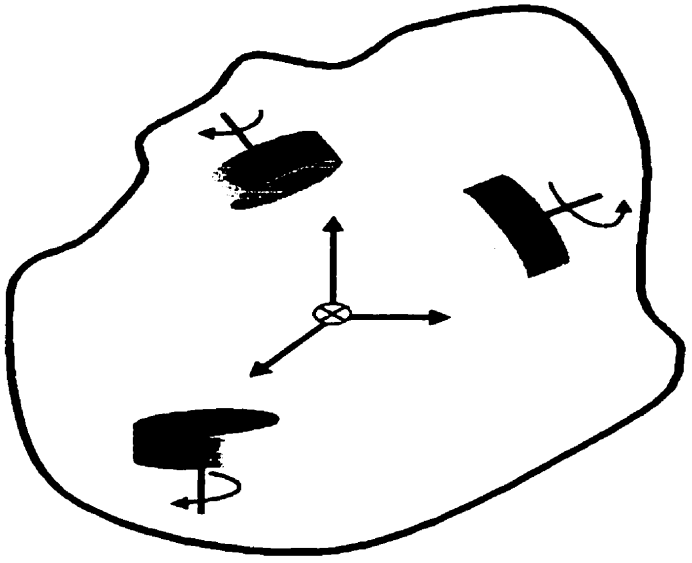

FIGURE 1.5. A body with three reaction wheels

By sensing the orientation of the spacecraft, the control system seeks to deal with the unwanted angular momentum contributed by external torques, by transferring it to the reaction wheels. This transferral is accomplished by applying control laws to the wheels. These wheels are aptly called reaction wheels because the equal and

opposite torque from the wheels on the spacecraft tend to cancel the external torque, leaving the momentum of the spacecraft unchanged (**Hughes**, *1986*).

4. The Object-oriented Approach

Considerable effort has been directed towards the dynamics, modeling, and computer simulation of multibody systems because the micro-gravity environment of space is not easily amenable for experimentation on the ground (**Min et al.**, *1999*). Most previous investigations, have considered specific models and have adopted a procedure-oriented approach. Modeling by this method is composed of a large number of procedures. This method is prone to errors and does not easily accommodate the possibility of modifications, as it is too laborious. But recently several researchers have focussed attention to the application of object-oriented approaches to multibody dynamics formulations (**Otter et al.**, *1993*). Following this methodology, the system is viewed as a combination of distinctive objects having certain characteristic data and corresponding operations. An action of the system is typified as a procedure which swaps and renews the information through its own internal operation. This makes the object-oriented approach have a much lower probability of errors while modeling. Moreover it is considerably easy to upgrade and/or modify existing systems by simply adding or replacing some objects.

Multibody systems are comprised of many distinctive and consequential elements, such as solar panels, antennas, booms, and manipulator arms. The functionalities and characteristics of each of these elements can be generalized and modeled as objects. In addition, processes, such as the system assembly and the solution of the nonlinear equations are also designed as objects. Consequently, using object-oriented concepts, the modeling of multibody systems can be done in a modular fashion. Modeling is achieved by interconnection of the object modules in a simple and concise manner.

5. Motivation and Objective

The formalisms for computer-oriented generation of multibody system equations have been developed to a high degree of maturity during the past decades. Meanwhile, the modeling aspects in the various technological contexts and the interaction with other methodologies for computer-aided system design, are fertile research topics in multibody dynamics.

Using object-oriented approach, the multibody system can be broken down into generic classes and further bifurcated into specialized objects. Such a methodology has many advantages over the conventional procedure-oriented technique. While modeling complex multibody systems, the object-oriented modeling method is less prone to errors. It also enhances code re-usability, since it is a constantly evolving piece of software and is easy to alter and/or upgrade. As mentioned previously, the attitude stabilization and control of the motherbody is of extreme importance, and the use of reaction wheels is a very effective method of maintaining the orientation of the spacecraft. Objects that could simulate a spacecraft mounted with reaction wheels, and this system being a part of a larger multibody space system, have not been developed. Hence, the objective of this study involves the application of object-oriented modeling techniques for the efficient generation and solution of the dynamic equations of motion of a spacecraft containing reaction wheels. In order to preserve the autonomous portrayal of each individual body in the multibody space system, the technique adopted involves the modification of the Lagrangian method in conjunction with the Natural Orthogonal Complement of the kinematic constraint matrix.

This research project encompasses the mathematical formulation, as well as designing and coding of the objects that would simulate a spacecraft mounted with three reaction/momentum wheels. The objects designed would be part of a multibody space system software package, that could be used to simulate a variety of real-life space applications. The first step in this research work would be to develop

a mathematical model to study the dynamics of a general multibody space system. A variation of the Lagrangian formulation technique will be used to formulate the equations of motion. The next step will be to incorporate the reaction wheels along each body-fixed axes of the spacecraft. Using energy methods, the complete equations of motion of the spacecraft with reaction wheels will be derived. The kinematic constraints evolving between two connected bodies of the multibody system will be eliminated using the Natural Orthogonal Complement matrix. Finally objects for the reaction wheels mounted on the body-fixed axes of the spacecraft will be developed using ROSE (Real-time Object-oriented Software Environment) (**Min et al.**, *1999*). The objects designed will be such that control gains could be fed to the reaction wheels, which would change the spin rate of the wheels. This would consequently change their angular momentum, and thus compensate for the change in the angular momentum of the spacecraft. Such an object-oriented approach enables characteristic features such as code re-usability, versatility, and information hiding, which are the advantages of using such a modular approach (**Min et al.**, *2000*).

6. Organization of the Thesis

This thesis is divided into three distinct parts. The first part involves the rigorous formulation of the equations of motion of the motherbody with reaction wheels. This has been described in **chapter 2**. The chapter starts by introducing the kinematics involved for rigid body undergoing translation and rotation. Using the relations obtained from kinematics, the general dynamical equations for a body are obtained. Then a reaction wheel spinning about a fixed axis, with respect to the body-fixed axes of the spacecraft is considered. The terms originating due to the dynamic coupling between the spacecraft and the reaction wheels are added to the equations of motion of the motherbody, in order to deduce the complete set of equations governing the dynamics of a spacecraft containing multiple reaction wheels.

The second part gives a brief history of the application of object-oriented modeling techniques to multibody dynamics and the concept of the generic elements are also introduced. This lays the foundation for the formation of classes like **Body** and **Joint**. This has been explained in **chapter 3**. The equations of motion for each body of the multibody system are assembled here and the kinematic constraints are also eliminated. **Chapter 4** is concerned with the implementation of the equations of motion of the system into programmable code, and finally in the form of fully developed and functional objects.

The last part viz. **chapter 5**, involves validation tests and new simulations done for a variety of cases. Finally in conclusion of the thesis, i.e. **chapter 6**, a summary of the work is presented and suggestions are given for future work.

CHAPTER 2

Dynamical Equations of the System

1. Introduction

The system under study is composed of a main body(motherbody or satellite) containing reaction wheels, that serves as a platform on which there is provision for multiple appendages to be attached in any open chain configuration. Such space systems can be modeled for dynamical analysis as multibody mechanical systems. The crux of this chapter is the formulation of the dynamical equations of motion of a spacecraft containing reaction wheels.

For the study under consideration, the main body or satellite is modeled to be a rigid body, while the multiple short appendages are modeled to be rigid links. The joints are modeled as rigid and could be of prismatic, revolute or free floating type. The kinematics presented here, is described in the most general case which could be applied to any i^{th} body of the multibody system. A suitable set of coordinates that describes the motion of a rigid body will be presented. Also, the position and velocity vectors of any point on body i are obtained in order to use them for the derivation of the equations of motion.

2. Kinematics

2.1. Coordinates for a Rigid Body. If the rigid body i is considered to be an unconstrained body, then under rigid body conditions, it can be fully described by the position and orientation of the body-fixed frame X_i, Y_i, Z_i with respect to the inertial frame X_o, Y_o, Z_o, as shown in figure 2.1. The location of the origin of the

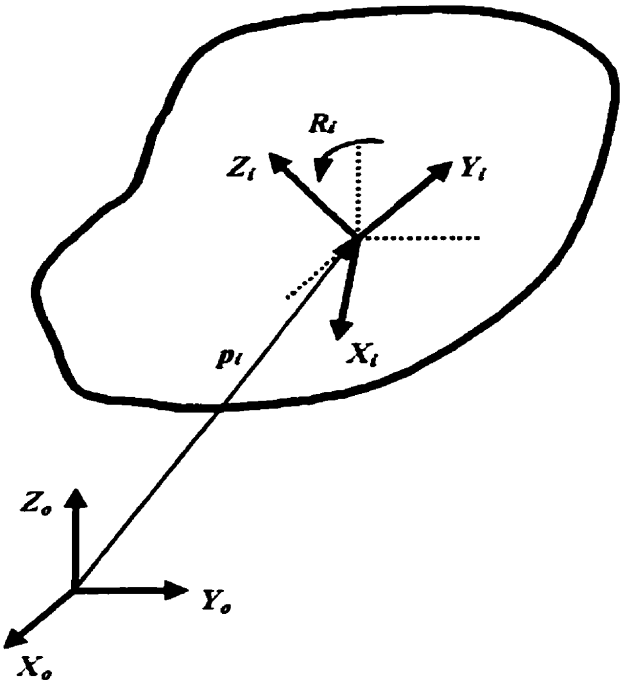

FIGURE 2.1. The representation of a rigid body

frame X_i, Y_i, Z_i from the origin of the frame X_o, Y_o, Z_o is described by the position vector $\mathbf{p}_i$ and the orientation is specified by the rotation matrix $\mathbf{R}_i$. The nine elements of this matrix $\mathbf{R}_i$ are direction cosines of the unit vectors along X_i, Y_i, Z_i axes, which uniquely describe the orientation of the body-fixed frame X_i, Y_i, Z_i in terms of the X_o, Y_o, Z_o coordinates. There exist only three independent parameters within the nine elements, and hence there exist six constraint equations, which are due to the orthogonality property of $\mathbf{R}_i$ .i.e.

$$\mathbf{R}_i^T \mathbf{R}_i = \mathbf{1} \tag{2.1}$$

Thus there are only three independent parameters, the most popular of which are : Euler angles and Bryant(Cardan) angles. However it has been proven that no three-parameter set is nonsingular (**Stuelpnagel**, *1964*). An alternative to overcome the singularities of the three-parameter set for orientation, is to choose a set of four redundant parameters with one constraint equation. This four-parameter set is referred to as quaternions, and some of these are: natural invariants, Euler parameters, and linear invariants.

2.2. Definitions. The Euler parameters associated with body i are defined by,

$$\mathbf{r}_i = \sin\left(\frac{\theta_i}{2}\right) \hat{\mathbf{e}}_i \tag{2.2}$$

and,

$$r_{o_i} = \cos\left(\frac{\theta_i}{2}\right) \tag{2.3}$$

The quaternion formed by the Euler parameters is then defined as,

$$\hat{\mathbf{q}}_i = \left\{ \begin{array}{c} \mathbf{r}_i \\ r_{o_i} \end{array} \right\} \tag{2.4}$$

Alternatively, in terms of the Euler angle θ_i and the Euler axis $\hat{\mathbf{e}}_i$,

$$\hat{\mathbf{q}}_i = \left\{ \begin{array}{c} \sin\left(\frac{\theta_i}{2}\right) \hat{\mathbf{e}}_i \\ \cos\left(\frac{\theta_i}{2}\right) \end{array} \right\} \tag{2.5}$$

Since $\sin(\cdot)$ and $\cos(\cdot)$ are dependent upon each other, the quaternions satisfy the algebraic constraint equation,

$$\hat{\mathbf{q}}_i^T \hat{\mathbf{q}}_i = 1 \tag{2.6}$$

The rotation matrix $\mathbf{R}_i$, expressed in terms of Euler parameters is then given by,

$$\mathbf{R}_i = \left(2 r_{o_i}^2 - 1\right) \mathbf{1} + 2 \mathbf{r}_i \mathbf{r}_i^T + 2 r_{o_i} \mathbf{r}_i^{\times} \tag{2.7}$$

The superscript '×' represents the cross product operation. The explicit formulae for the inverse problem in which the matrix $\mathbf{R}_i$ is given and the corresponding Euler parameters are determined, are as follows (**Wittenburg**, *1974*),

$$r_{o_i} = \sqrt{\frac{tr\,(\mathbf{R}_i) + 1}{4}} \tag{2.8}$$

$$r_{i_{(j)}} = \sqrt{\frac{\left(R_{i_{(j\,j)}} + 1\right)}{2} - \frac{(tr\,(\mathbf{R}_i) + 1)}{4}} \;; j = 1.2.3 \tag{2.9}$$

where the subscripts $r_{i_{(j)}}$ and $R_{i_{(j\,j)}}$ represent the j^{th} and $(j,j)^{th}$ elements of the corresponding vector and matrix, respectively and tr($\mathbf{R}_i$) denotes the trace of $\mathbf{R}_i$.

The 7−dimensional extended position vector, $\mathbf{q}_i$, contains the position vector $\mathbf{p}_i$ of the origin of the frame X_i, Y_i, Z_i on the i^{th} body and the orientation $\hat{\mathbf{q}}_i$ of that body. It is also referred to as the pose of the body and is given as.

$$\mathbf{q}_i = \left\{ \begin{array}{c} \mathbf{p}_i \\ \hat{\mathbf{q}}_i \end{array} \right\} \tag{2.10}$$

The 6−dimensional extended velocity vector $\mathbf{v}_i$ consists of the linear or translational velocity $\dot{\mathbf{p}}_i$ of the origin of the frame X_i, Y_i, Z_i on the i^{th} body and the angular velocity $\boldsymbol{\omega}_i$ of that body. It is also referred to as the twist of the body and is given by.

$$\mathbf{v}_i = \left\{ \begin{array}{c} \dot{\mathbf{p}}_i \\ \boldsymbol{\omega}_i \end{array} \right\} \tag{2.11}$$

The twist $\mathbf{v}_i$ and the time derivative of the pose $\dot{\mathbf{q}}_i$ are related as.

$$\mathbf{v}_i = \mathbf{L}_i\,\dot{\mathbf{q}}_i \tag{2.12}$$

where $\dot{\mathbf{q}}_i$ is a 7×1 vector, given by,

$$\dot{\mathbf{q}}_i = \begin{Bmatrix} \dot{\mathbf{p}}_i \\ \dot{\hat{\mathbf{q}}}_i \end{Bmatrix} \tag{2.13}$$

and $\mathbf{L}_i = \mathbf{L}_i\,(\mathbf{q}_i,\, t)$ which is a 6×7 matrix, defined by,

$$\mathbf{L}_i = \begin{bmatrix} \mathbf{1}_{3\,3} & \mathbf{0}_{3\,4} \\ \mathbf{0}_{3\,3} & \hat{\mathbf{L}}_i \end{bmatrix} \tag{2.14}$$

where $\hat{\mathbf{L}}_i$ is a 3×4 matrix, given by,

$$\hat{\mathbf{L}}_i = 2 \left[\cos\left(\frac{\theta_i}{2}\right) \mathbf{1} + \sin\left(\frac{\theta_i}{2}\right) \hat{\mathbf{e}}_i^{\times} - \sin\left(\frac{\theta_i}{2}\right) \hat{\mathbf{e}}_i \right] \tag{2.15}$$

Also,

$$\dot{\mathbf{q}}_i = \mathbf{\Lambda}_i\, \mathbf{v}_i \tag{2.16}$$

and,

$$\ddot{\mathbf{q}}_i = \mathbf{\Lambda}_i\, \dot{\mathbf{v}}_i + \dot{\mathbf{\Lambda}}_i\, \mathbf{v}_i \tag{2.17}$$

where $\mathbf{\Lambda}_i = \mathbf{\Lambda}_i\,(\mathbf{q}_i,\, t)$ is a 7×6 matrix and is given by,

$$\mathbf{\Lambda}_i = \begin{bmatrix} \mathbf{1}_{3\,3} & \mathbf{0}_{3\,3} \\ \mathbf{0}_{4\,3} & \hat{\mathbf{\Lambda}}_i \end{bmatrix} \tag{2.18}$$

where $\hat{\mathbf{\Lambda}}_i$ is a 4×3 matrix, given by,

$$\hat{\mathbf{\Lambda}}_i = \frac{1}{2} \begin{bmatrix} \cos\left(\frac{\theta_i}{2}\right) \mathbf{1} - \sin\left(\frac{\theta_i}{2}\right) \hat{\mathbf{e}}_i^{\times} \\ -\sin\left(\frac{\theta_i}{2}\right) \hat{\mathbf{e}}_i^{T} \end{bmatrix} \tag{2.19}$$

Moreover,

$$\mathbf{L}_i\, \mathbf{\Lambda}_i = \mathbf{1} \tag{2.20}$$

and also,

$$\hat{\mathbf{L}}_i \hat{\mathbf{\Lambda}}_i = \mathbf{1} \tag{2.21}$$

Further, $\mathbf{\Lambda}_i$ and $\hat{\mathbf{\Lambda}}_i$ can be evaluated from $\mathbf{L}_i$ and $\hat{\mathbf{L}}_i$ respectively, using the Moor-Penrose pseudo inverse,

$$\mathbf{\Lambda}_i = \mathbf{L}_i^T \left(\mathbf{L}_i \mathbf{L}_i^T\right)^{-1} \tag{2.22}$$

And,

$$\hat{\mathbf{\Lambda}}_i = \hat{\mathbf{L}}_i^T \left(\hat{\mathbf{L}}_i \hat{\mathbf{L}}_i^T\right)^{-1} \tag{2.23}$$

3. Dynamics

3.1. Introduction. The Newton-Euler Method is a very efficient recursive technique for doing computations involving the inverse and forward dynamics of serial, rigid-link manipulators. However, while analysing complicated systems this method is extremely cumbersome. Alternatively, the Euler Lagrange method is conceptually much simpler. However, the straightforward implementation of this method requires a great amount of lengthy partial differentiations, which also render these equations computationally less efficient than the other methods.

In this thesis, the derivations of the dynamical equations of the spacecraft with reaction wheels and any other connected bodies has been done using a variation of the Euler-Lagrange formulation method. In the case of this variation of Lagrangian dynamics, the kinetic and potential energies of each body are considered and then the equations of motion are derived. The equations of motion of each body are then assembled to get the dynamical equations motion of the whole system. This method introduces the non-working constraint wrenches, as in the case of the Newton-Euler formulation, but they are eliminated using the concept of Natural Orthogonal Complement (**Cyril et al.**, *1991*), which is described later.

3.2. Formulation of Equations of Motion for the i^{th} Body. The kinetic energy for each body, which could be the spacecraft, motherbody, or any attached appendage is,

$$T_i = T_i\left(\mathbf{q}_i, \dot{\mathbf{q}}_i\right) \tag{2.24}$$

The kinetic energy can be written in terms of the twist $\mathbf{v}_i$ as,

$$T_i = \frac{1}{2}\mathbf{v}_i^T \mathbf{M}_i \mathbf{v}_i \tag{2.25}$$

where $\mathbf{M}_i = M_i\left(\mathbf{q}_i, t\right)$ is the 6×6 extended mass matrix of body i. The expression for the extended mass matrix can be derived from the kinetic energy and is written as,

$$\mathbf{M}_i = \begin{bmatrix} \mathbf{M}_i^{dd} & \mathbf{M}_i^{dr} \\ \mathbf{M}_i^{rd} & \mathbf{M}_i^{rr} \end{bmatrix} \tag{2.26}$$

where,

$$\mathbf{M}_i^{dd} \equiv \int_i \mathbf{1}\, dm_i = m_i \mathbf{1} \tag{2.27}$$

$$\mathbf{M}_i^{dr} \equiv -\int_i \mathbf{r}_{o_i}^{\times}\, dm_i = -m_i \mathbf{c}_{o_i}^{\times} \tag{2.28}$$

$$\mathbf{M}_i^{rr} \equiv -\int_i \mathbf{r}_{o_i}^{\times}\mathbf{r}_{o_i}^{\times}\, dm = \mathbf{M}_{o_i}^{rr} \tag{2.29}$$

In the above equations m_i, $\mathbf{c}_{o_i}$ and $\mathbf{M}_{o_i}^{rr}$ are the total mass, position vector of the center of mass, and the second moment of inertia of the i^{th} body around its center of mass, respectively.

The dynamical equations of body i are derived using the Euler-Lagrange equation, which is given as,

$$\frac{d}{dt}\left(\frac{\partial T_i}{\partial \dot{\mathbf{q}}_i}\right) - \frac{\partial T_i}{\partial \mathbf{q}_i} = \mathbf{w}_i \tag{2.30}$$

where, $\mathbf{w}_i$ is a 6×1 dimensional vector accounting for all nonconservative wrenches.

$$\mathbf{w}_i = \mathbf{w}_i^E + \mathbf{w}_i^K + \mathbf{w}_i^A \tag{2.31}$$

where,

- $\mathbf{w}_i^A$ is the algebraic constraint wrench originating from the fact that.

$$\hat{\mathbf{q}}_i^T \hat{\mathbf{q}}_i = \mathbf{1} \tag{2.32}$$

- $\mathbf{w}_i^E$ is the external wrench.
- $\mathbf{w}_i^K$ is the kinematic constraint wrench.

The potential energy has been ignored in the Euler-Lagrange equation (2.30). Such a consideration has been done because of the fact that in micro-gravity environment the effect of the gravitational potential energy is small compared to the nonconservative wrenches. Using local velocity transformation. stated in equation (2.12) and rewritten again for convenience.

$$\mathbf{v}_i = \mathbf{L}_i \dot{\mathbf{q}}_i$$

The kinetic energy of body i. from equation (2.25). is now rewritten as.

$$T_i = \frac{1}{2} \mathbf{q}_i^T \mathbf{I}_i \mathbf{q}_i \tag{2.33}$$

where,

$$\mathbf{I}_i = \mathbf{L}_i^T \mathbf{M}_i \mathbf{L}_i \tag{2.34}$$

Applying the Euler-Lagrange equation stated in equation (2.30), the equation of motion for the i^{th} body is given as,

$$\mathbf{I}_i \ddot{\mathbf{q}}_i = -\dot{\mathbf{I}}_i \dot{\mathbf{q}}_i + \frac{1}{2} \frac{\partial}{\partial \mathbf{q}_i} \left(\dot{\mathbf{q}}_i^T \mathbf{I}_i \dot{\mathbf{q}}_i \right) + \mathbf{w}_i^E + \mathbf{w}_i^K + \mathbf{w}_i^A \tag{2.35}$$

The equation of motion, represented by equation (2.35), for the i^{th} body is pre-multiplied by $\mathbf{\Lambda}_i^T$, in order to eliminate the algebraic constraint $\mathbf{w}_i^A$, from equation (A.7) in Appendix A, and substituting the expression for $\ddot{\mathbf{q}}_i$, derived in equation (2.17), the following equation is obtained,

$$\begin{aligned} \mathbf{M}_i \dot{\mathbf{v}}_i &= -\mathbf{\Lambda}_i^T \mathbf{I}_i \dot{\mathbf{\Lambda}}_i \mathbf{v}_i - \mathbf{\Lambda}_i^T \dot{\mathbf{I}}_i \mathbf{\Lambda}_i \mathbf{v}_i + \frac{1}{2} \mathbf{\Lambda}_i^T \frac{\partial}{\partial \mathbf{q}_i} \left(\mathbf{v}_i^T \mathbf{M}_i \mathbf{v}_i \right) \\ &\quad + \mathbf{\Lambda}_i^T \mathbf{w}_i^E + \mathbf{\Lambda}_i^T \mathbf{w}_i^K \end{aligned} \tag{2.36}$$

Using the relations derived in equation (2.20), and equations (B.5), (B.6), and (B.13) in Appendix B, equation (2.36) can be expressed as,

$$\begin{aligned} \mathbf{M}_i \dot{\mathbf{v}}_i &= -\dot{\mathbf{M}}_i \mathbf{v}_i - 2 \mathbf{\Lambda}_i^T \dot{\mathbf{L}}_i^T \mathbf{M}_i \mathbf{v}_i + \frac{1}{2} \mathbf{\Lambda}_i^T \left(\mathbf{v}_i^T \frac{\partial \mathbf{M}_i}{\partial \mathbf{q}_i} \mathbf{v}_i \right) \\ &\quad + \boldsymbol{\phi}_i^E + \boldsymbol{\phi}_i^K \end{aligned} \tag{2.37}$$

where,

$$\boldsymbol{\phi}_i^E = \mathbf{\Lambda}_i^T \mathbf{w}_i^E$$

$$\boldsymbol{\phi}_i^K = \mathbf{\Lambda}_i^T \mathbf{w}_i^K$$

Equation (2.37) can be stated in a compact form as,

$$\mathbf{M}_i \dot{\mathbf{v}}_i = \boldsymbol{\phi}_i^S + \boldsymbol{\phi}_i^E + \boldsymbol{\phi}_i^K \tag{2.38}$$

which is the generalized Newton-Euler equation, where $\boldsymbol{\phi}_i^S$ is the system wrench given by,

$$\boldsymbol{\phi}_i^S = -\dot{\mathbf{M}}_i \mathbf{v}_i - 2 \mathbf{\Lambda}_i^T \dot{\mathbf{L}}_i^T \mathbf{M}_i \mathbf{v}_i + \frac{1}{2} \mathbf{\Lambda}_i^T \left(\mathbf{v}_i^T \frac{\partial \mathbf{M}_i}{\partial \mathbf{q}_i} \mathbf{v}_i \right) \tag{2.39}$$

4. Dynamical Equations of Motion for a Spacecraft with Reaction Wheels

The spacecraft can be regarded as a rigid body and hence the concepts and formulation techniques that were introduced in the previous section for a body i could be extended to the spacecraft (subscript B). The reaction wheels are mounted on a fixed axis frame with respect to the body coordinate frame of the spacecraft. The kinetic energy of a spacecraft containing a reaction wheel is given by,

$$T_{SC} = T_B + T_w \tag{2.40}$$

where,

- T_{SC} is the total kinetic energy
- T_B is the kinetic energy of the spacecraft
- T_w is the kinetic energy of the reaction wheel

Thus the total kinetic energy T_{SC} can be separated into two parts T_B and T_w. In the foregoing formulation the Euler-Lagrange equation is applied to the sum of T_B and T_w; however, for the ease of formulation the contributions from T_B and T_w are evaluated separately and then the evaluated terms are added together in order to get the complete dynamic equations of motion of the spacecraft with the reaction wheels.

4.1. The Spacecraft. The kinetic energy (T_B) for the spacecraft is given as.

$$T_B = \frac{1}{2}\mathbf{v}_B^T \mathbf{M}_B \mathbf{v}_B \tag{2.41}$$

where,

- $\mathbf{v}_B$ is the 6−dimensional twist of the spacecraft, as defined in equation (2.11).
- $\mathbf{M}_B$ is the $\bar{6} \times 6$ extended mass matrix of the spacecraft. The expression for the extended mass matrix can be derived from the kinetic energy and is

written as,

$$\mathbf{M}_B = \begin{bmatrix} \mathbf{M}_B^{dd} & \mathbf{M}_B^{dr} \\ \mathbf{M}_B^{rd} & \mathbf{M}_B^{rr} \end{bmatrix} \tag{2.42}$$

The terms of the extended mass matrix of the spacecraft, given in equation (2.42) can be evaluated from the expressions given in equations (2.27), (2.28) and (2.29). On applying the Euler-Lagrange equation to equation (2.41) and using the result obtained from equation (2.37), the contribution of the kinetic energy of the motherbody to the equation of motion of the considered system is,

$$\begin{aligned} \mathbf{M}_B \dot{\mathbf{v}}_B &= -\dot{\mathbf{M}}_B \mathbf{v}_B - 2\,\mathbf{\Lambda}_B^T \dot{\mathbf{L}}_B^T \mathbf{M}_B \mathbf{v}_B + \frac{1}{2}\mathbf{\Lambda}_B^T \left(\mathbf{v}_B^T \frac{\partial \mathbf{M}_B}{\partial \mathbf{q}_B} \mathbf{v}_B \right) \\ &\quad + \boldsymbol{\phi}_B^E + \boldsymbol{\phi}_B^K \end{aligned} \tag{2.43}$$

4.2. Reaction Wheel. The derivation presented below is for one reaction wheel which can be extended to three reaction wheels. The inertia and wrench terms that are generated from the dynamical equations of motion of the reaction wheels are combined with the inertia and wrench terms of the spacecraft, which have been derived in equation (2.43).

The kinetic energy of the wheel is given as,

$$T_w = \frac{1}{2}\mathbf{v}_w^T \mathbf{M}_w \mathbf{v}_w \tag{2.44}$$

where $\mathbf{M}_w$ is the 6×6 extended mass matrix of reaction wheel. The expression for the extended mass matrix of the wheel can be derived as,

$$\mathbf{M}_w = \begin{bmatrix} \mathbf{M}_w^{dd} & \mathbf{M}_w^{dr} \\ \mathbf{M}_w^{rd} & \mathbf{M}_w^{rr} \end{bmatrix} \tag{2.45}$$

where,

$$\mathbf{M}_w^{dd} \equiv \int_w \mathbf{1}\, dm_w = m_w \mathbf{1} \tag{2.46}$$

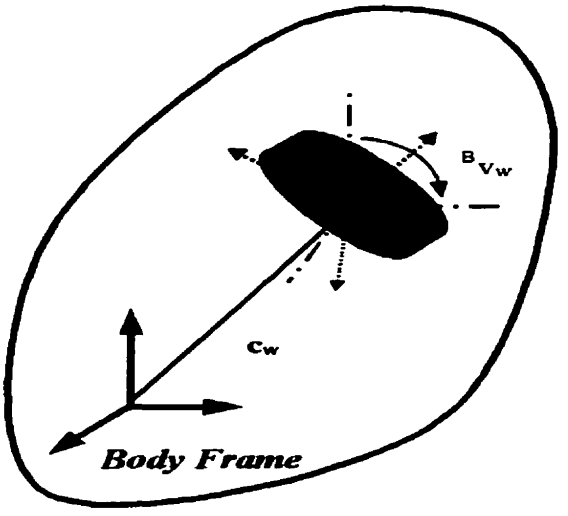

FIGURE 2.2. Reaction wheel in the motherbody

$$\mathbf{M}_w^{dr} = -m_w \mathbf{c}_w^{\times} \tag{2.47}$$

In the above equations m_w and $\mathbf{M}_w^{rr}$ are the total mass and the second moment of inertia of the reaction wheel expressed in the spacecraft body frame, respectively, while $\mathbf{c}_w$ is the position vector of the center of mass of the wheel from the origin of the body frame of the motherbody, as shown in figure 2.2. ${}^{B}\mathbf{v}_w$ is the twist of the wheel relative to the motherbody. The total twist of the reaction wheel, $\mathbf{v}_w$, which is expressed in the body frame of the motherbody is given by,

$$\mathbf{v}_w = \mathbf{v}_B + {}^{B}\mathbf{v}_w \tag{2.48}$$

${}^{B}\mathbf{v}_w$ is a 6-dimensional vector. All the elements of ${}^{B}\mathbf{v}_w$ are zero, except one, depending on the axis of spin of the reaction wheel. The fourth, fifth or sixth element of the vector ${}^{B}\mathbf{v}_w$ constitutes the spin rate (relative angular velocity) of wheel if it spins about its X-axis, Y-axis or Z-axis, respectively. This relative angular speed of the reaction wheel is denoted by ω_{wheel} and it could be:

(i) A constant nominal spin rate.

(ii) Any function of time.

(iii) In the form of a P.I.D. control law, such as,

$$\omega_{wheel} = \mathbf{K}_1 \hat{\mathbf{q}}_B + \mathbf{K}_2 \int \hat{\mathbf{q}}_B \, dt + \mathbf{K}_3 \dot{\hat{\mathbf{q}}}_B \tag{2.49}$$

where, $\mathbf{K}_1$, $\mathbf{K}_2$ and $\mathbf{K}_3$ are 1×4 control gain vectors and $\hat{\mathbf{q}}_B$ is the body quaternion of the spacecraft. The equations of motion of the spacecraft with the reaction wheels have been formulated to accommodate such a P.I.D. control law.

Substituting the expression for the total velocity of the reaction wheel, $\mathbf{v}_w$ in equation (2.44), the kinetic energy of the wheel on expanding is,

$$T_w = \frac{1}{2} \left(\mathbf{v}_B^T \mathbf{M}_w \mathbf{v}_B + {}^B\mathbf{v}_w^T \mathbf{M}_w \mathbf{v}_B + \mathbf{v}_B^T \mathbf{M}_w {}^B\mathbf{v}_w + {}^B\mathbf{v}_w^T \mathbf{M}_w {}^B\mathbf{v}_w \right) \tag{2.50}$$

which is rewritten as,

$$T_w = \frac{1}{2} \mathbf{v}_B^T \mathbf{M}_w \mathbf{v}_B + \mathbf{v}_B^T \mathbf{M}_w {}^B\mathbf{v}_w + \frac{1}{2} {}^B\mathbf{v}_w^T \mathbf{M}_w {}^B\mathbf{v}_w \tag{2.51}$$

Let,

$$T_w = T_1 + T_2 + T_3$$

where,

- $T_1 = \frac{1}{2} \mathbf{v}_B^T \mathbf{M}_w \mathbf{v}_B$
- $T_2 = \mathbf{v}_B^T \mathbf{M}_w {}^B\mathbf{v}_w$
- $T_3 = \frac{1}{2} {}^B\mathbf{v}_w^T \mathbf{M}_w {}^B\mathbf{v}_w$

4.3. Complete Dynamic Equations of Motion for the Spacecraft with the Reaction Wheel. The inertia (Left hand) terms and the wrench (Right hand) terms due to the kinetic energy of the reaction wheel derived in equation (C.32), given in Appendix C, are combined with the inertia and wrench terms of the spacecraft to get the dynamical equations of motion for the spacecraft containing the reaction wheel. The inertia and wrench terms of the spacecraft has been derived in equation (2.43). Thus the complete equation of motion of the spacecraft with the

reaction wheel is,

$$\begin{aligned}
\mathbf{M}_B\,\dot{\mathbf{v}}_B \quad & + \mathbf{M}_w\,\dot{\mathbf{v}}_B + \mathbf{\Lambda}_B^T \left(\frac{\partial^B \mathbf{v}_w}{\partial \dot{\mathbf{q}}_B}\right)^T \mathbf{M}_w\,\dot{\mathbf{v}}_B = -\dot{\mathbf{M}}_B\,\mathbf{v}_B - 2\,\mathbf{\Lambda}_B^T\,\dot{\mathbf{L}}_B^T\,\mathbf{M}_B\,\mathbf{v}_B \\
& + \frac{1}{2}\,\mathbf{\Lambda}_B^T \left(\mathbf{v}_B^T \frac{\partial \mathbf{M}_B}{\partial \mathbf{q}_B}\,\mathbf{v}_B\right) - 2\,\mathbf{\Lambda}_B^T\,\dot{\mathbf{L}}_B^T\,\mathbf{M}_w\,\mathbf{v}_B + \mathbf{\Lambda}_B^T \left(\frac{\partial^B \mathbf{v}_w}{\partial \mathbf{q}_B}\right)^T \mathbf{M}_w\,\mathbf{v}_B \\
& - 2\,\mathbf{\Lambda}_B^T\,\dot{\mathbf{L}}_B^T\,\mathbf{M}_w\,{}^B\mathbf{v}_w - \mathbf{M}_w \frac{d\,{}^B\mathbf{v}_w}{dt} - \mathbf{\Lambda}_B^T \frac{d}{dt}\left(\frac{\partial^B \mathbf{v}_w}{\partial \dot{\mathbf{q}}_B}\right)^T \mathbf{M}_w \mathbf{v}_B \\
& - \mathbf{\Lambda}_B^T \left[\frac{d}{dt}\left(\frac{\partial^B \mathbf{v}_w}{\partial \dot{\mathbf{q}}_B}\right)^T \mathbf{M}_w\,{}^B\mathbf{v}_w\right] - \mathbf{\Lambda}_B^T \left[\left(\frac{\partial^B \mathbf{v}_w}{\partial \dot{\mathbf{q}}_B}\right)^T \mathbf{M}_w \frac{d\,{}^B\mathbf{v}_w}{dt}\right] \\
& + \mathbf{\Lambda}_B^T \left[\left(\frac{\partial^B \mathbf{v}_w}{\partial \mathbf{q}_B}\right)^T \mathbf{M}_w\,{}^B\mathbf{v}_w\right] + \boldsymbol{\phi}_B^E + \boldsymbol{\phi}_B^K \qquad (2.52)
\end{aligned}$$

The equation of motion for any i^{th} connected body appended onto the spacecraft is given by,

$$\begin{aligned}
\mathbf{M}_i\,\dot{\mathbf{v}}_i \;\; = \;\; & -\dot{\mathbf{M}}_i\,\mathbf{v}_i - 2\,\mathbf{\Lambda}_i^T\,\dot{\mathbf{L}}_i^T\,\mathbf{M}_i\,\mathbf{v}_i + \frac{1}{2}\,\mathbf{\Lambda}_i^T \left(\mathbf{v}_i^T \frac{\partial \mathbf{M}_i}{\partial \mathbf{q}_i}\,\mathbf{v}_i\right) \\
& + \boldsymbol{\phi}_i^E + \boldsymbol{\phi}_i^K \qquad (2.53)
\end{aligned}$$

Equation (2.52) is the dynamic equation of motion of the motherbody containing a reaction wheel. The inertia and wrench terms of this equation have been converted into programmable code and incoporated into functional objects, which is described in the subsequent chapters.

CHAPTER 3

Object-oriented Concepts and Multibody Dynamics

1. Introduction

In an object-oriented approach, a complex system is viewed as a meaningful collection of objects that collaborate to achieve some higher level of operation. Object-oriented modeling methods have evolved to help developers exploit the expressive power of object-oriented programming languages, using class and object as building blocks (**Booch**, *1994*). Classes and objects are intimately related concepts. Specifically, every object belongs to a certain class. The object-oriented modeling offers significant benefits such as,

- The object models are produced from stable intermediate forms which are more resilient to change.
- Systems developed using the object-oriented concepts can be allowed to evolve over time, rather than be abandoned or completely redesigned in response to the first major change in requirements.
- Object-oriented modeling reduces the risks and errors inherent in developing complex systems, primarily because integration of the software is spread out across the life cycle rather than occurring as one major event.
- It engineers an illusion of simplicity and is user-friendly.

2. Object-oriented Concepts Applied to Multibody Systems

Most past research has focussed on the procedure-oriented computation techniques for analyzing the dynamics of multibody systems. In this method of computation, the main task is broken down into numerous simple instruction units that are processed in a serial fashion. Unfortunately this method is extremely cumbersome for large and complex multibody systems. The object-oriented modeling consists of identifying objects and the computations done by those objects, and creating simulations of those objects, their processes, and the required communications between the objects (**Sebest**, *1989*). As mentioned in the previous section, such a formulation technique is less prone to errors and is relatively easy to modify and/or upgrade.

Due to the apparent and numerous advantages of using object-oriented modeling techniques, various researchers have applied these concepts for the dynamic simulation of multibody systems. **Otter and Hocke** (*1993*) can be credited as one of the first research groups who introduced the concept of object-oriented programming into a data model for the exchange of rigid multibody system descriptions. They used a hierarchical framework for characterizing objects and were concerned only with the dynamic simulation of rigid body systems. Wallrapp extended the work of Otter and Hocke by adding classes that could represent the flexible members of the multibody system (**Wallrapp**, *1993*). The work done by these researchers was aimed at providing a standard input for multibody system software packages and did not specify the method used to formulate the equations of motion.

Kecskeméthy applied object-oriented modeling for the efficient generation and solution of the equations of motion for rigid multibody systems (**Kecskeméthy**, *1995*). He classified the multibody system into state objects and transmission elements. State objects were responsible for holding and passing on information about position, velocity, acceleration, and load at an arbitrary location, while the transmission elements transmitted this information from one set of state objects to another.

The assembly process consisted of attaching specific copies of state objects to the inputs and outputs of the transmission elements. Lückel et al. adopted a computationally efficient recursive Newton-Euler formalism for the dynamic simulation of rigid multibody systems (**Lückel et al.**, *1993*). The use of work-energy relations was the focus of research for the dynamic simulation of multibody systems by Anantharaman (**Anantharaman**, *1996*). In his research, the equations of motion for the multibody system were derived using symbolic differentiation of the virtual work of the system.

In order to accommodate the flexibility as well as maintain the independent representation of each individual body in a multibody system, Min et al. adopted the formalism based on the Euler-Lagrange method in conjunction with the use of the Natural Orthogonal Complement of the kinematic constraint matrix (**Min et al.**, *1999*). In that work, the multibody dynamics model has been treated as a combination of **Body**, **Joint**, **System**, and **Solver** classes. The objects defined in these classes are refined from the generic types in a top-down fashion by taking advantage of the inheritance concept, as opposed to the procedure-oriented approach which functions at a very specific level. The methodology followed in this research is an extension of the work done by Min et al. This thesis involves the modeling of objects that would simulate the dynamic response of a spacecraft carrying reaction wheels. The spacecraft could be a complex multibody space system.

3. Kinematic Objects

As mentioned previously, multibody space systems can be composed of many distinctive components, such as solar panels, booms, manipulator links, antennas, actuators, reaction wheels, control moment gyros, and jet thrusters. The processes and operations for each of these components can be identified and characterized into objects. The following section describes the essential kinematic relationships that have been embedded into objects for the transfer of motion states from one body to

the next body via joints in a multibody system. The objects mentioned in this thesis are written in *italics*.

3.1. The Generic Element. Kinematics is responsible for holding and passing the motion states of the body. The transfer of motion states can occur within a *Link* and within a *Joint* due to the motion of the rigid body. The relationships presented below are given in the most general form for a generic kinematic element, during the transfer of motion states from one frame to another. These relationships have been extended to be incorporated in the objects *Link* and *Joint*.

The fundamental motion states of the rigid body are position ($\mathbf{p}$), velocity ($\dot{\mathbf{p}}$) and acceleration ($\ddot{\mathbf{p}}_{\bar{\mathbf{y}}=0}$) for translation, and rotation matrix ($\mathbf{R}$), angular velocity ($\boldsymbol{\omega}$), and angular acceleration ($\dot{\boldsymbol{\omega}}_{\bar{\mathbf{y}}=0}$) for rotation respectively. They are held in an object titled *Frame*. In the above $(\cdot)_{\bar{\mathbf{y}}=0}$ stands for the evaluation of a quantity when the generalized acceleration vector ($\ddot{\mathbf{y}}$) of the multibody system is set to zero, where $\mathbf{y}$ is the generalized coordinate vector of the system. These values are used instead of real accelerations, since they are useful for the assembly of the global system dynamics. The kinematic motion states are expressed with respect to the inertial reference frame $\mathbf{O}$. The frame $\mathbf{O}_m$ represents the local body frame of the rigid body. $\mathbf{O}_s$ represents the new frame after the relative change in position and orientation due to rigid body motion. $\mathbf{p}_s$ is the position vector that locates the origin of the frame $\mathbf{O}_s$ from the origin of the inertial reference frame $\mathbf{O}$, while $\mathbf{R}_s$ is the rotation matrix that represents the orientation of the frame $\mathbf{O}_s$ with respect to the inertial reference frame $\mathbf{O}$. $\mathbf{p}_m$ is the position vector that locates the origin of the frame $\mathbf{O}_m$ from the origin of the inertial reference frame $\mathbf{O}$, while $\mathbf{R}_m$ is the rotation matrix that represents the orientation of the frame $\mathbf{O}_m$ with respect to the inertial reference frame $\mathbf{O}$. The fundamental operation of the generic kinematic element is the transmission of motion states from one frame into another as depicted in figure 3.1. It consists of the following three transmissions.

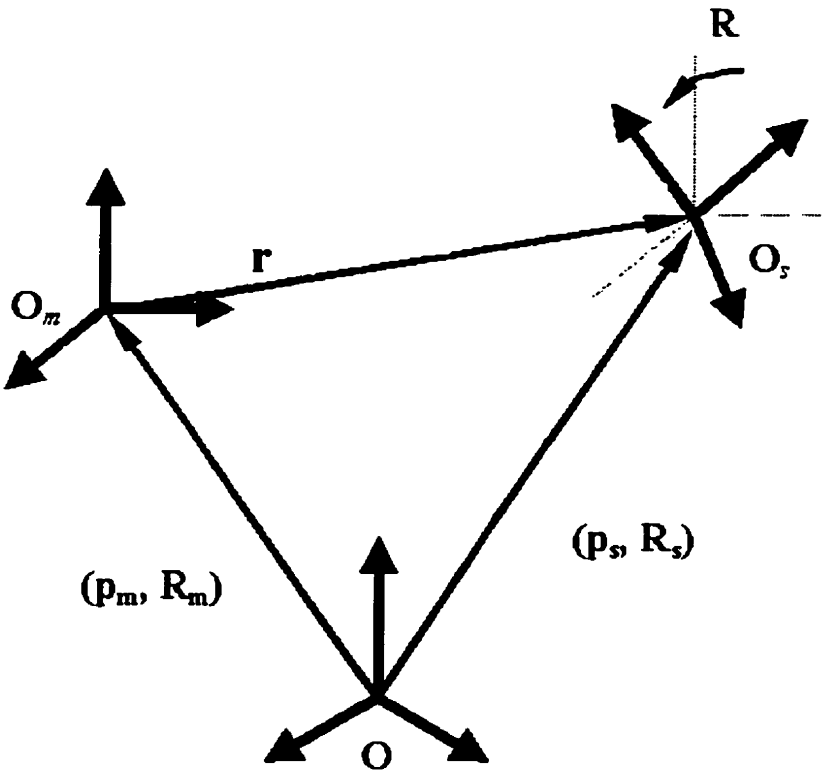

FIGURE 3.1. Generic kinematic element

- Displacement

$$\mathbf{R}^T (\mathbf{p}_m + \mathbf{r}) = \mathbf{p}_s \tag{3.1}$$

$$\mathbf{R}_m \mathbf{R} = \mathbf{R}_s \tag{3.2}$$

- Velocity

$$\mathbf{R}^T \left(\dot{\mathbf{p}}_m + \boldsymbol{\omega}_m^{\times} \mathbf{r}\right) = \dot{\mathbf{p}}_s \tag{3.3}$$

$$\mathbf{R}^T (\boldsymbol{\omega}_m + \boldsymbol{\omega}) = \boldsymbol{\omega}_s \tag{3.4}$$

- Acceleration

$$\mathbf{R}^T \left(\ddot{\mathbf{p}}_{m_{\dot{\mathbf{y}}=0}} + \dot{\boldsymbol{\omega}}_{m_{\dot{\mathbf{y}}=0}}^{\times} \mathbf{r} + \boldsymbol{\omega}_m^{\times} \boldsymbol{\omega}_m^{\times} \mathbf{r}\right) = \ddot{\mathbf{p}}_{s_{\dot{\mathbf{y}}=0}} \tag{3.5}$$

$$\mathbf{R}^T \left(\dot{\boldsymbol{\omega}}_{m_{\bar{y}=0}} + \boldsymbol{\omega}_m^{\times} \boldsymbol{\omega} \right) = \dot{\boldsymbol{\omega}}_{s_{\bar{y}=0}} \tag{3.6}$$

In the above expressions, $\mathbf{r}$ and $\boldsymbol{\omega}$ represent the relative displacement and relative angular velocity, respectively, between frames $\mathbf{O}_m$ and $\mathbf{O}_s$, while the superscript '$\times$' represents the cross product operation.

3.2. Link. *Link* is a kinematic object that transfers motion states within a body. In order to provide some simplicity while modeling complex multibody systems, the objects *Outward Link* and *Inward Link* are developed for a rigid body. The *Outward Link* is responsible for transfer of kinematic states from the local body frame $\mathbf{O}_B$ to the outside frame $\mathbf{O}_J$ (the term "outside frame" represents the frame towards the terminal bodies/outside of the multibody system, at the connection point between the joint and the body). The *Inward Link* transfers the motion states from the inside frame $\mathbf{O}_J$ (the term "inside frame" represents the frame towards the base/inside of the multibody system, at the connection point between the joint and the body) to the local body frame $\mathbf{O}_B$. The figure 3.2 depicts the schematic of a generic *Link* (*Outward Link* and *Inward Link*). $\mathbf{r}$ is the nominal length vector from the origin of frame $\mathbf{O}_B$ to the origin of the frame $\mathbf{O}_J$, while $\mathbf{R}$ is the rotation matrix of frame $\mathbf{O}_J$ with respect to frame $\mathbf{O}_B$ due to normal twist of the body. $\mathbf{r}$ is a constant vector and $\mathbf{R}$ is a constant matrix and they are determined by the nominal body architecture.

Along with the transmission of motion states, the link restrains the relative motion of a frame with respect to another. The kinematic constraint equations of the link can be obtained by the modification of the velocity transmission relations, equations (3.3) and (3.4). For outward operation (*Outward Link*), the constraint relation is,

$$\mathbf{X}_L^O \begin{Bmatrix} \dot{\mathbf{p}}_B \\ \boldsymbol{\omega}_B \end{Bmatrix} = \begin{Bmatrix} \dot{\mathbf{p}}_J \\ \boldsymbol{\omega}_J \end{Bmatrix} \tag{3.7}$$

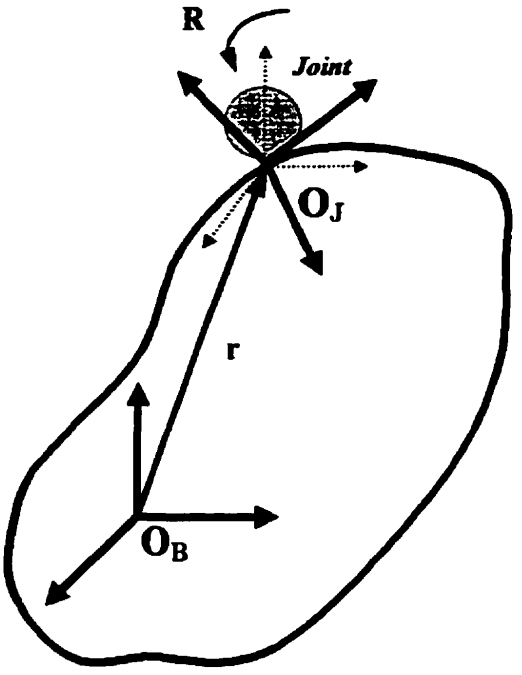

FIGURE 3.2. Generic rigid link

where,

$$\mathbf{X}_L^O = \begin{bmatrix} \mathbf{R}^T & -\mathbf{R}^T\mathbf{r}^\times \\ \mathbf{0} & \mathbf{R}^T \end{bmatrix}$$

and for the inward operation (*Inward Link*), the constraint relation is,

$$\begin{Bmatrix} \dot{\mathbf{p}}_B \\ \boldsymbol{\omega}_B \end{Bmatrix} = \mathbf{X}_L^I \begin{Bmatrix} \dot{\mathbf{p}}_J \\ \boldsymbol{\omega}_J \end{Bmatrix} \tag{3.8}$$

where,

$$\mathbf{X}_L^I = \begin{bmatrix} \mathbf{R} & \mathbf{r}^\times\mathbf{R} \\ \mathbf{0} & \mathbf{R} \end{bmatrix}$$

In the above equations, $\dot{\mathbf{p}}_B$ and $\boldsymbol{\omega}_B$ are the linear velocity vector and angular velocity vector of the rigid body expressed in the inertial reference frame, respectively. $\dot{\mathbf{p}}_J$ and $\boldsymbol{\omega}_J$ are the linear velocity vector and angular velocity vector of the rigid body at the inward or outward location, respectively. In equations (3.7) and (3.8), $\mathbf{X}_L^O$ and $\mathbf{X}_L^I$ are spatial transformations for the outward type link and the inward type

link, respectively. They are essential for assembly of the global kinematic constraint equation of the whole system, which will be explained later.

3.3. Joint. *Joint* is an object that transfers the kinematic states between two interconnecting bodies. Joints can be of revolute, prismatic, universal, or spherical types. Figure 3.3 depicts the schematic of a generic *Joint*. $\mathbf{O}_J$ and $\mathbf{O}_J^I$ represent the joint frames before and after the joint has undergone motion (translation and/or rotation), respectively. If $\mathbf{r}$ is a vector that represents the translational displacement of the joint, as in the case of a prismatic joint, and if $\mathbf{R}$ is a matrix that represents the rotation of the joint, as in the case of a revolute joint, then the state quantities of the *Joint* are expressed below in table 3.1 as,

Translation	Rotation
$\mathbf{r} = r(\boldsymbol{\theta})$	$\mathbf{R} = R(\boldsymbol{\theta})$
$\dot{\mathbf{r}} = \mathbf{Z}_v \dot{\boldsymbol{\theta}}$	$\boldsymbol{\omega} = \mathbf{Z}_\omega \dot{\boldsymbol{\theta}}$
$\ddot{\mathbf{r}}_{\dot{\mathbf{y}}=0} = \dot{\mathbf{Z}}_v \dot{\boldsymbol{\theta}} + \mathbf{Z}_v \ddot{\boldsymbol{\theta}}_{\dot{\mathbf{y}}=0}$	$\dot{\boldsymbol{\omega}}_{\dot{\mathbf{y}}=0} = \dot{\mathbf{Z}}_\omega \dot{\boldsymbol{\theta}} + \mathbf{Z}_\omega \ddot{\boldsymbol{\theta}}_{\dot{\mathbf{y}}=0}$

TABLE 3.1. State quantities of a joint

In table 3.1, $\boldsymbol{\theta}$ is the joint coordinate vector composed of the translational displacement and/or rotational angles of the joint. $\mathbf{Z}_v$, $\dot{\mathbf{Z}}_v$, $\mathbf{Z}_\omega$, and $\dot{\mathbf{Z}}_\omega$ are the joint characteristic matrices and are dependent on the type of joint. For example, $(\mathbf{Z}_v, \dot{\mathbf{Z}}_v, \mathbf{Z}_\omega, \dot{\mathbf{Z}}_\omega) = (\hat{\mathbf{z}}_p, \mathbf{0}_{3\times1}, \mathbf{0}_{3\times1}, \mathbf{0}_{3\times1})$ for a prismatic joint undergoing translation along the $\hat{\mathbf{z}}_p$ axis, while $(\mathbf{Z}_v, \dot{\mathbf{Z}}_v, \mathbf{Z}_\omega, \dot{\mathbf{Z}}_\omega) = (\mathbf{0}_{3\times1}, \mathbf{0}_{3\times1}, \hat{\mathbf{z}}_r, \mathbf{0}_{3\times1})$ for a revolute joint undergoing rotation about the $\hat{\mathbf{z}}_r$ axis.

A joint also defines a restriction on the relative motion of a frame on one body with respect to a frame on an adjacent body. From the velocity transmission relations given by equations (3.3) and (3.4), the kinematic constraint equation for the joint is,

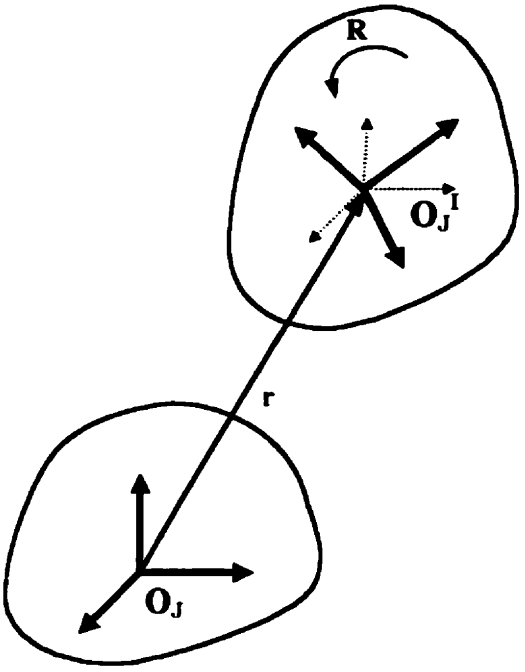

FIGURE 3.3. Generic joint

$$\mathbf{X}_J \begin{Bmatrix} \dot{\mathbf{p}}_J \\ \boldsymbol{\omega}_J \end{Bmatrix} + \mathbf{J}_J \dot{\boldsymbol{\theta}} = \begin{Bmatrix} \dot{\mathbf{p}}_J^I \\ \boldsymbol{\omega}_J^I \end{Bmatrix} \tag{3.9}$$

where,

$$\mathbf{X}_J = \begin{bmatrix} \mathbf{R}^T & -\mathbf{R}^T \mathbf{r}^\times \\ \mathbf{0} & \mathbf{R}^T \end{bmatrix} \tag{3.10}$$

And,

$$\mathbf{J}_J = \begin{bmatrix} \mathbf{R}^T \mathbf{Z}_v \\ \mathbf{R}^T \mathbf{Z}_\omega \end{bmatrix} \tag{3.11}$$

In the above equations, $\dot{\mathbf{p}}_J$ and $\boldsymbol{\omega}_J$ are the linear velocity vector and the angular velocity vector, respectively, before the joint has undergone motion and are expressed in the inertial reference frame, while $\dot{\mathbf{p}}_J^I$ and ω_J^I are the linear velocity vector and the angular velocity vector, respectively, after the joint has undergone motion and

are also expressed in the inertial reference frame. In equations (3.10) and (3.11), $\mathbf{X}_J$ and $\mathbf{J}_J$ are the spatial transformation and the local Jacobian matrices of the joint, respectively. They play a crucial role in the assemblage of the global kinematic constraint equation of the system, which is described later.

4. Dynamic Objects

Dynamic objects are responsible for yielding the equation of motion of a body, which is given in the general form as (**Jaar**, *1993*),

$$\mathbf{M}(\mathbf{y})\ \dot{\mathbf{v}} = \boldsymbol{\phi}(\mathbf{y}, \mathbf{v}, t) \tag{3.12}$$

where,

- $\mathbf{M}$ is the 6×6 extended mass matrix of the body.
- $\boldsymbol{\phi}$ is the 6−dimensional wrench of the body consisting of the external forces and moments acting on the body, and the mixed terms i.e. terms which are functions of the generalized coordinate vector $\mathbf{y}$, extended velocity vector $\mathbf{v}$ and also time t.

The generic dynamics objects are *Inertia* and *Wrench*, which represents the motion resistance and the motion agent, respectively. The primary operation of *Inertia* is to build the extended mass matrix and its time derivative of the body. While *Wrench* is responsible for evaluation of the right hand side of equation (3.12). The previous chapter was concerned with the formulation of the dynamical equations of motion of the system, which included the inertia and wrench terms. These terms have been coded in the objects *Inertia* and *Wrench*.

In the next section the kinematic constraint equations of the body and the joint, which were derived earlier, will be used to formulate the global kinematic constraint equation of the multibody system and hence the Natural Orthogonal Complement matrix of the system. The Natural Orthogonal Complement matrix is used to eliminate the kinematic constraint wrench of the system.

5. Assembly

Multibody systems in the most general form can be considered to be composed of N bodies. After assembling the individual body equations, which includes the motherbody and the connected auxiliary bodies, the dynamical equations of the complete multibody system are obtained in the form (**Cyril et al.**, *1991*),

$$\mathbf{M}\dot{\mathbf{v}} = \boldsymbol{\phi}^S + \boldsymbol{\phi}^E + \boldsymbol{\phi}^K \tag{3.13}$$

where $\mathbf{M}$ is the $6N \times 6N$ generalized mass matrix, $\dot{\mathbf{v}}$ represents the $6N-$dimensional time derivative of the generalized twist, while $\boldsymbol{\phi}^S$, $\boldsymbol{\phi}^E$, and $\boldsymbol{\phi}^K$ are the $6N-$dimensional generalized system, generalized external, and generalized constraint wrenches, respectively. The dynamic equation for the multibody system, given in equation (3.13) can be rewritten more explicitly as,

$$\begin{bmatrix} \ddots & & \mathbf{0} \\ & \mathbf{M}_i & \\ \mathbf{0} & & \ddots \end{bmatrix} \begin{Bmatrix} \vdots \\ \dot{\mathbf{v}}_i \\ \vdots \end{Bmatrix} = \begin{Bmatrix} \vdots \\ \boldsymbol{\phi}_i^S \\ \vdots \end{Bmatrix} + \begin{Bmatrix} \vdots \\ \boldsymbol{\phi}_i^E \\ \vdots \end{Bmatrix} + \begin{Bmatrix} \vdots \\ \boldsymbol{\phi}_i^K \\ \vdots \end{Bmatrix} \tag{3.14}$$

where $\mathbf{M}_i$, $\dot{\mathbf{v}}_i$, $\boldsymbol{\phi}_i{}^S$, $\boldsymbol{\phi}_i^E$, and $\boldsymbol{\phi}_i^K$ are the 6×6 extended mass matrix, the $6-$dimensional time derivative of the twist, system wrench, external wrench, and constraint wrench, respectively, associated with the i^{th} body. The constraint wrench $\boldsymbol{\phi}^K$ is eliminated by multiplying the assembled equations of motion from the left by $\mathbf{N}^T$,the transpose of the Natural Orthogonal Complement matrix, to obtain the independent dynamical equations of the multibody system.

5.1. Formulation for the Natural Orthogonal Complement Matrix.

As mentioned earlier in this chapter, the rigid body has been decomposed into two distinct parts viz. the outward link and the inward link. The kinematic constraint is due to the combination of the outward link in the lower body $i-1$, the inward link in the body i, and the joint i between them, as shown in figure (3.4). Using equations (3.7), (3.8), and (3.9), the individual constraint equations in terms of the

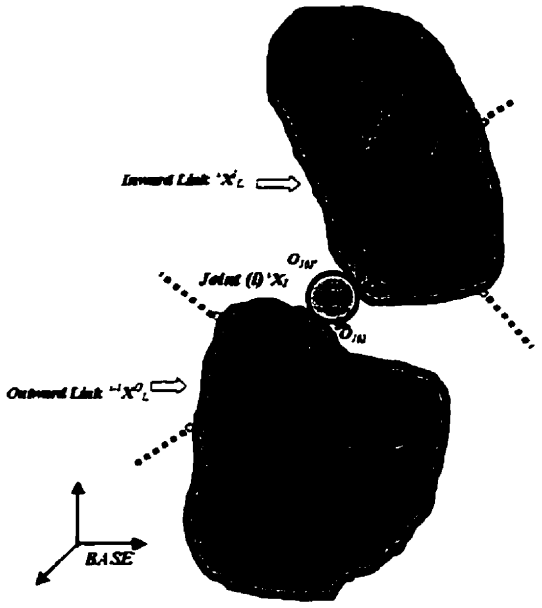

FIGURE 3.4. Connected Bodies

spatial transformation and local Jacobian matrices are given as,

$$ {}^{i-1}\mathbf{X}_L^O \left\{ \begin{array}{c} \dot{\mathbf{p}}_{i-1} \\ \boldsymbol{\omega}_{i-1} \end{array} \right\} = \left\{ \begin{array}{c} \dot{\mathbf{p}}_{J_i} \\ \boldsymbol{\omega}_{J_i} \end{array} \right\} \tag{3.15} $$

$$ {}^{i}\mathbf{X}_J \left\{ \begin{array}{c} \dot{\mathbf{p}}_{J_i} \\ \boldsymbol{\omega}_{J_i} \end{array} \right\} + {}^{i}\mathbf{J}_J \dot{\boldsymbol{\theta}}_i = \left\{ \begin{array}{c} \dot{\mathbf{p}}^I_{J_i} \\ \boldsymbol{\omega}^I_{J_i} \end{array} \right\} \tag{3.16} $$

$$ {}^{i}\mathbf{X}_L^I \left\{ \begin{array}{c} \dot{\mathbf{p}}^I_{J_i} \\ \boldsymbol{\omega}^I_{J_i} \end{array} \right\} = \left\{ \begin{array}{c} \dot{\mathbf{p}}_i \\ \boldsymbol{\omega}_i \end{array} \right\} \tag{3.17} $$

Substituting equations (3.15) and (3.16) in equation (3.17), the kinematic constraint equation between the body i and the lower body $i-1$ is derived as,

$$ {}^{i}\mathbf{X}_L^I \; {}^{i}\mathbf{X}_J \; {}^{i-1}\mathbf{X}_L^O \left\{ \begin{array}{c} \dot{\mathbf{p}}_{i-1} \\ \boldsymbol{\omega}_{i-1} \end{array} \right\} + {}^{i}\mathbf{X}_L^I \; {}^{i}\mathbf{J}_J \, \dot{\boldsymbol{\theta}}_i = \left\{ \begin{array}{c} \dot{\mathbf{p}}_i \\ \boldsymbol{\omega}_i \end{array} \right\} \tag{3.18} $$

In the tree-type topology the serial combination of the joint coordinates $\boldsymbol{\theta}_i$ is expressed as $\mathbf{y} = \left[\ldots \boldsymbol{\theta}_i^T \ldots \right]^T$. There exists a mapping between the generalized speed $\dot{\mathbf{y}}$ and the rate of change of the joint angles $\dot{\boldsymbol{\theta}}_i$ and also between the generalized twist $\left\{ \dot{\mathbf{p}}_i^T \; \boldsymbol{\omega}_i^T \right\}^T$ such that,

$$ \dot{\boldsymbol{\theta}}_i = \boldsymbol{\Upsilon}_i \, \dot{\mathbf{y}} \tag{3.19} $$

$$ \left\{ \begin{array}{c} \dot{\mathbf{p}}_i \\ \boldsymbol{\omega}_i \end{array} \right\} = \boldsymbol{\Gamma}_i \, \dot{\mathbf{y}} \tag{3.20} $$

where the connectivity matrix $\boldsymbol{\Upsilon}_i$ is composed of elements that are either 0 or 1. while the mapping matrix $\boldsymbol{\Gamma}_i$ is not that apparent to infer. Now substituting the mapping expressions stated in equations (3.19) and (3.20) into the constraint equation (3.18), the resulting relationship after simplifications is,

$$ {}^{i}\mathbf{X}_L^I \; {}^{i}\mathbf{X}_J \; {}^{i-1}\mathbf{X}_L^O \, \boldsymbol{\Gamma}_{i-1} + {}^{i}\mathbf{X}_L^I \; {}^{i}\mathbf{J}_J \, \boldsymbol{\Upsilon}_i = \boldsymbol{\Gamma}_i \qquad i > 1 \tag{3.21} $$

$$ {}^{1}\mathbf{X}_L^I \; {}^{1}\mathbf{J}_J \, \boldsymbol{\Upsilon}_1 = \boldsymbol{\Gamma}_1 \tag{3.22} $$

Equation (3.22) is the application of equation (3.21) at the base i.e. $i = 1$. Equations (3.21) and (3.22) constitute a recursive formula to compute mapping matrices $\boldsymbol{\Gamma}_i$ from the motherbody to the terminal body of the multibody system. Thus, the Natural Orthogonal Complement matrix of the kinematic constraints is obtained as.

$$\mathbf{N} = \begin{bmatrix} \boldsymbol{\Gamma}_1 \\ \vdots \\ \boldsymbol{\Gamma}_i \\ \vdots \\ \boldsymbol{\Gamma}_N \end{bmatrix} \tag{3.23}$$

The dynamical equations of a multibody system written in equation (3.13) contain non-working constraint wrenches due to the physical coupling between adjacent bodies. These constraint wrenches introduce additional variables in the dynamical equations, as a result, the dimension of the system of equations is increased. Thus the constraint equations are not desirable and hence, have to be eliminated from the dynamical equations. The Natural Orthogonal Complement matrix $\mathbf{N}$ maps the generalized speed $\dot{\mathbf{y}}$ and the generalized twist $\mathbf{v}$, such that,

$$\mathbf{v} = \mathbf{N}\dot{\mathbf{y}} \tag{3.24}$$

It has been shown that, by using the principle of virtual work and the fact that the kinematic constraint wrench is a non-working wrench, the Natural Orthogonal Complement matrix $\mathbf{N}$ is orthogonal to the kinematic constraint wrench $\boldsymbol{\phi}^K$ (**Cyril et al.**, *1991*). Thus,

$$\mathbf{N}^T \boldsymbol{\phi}^K = \mathbf{0} \tag{3.25}$$

Taking the time derivative of the generalized twist $\mathbf{v}$, given in equation (3.24),

$$\dot{\mathbf{v}} = \dot{\mathbf{N}}\dot{\mathbf{y}} + \mathbf{N}\ddot{\mathbf{y}} \tag{3.26}$$

Pre-multiplying the dynamical equation of motion (3.13) of the multibody system with $\mathbf{N}^T$, and using the relations derived in equations (3.24), (3.25), and (3.26), the

dynamical equation of motion of the multibody system is,

$$\left(\mathbf{N}^T \mathbf{M} \mathbf{N}\right) \ddot{\mathbf{y}} = -\mathbf{N}^T \mathbf{M} \dot{\mathbf{N}} \dot{\mathbf{y}} + \mathbf{N}^T \boldsymbol{\phi}^S + \mathbf{N}^T \boldsymbol{\phi}^E \tag{3.27}$$

Evaluation of $\dot{\mathbf{N}}^T$ involves extensive computations, hence the following relation is used,

$$\dot{\mathbf{N}} \dot{\mathbf{y}} = \dot{\mathbf{v}}_{\dot{\mathbf{y}}=0} \tag{3.28}$$

Using equation (3.28), equation (3.27) is rewritten in a more compact form. This is the equation of motion of the complete multibody system obtained in terms of the minimal generalized coordinates as,

$$\mathbf{I} \ddot{\mathbf{y}} = \mathbf{c}\left(\mathbf{y}, \dot{\mathbf{y}}\right) + \boldsymbol{\tau} \tag{3.29}$$

where,

$$\mathbf{I} = \mathbf{N}^T \mathbf{M} \mathbf{N}$$

$$\mathbf{c} = \mathbf{N}^T \left(-\mathbf{M} \dot{\mathbf{v}}_{\dot{\mathbf{y}}=0} + \boldsymbol{\phi}^S\right)$$

$$\boldsymbol{\tau} = \mathbf{N}^T \boldsymbol{\phi}^E$$

CHAPTER 4

Implementation

The multibody system under consideration has a base or a motherbody to which a series of bodies can be attached in any open chain configuration. The appendages are connected to each other via joints. The kinematics and dynamics of these various elements of the multibody space system have been formulated and coded into objects. As mentioned earlier, objects having common functionalities and characteristics can be grouped into a class. In this research work, the multibody simulation archetype constitutes of **Body**, **Joint**, **System**, and **Solver** classes (**Min et al.**, *2000*). This chapter discusses the aforementioned classes.

1. Body

The class **Body** is an abstraction of objects having mass as well as finite dimensions. The objects grouped in this class represent the functionality that characterizes the complete kinematics and dynamics of a rigid body. The objects *Frame*, *Base*, *Link*, *Inertia*, and *Wrench* belong to the class **Body**.

The object *Frame* characterizes the local body frame of the rigid body. It stores the kinematic states of the body and is updated recursively from the base to the terminal bodies of the system. The kinematic states of the body include the position

and orientation, the linear and angular velocities, and the linear and angular accelerations of the body. The transmission of these kinematic states from one frame to the next frame is through the objects like *Link* and *Joint*.

A multibody system has an inertial reference frame. The local body frame of each body in the multibody system has been resolved in the inertial reference frame, in order to enable the global dynamics assembly of the system. The *Base* is reckoned as a special type of the frame having a stationary kinematic state. This implies that the coordinate frame associated with the *Base* is regarded as the inertial reference frame of the system. It is possible to induce motion to the base or motherbody in the form of external velocity and acceleration. This enables the simulation of a gravity environment by providing an external linear acceleration to the *Base*. Orbital motion of the spacecraft can also be simulated by providing external angular velocity to the *Base*.

In a complex multibody system each body can be connected with one or more bodies. Hence the objects must be designed so as to accommodate any such general formulation. A body is separated into two parts and is visualized as two distinguishable objects, viz. *Inward Link* and *Outward Link*. As shown in figure 4.1, the *Outward Link* of body i is connected to *Inward Links* of bodies $i+1$ and $i+2$, which characterizes the fact that bodies *i+1* and *i+2* are both connected to body i. The objects *Inward Link* and *Outward Link* are designed to transfer kinematic states within a body. The spatial transformation matrices derived in equations (3.7) and (3.8) are computed in the objects *Outward Link* and *Inward Link*, respectively, which are used for the formulation of the Natural Orthogonal Complement matrix in the *System* object.

Inertia and *Wrench* are built for the dynamics of the system. The dynamic equation of motion for any body (motherbody or any connected appendage), in terms

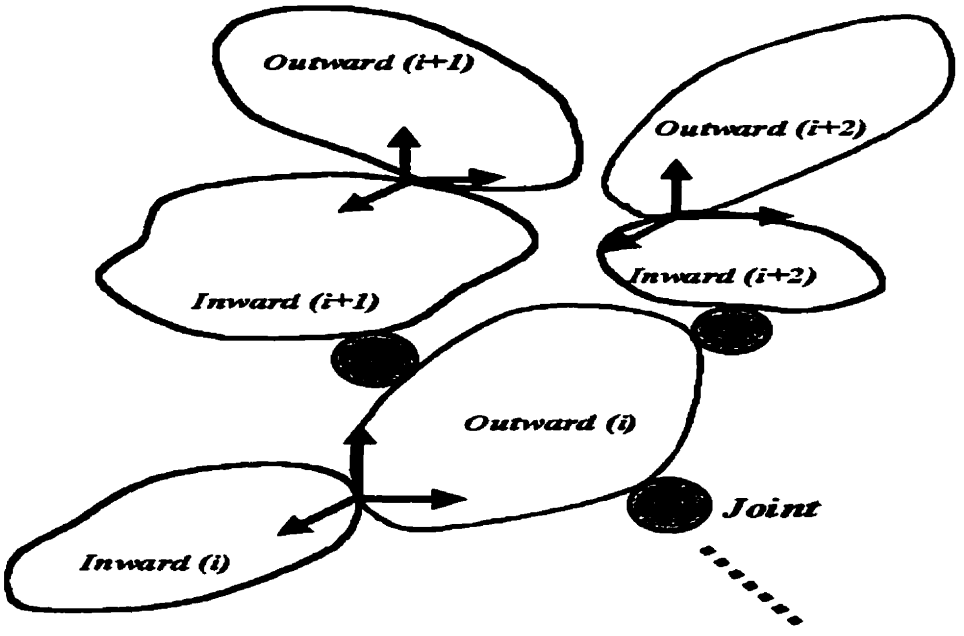

FIGURE 4.1. Abstraction of Inward and Outward Links

of the extended velocity vector $\mathbf{v}_i$, is given by (**Cyril et al.**, *1991*),

$$\mathbf{M}_i \dot{\mathbf{v}}_i = \boldsymbol{\phi}_i^S + \boldsymbol{\phi}_i^E + \boldsymbol{\phi}_i^K \tag{4.1}$$

where $\mathbf{M}_i$ is the extended mass matrix of the body, while $\boldsymbol{\phi}_i^S$, $\boldsymbol{\phi}_i^E$ and $\boldsymbol{\phi}_i^K$ are the wrenches due to the non-inertial and relative motions of the body, the external forces and moments, and the kinematic constraints imposed by the links and joints connected to the body, respectively.

The object *Inertia* computes the extended mass matrix and its time derivative of any body attached to the motherbody. The object *Inertia (Body and Wheel)* computes the motherbody's extended mass matrix and its time derivative, and also the extended mass-matrix of the reaction wheels. The motherbody's extended mass matrix and its time derivative are computed if the mass, mass moment of inertia,

and location of the center of mass of the motherbody with respect to the local body coordinate frame are supplied to the object. The extended mass matrix of the reaction wheel is also computed once its mass and mass moment of inertia are inputed to the object *Inertia (Body and Wheel)*. Figure 4.2 depicts the graphical icon created, that represents the object *Inertia (Body and Wheel)*. The connection point **Inertia** exports the extended mass matrix and its time derivative of the motherbody and the extended mass matrix of the reaction wheels into the *Wrench* object. While the connection point **M** exports the total extended mass matrix for the motherbody with the wheels into the object *System*, where it is used for the global dynamics assembly of the system. The angular velocity and the relative rotation matrix of the motherbody with reaction wheels are imported into the object via the connection point **w** and **R**, respectively, which are required for the computation of the extended mass matrix and its time derivative of the motherbody with reaction wheels. They are imported from the kinematic states of the body supplied by the object *Frame*.

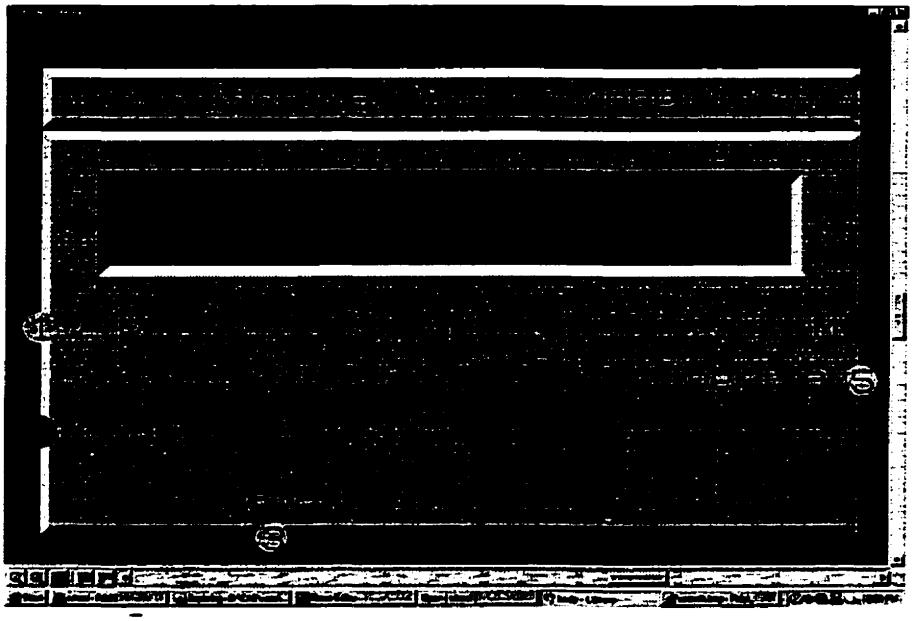

FIGURE 4.2. OBJECT: Inertia of the Mother body and wheels

The dynamic object *Wrench* computes the wrench of any body connected to the motherbody. It combines all the motion agents on the body and evaluates the right hand side of equation (4.1). During the global dynamics assembly of the system another term having dimension of wrench appears and it is accounted for in the system wrench of the individual body. This term appears due to the use of the expression $\dot{\mathbf{N}}\dot{\mathbf{y}} = \dot{\mathbf{v}}_{\ddot{\mathbf{y}}=\mathbf{0}}$, as derived in equation (3.28). Therefore, the system wrench of the body which is computed in this object is given by,

$$\boldsymbol{\phi}_i = -\mathbf{M}_i \dot{\mathbf{v}}_{i_{\ddot{\mathbf{y}}=\mathbf{0}}} + \boldsymbol{\phi}_i^S \tag{4.2}$$

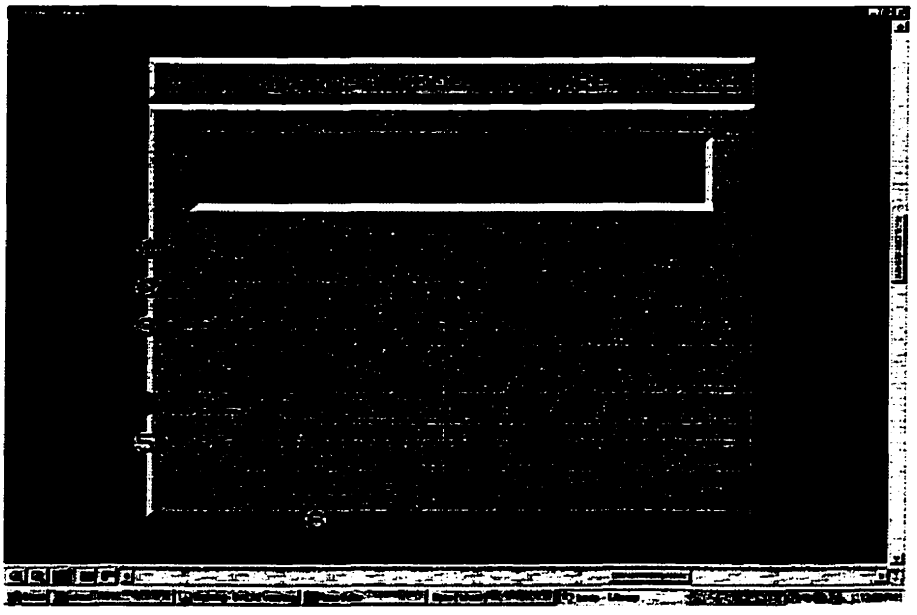

FIGURE 4.3. OBJECT: Wrench of the Mother body and wheels

Figure 4.3 depicts the graphical icon created, that represents the object *Wrench (Body and Wheel)*. As stated previously, the extended mass matrix and its time derivative of the motherbody with reaction wheels are fed into this object via the connection point **Inertia**. In this object the external wrench $\boldsymbol{\phi}_i^E$ can be inputed into the system via the connection point **ext**. The relative rotation matrix, the twist,

and the time derivative of the twist are imported into the object via the connections **R**, **vel**, and **acc**, respectively. They are imported from the kinematic states of the body supplied by the object *Frame*. The output of this object is the total wrench $(\boldsymbol{\phi}_i + \boldsymbol{\phi}_i^E + \boldsymbol{\phi}_i^K)$, which is used for the global dynamics assembly of the system and is denoted by the connection point **W**. This wrench is supplied to the object *System*. The noteworthy attributes of the object *Wrench (Body and Wheel)* are:

(i) It is feasible to place the reaction wheels in any orientation with respect to the body coordinate frame.

(ii) There is a capability to specify a constant nominal spin rate of the reaction wheel.

(iii) One can specify the angular velocity of the reaction wheel as any function of time.

(iv) It is possible to specify the angular velocity of the wheel as a function of the body quaternion i.e. the wheel velocity could be in the form of a P.I.D. control law. Thus it is possible to specify the spin rate of each wheel in the form,

$$\omega_{wheel} = \mathbf{K}_1 \hat{\mathbf{q}}_B + \mathbf{K}_2 \int \hat{\mathbf{q}}_B \, dt + \mathbf{K}_3 \dot{\hat{\mathbf{q}}}_B \tag{4.3}$$

where, $\mathbf{K}_1$, $\mathbf{K}_2$ and $\mathbf{K}_3$ are 1×4 control gain vectors. The equations of motion of the spacecraft with the reaction wheels have been formulated to accommodate such a P.I.D. control law.

The objects in the class **Body** export the spatial transformation matrix of the link as the prototypical kinematics, as well as the inertia matrix and the wrench vector as the prototypical dynamics to the *system* object (**Min et al.**, *1999*). They are used to update the elements in the *Inertia*, *Wrench*, and *Link* objects.

2. Joint

The bodies of a multibody system are connected to each other via joints. The two fundamental joints are the prismatic and revolute joints, which are developed

from the generic joint element. The joint objects have a maximum of six degrees of freedom. For each joint, it is possible to provide external actuation that could be in the form of joint forces or torques. The joint objects export the spatial transformation and local Jacobian matrices, derived in equations (3.10) and (3.11), respectively, which are used for the formulation of the Natural Orthogonal Complement matrix in the object *System*.

The translatory motion of a *Prismatic Joint* can be expressed in one of three different coordinate systems depending on the nature of the motion viz. rectangular, cylindrical, and spherical. The two sets of Euler angles viz. $1-2-3$ Euler angles and $3-1-3$ Euler angles are available to describe the rotational motion of a *Revolute Joint* (**Min et al.**, *1999*).

3. Assembly

The process of assembling and solving the dynamic equations of motion of the multibody system are done in the classes **System** and **Solver**, respectively. The class **System** contains an object *System* that assembles the individual wrenches and inertia matrices of each body and combines them to form the equations of motion of the system. The equations of motion are then multiplied by the Natural Orthogonal Complement matrix in the *System* object. The Natural Orthogonal Complement matrix is built in the object *System*, by combining the spatial transformation matrices from the *Inward Link* and *Outward Link* objects and the spatial transformation and the local Jacobian matrices from the *Joint* object, for each of the bodies. Having gathered and computed the extended mass matrices and wrenches from the bodies, as well as the said Natural Orthogonal Complement matrix, the complete dynamic equations of motion of the system are formulated. The class **Solver** contains an object *Solver* that numerically integrates non-linear differential equations of motion of the system. The integrator is of Adams-Moulton type (**Min et al.**, *1999*)

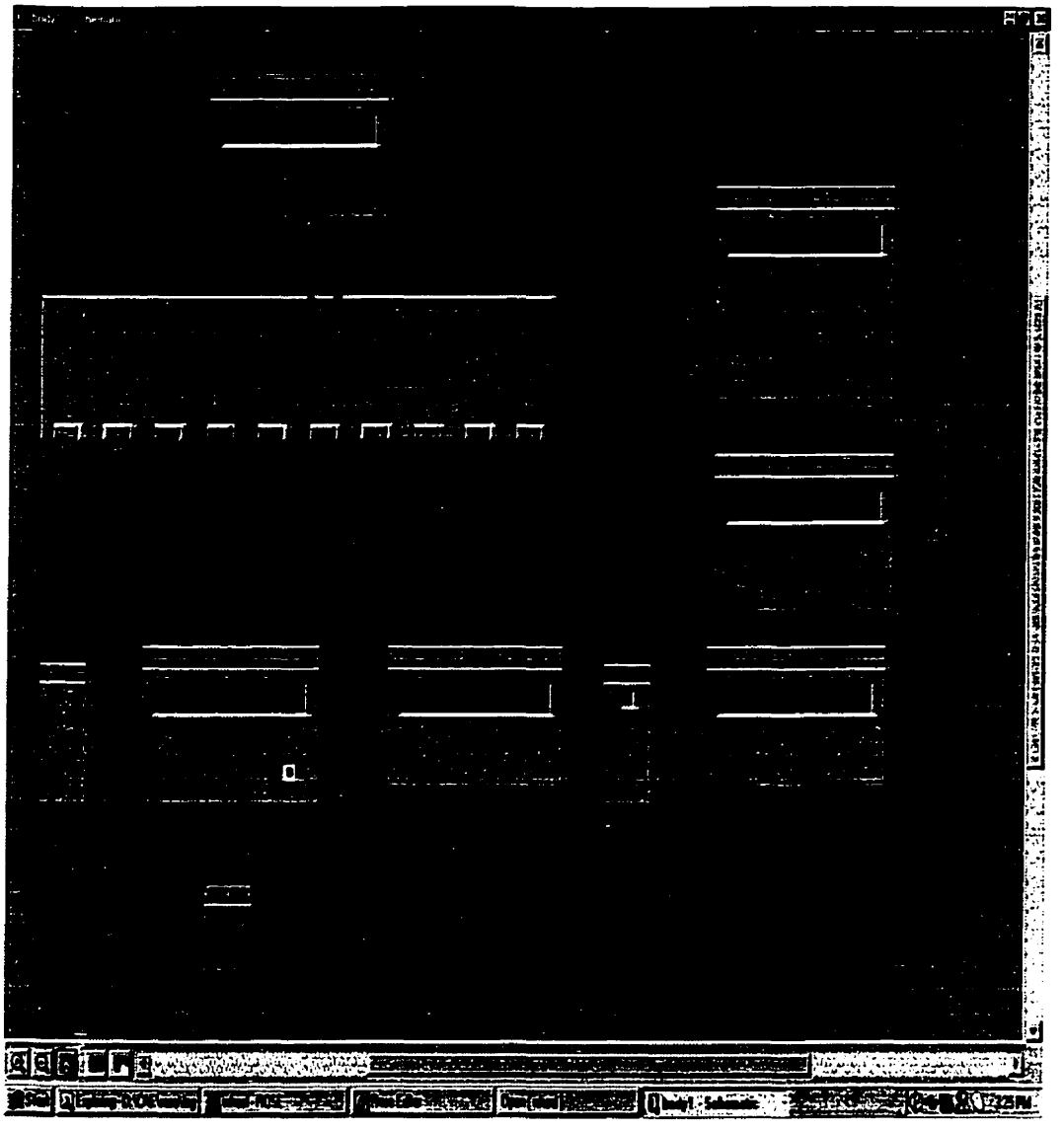

FIGURE 4.4. ROSE model for a spacecraft with three reaction wheels

Each object is implemented as a class module with a graphic icon in ROSE(Real-time Object-oriented Simulation Environment). The implementation in ROSE provides several benefits such as, automated code generation, interactive execution control, and rapid model development (**Min et al.**, *1999*). The actual modeling is achieved by the interconnection of the pre-casted object modules in an uncomplicated manner. Figure 4.4 depicts the interconnection of various objects in order to model a spacecraft mounted with three reaction wheels.

CHAPTER 5

Simulation and Results

In the previous chapters, the mathematical model for the multibody space system was developed. The dynamical equations of motion for the spacecraft with the reaction wheels was formulated, so as to incorporate them into the existing multibody software package. Using ROSE (Real-time Object Oriented Software Environment) the objects have been developed in a modular fashion and integrated with the existing objects.

This chapter is concerned with the verification and simulation conducted using the designed objects. In order to verify the accuracy of the designed objects, simulations were done using them and compared with results obtained using standard procedure. which were coded in MATLAB. So as to highlight the features and the control aspect of the designed objects, simulations for various examples have also been done.

1. Validation of Designed Objects

The first set of simulations were done to verify the validity of the designed objects. The methodology used for coding the objects was that, initially objects for rigid bodies were coded and then the procedures were written for the dynamic coupling terms between the motherbody and the reaction wheel. The simulation results that

are presented in this section deal with rigid bodies. The simulation results obtained using the designed objects are compared with those obtained by conventional method.

1.1. R R Manipulator. The first simulation was done for a R R manipulator, as shown in figure 5.1. The physical data parameters for the R R manipulator are given in table 1.1. The R R manipulator was subjected to similar initial conditions in both ROSE and MATLAB. For the results obtained from MATLAB and ROSE, the variation of the joint angles, viz. α and β, with time are plotted in figure 5.2 and the variations of the time derivative of the joint angles viz. $\dot{\alpha}$ and $\dot{\beta}$, with time are plotted in figure 5.3. The results obtained in the two cases are equivalent.

No.	Link Length (m)	Mass $(kg.)$	Moment of Inertia $(kg.m^2)$
1	2.0	10.0	3.33
2	4.0	10.0	13.33

TABLE 5.1. Data for the R R manipulator

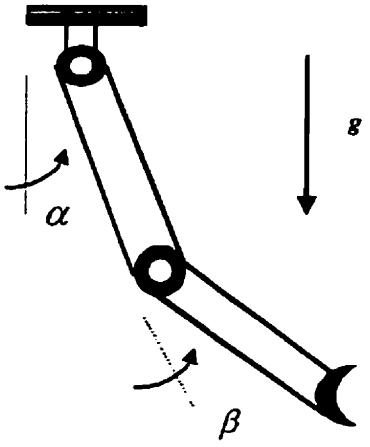

FIGURE 5.1. R R Manipulatior

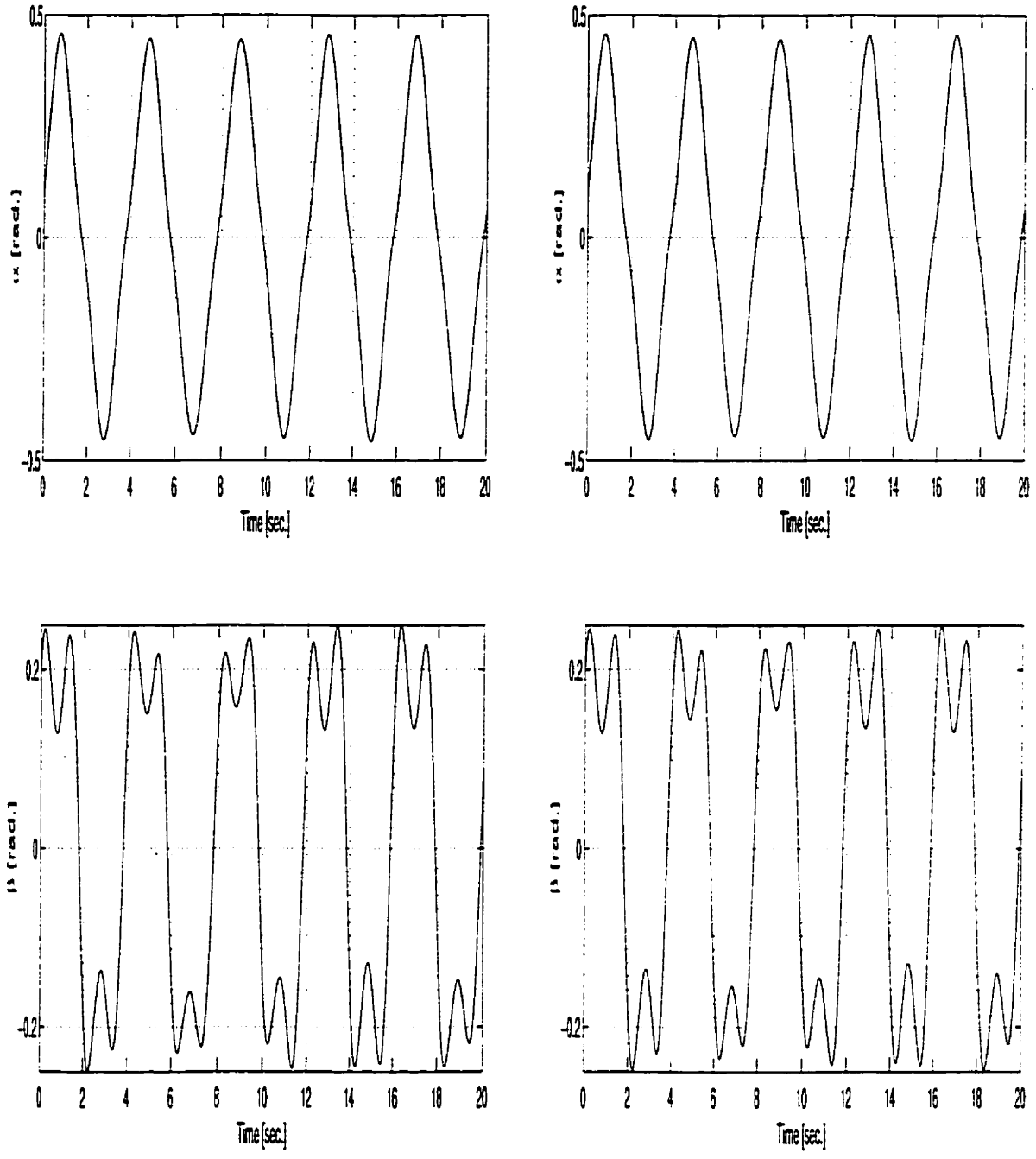

(a) (b)

FIGURE 5.2.- Variation of α and β with time using (a) MATLAB (b) ROSE

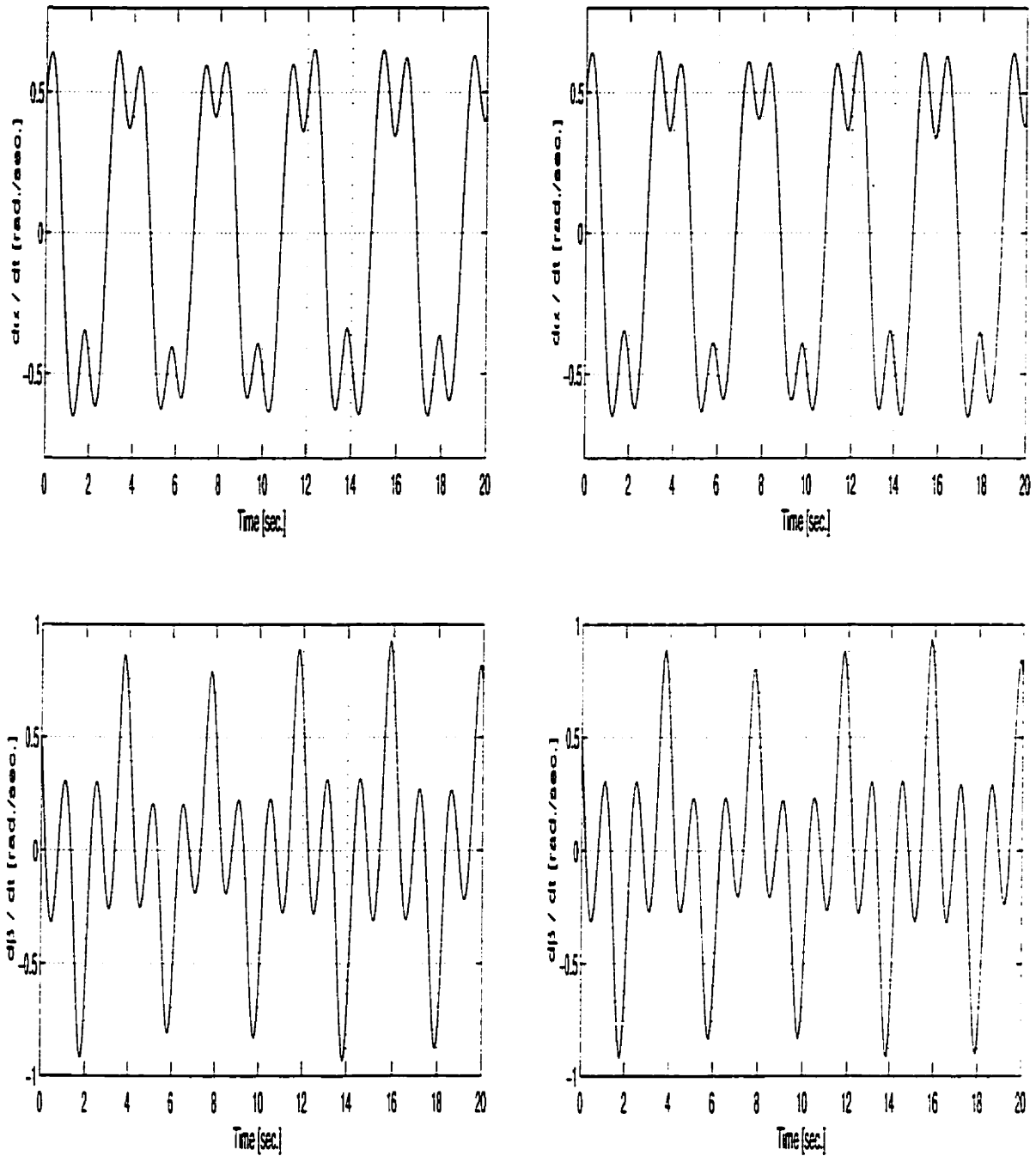

(a) (b)

FIGURE 5.3.- Variation of $\dot{\alpha}$ and $\dot{\beta}$ with time using (a) MATLAB (b) ROSE

1.2. Body With Two Arms : Planar Motion. The next simulations were done for a body with two appendages undergoing planar motion, as shown in figure 5.4. The simulation data parameters for the body and the two arms are given in table 5.2. For the results obtained from MATLAB and ROSE, the variation of the joint angles viz. α, β, and γ, with time are shown in figure 5.5 and the variation of the time derivative of the joint angles viz. $\dot{\alpha}$, $\dot{\beta}$, and $\dot{\gamma}$, with time are shown in figure 5.6. The variations in amplitude of the responses got from MATLAB and ROSE are correlating.

Body	**Mass**$(kg.)$	**Moment of Inertia** $(kg.m.^2)$
Motherbody	500.0	1041.7
Link 1	25.0	208.3
Link 2	25.0	208.3

TABLE 5.2. Data for a body with two appendages undergoing planar motion

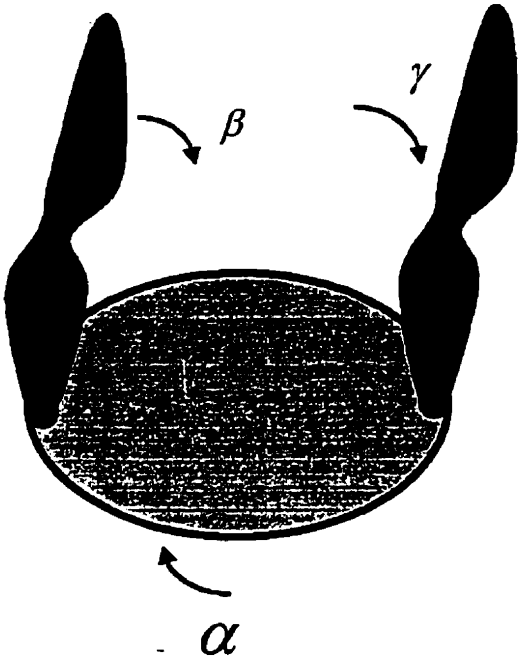

FIGURE 5.4. Body with two arms undergoing planar motion

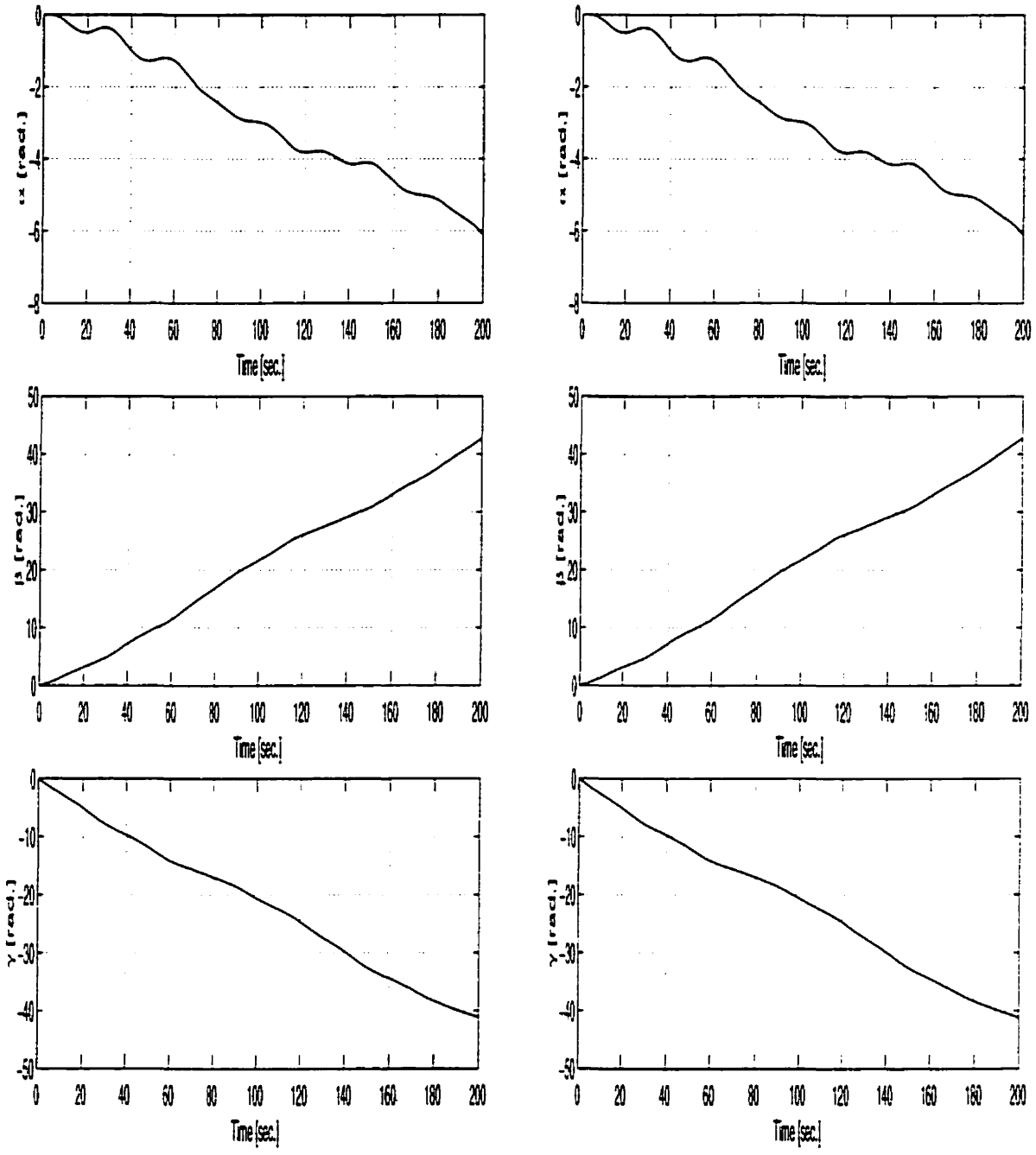

FIGURE 5.5. Variation of α, β and γ with time using (a) MATLAB (b) ROSE

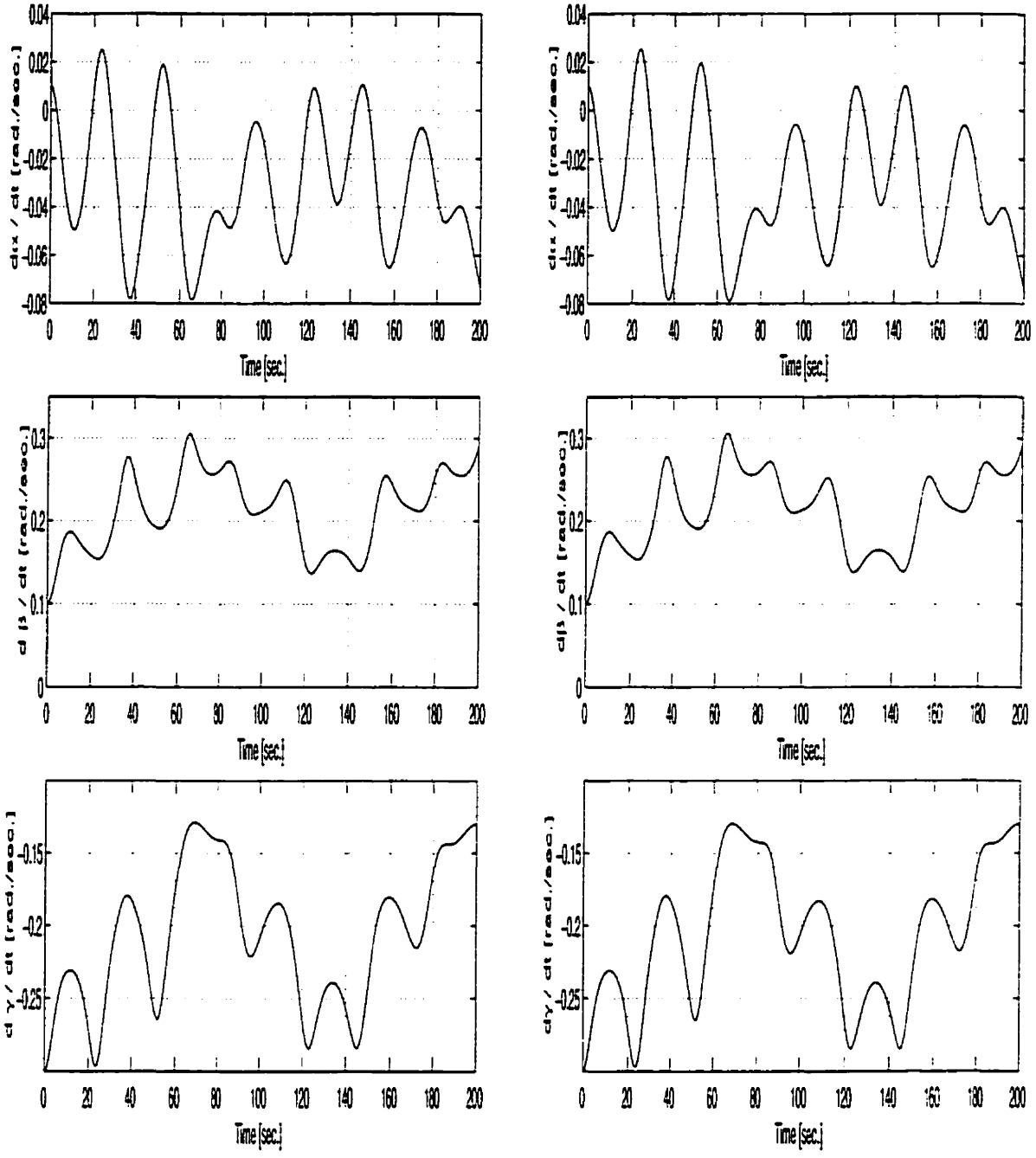

(a) (b)

FIGURE 5.6. Variation of $\dot{\alpha}$, $\dot{\beta}$ and $\dot{\gamma}$ with time using (a) MATLAB (b) ROSE

1.3. Satellite Spinning about Major axis : 3 D Motion. The third set of simulations involved a satellite spinning about its major axis, while there were small perturbations about the other two axes, as shown in figure 5.7. The physical data of the satellite are given in table 5.3. Using MATLAB and ROSE, the variations in attitude and attitude rates with time, are shown in figures 5.8 and 5.9, respectively. There is a maximum deviation of 0.06% in amplitude from the responses obtained from ROSE, as compared to those obtained via MATLAB. This may be due to fact that a constant step size of 1×10^{-4} was used in ROSE, as compared to the more accurate adaptive step size used by MATLAB.

Mass$(kg.)$	$\mathbf{I}_{xx}(kg.m.^2)$	$\mathbf{I}_{yy}$ $(kg.m.^2)$	$\mathbf{I}_{zz}$ $(kg.m.^2)$
200.0	379.2	379.2	625

TABLE 5.3. Data for a spinning satellite

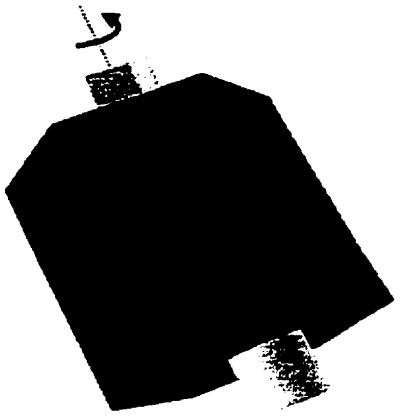

FIGURE 5.7. Satellite spinning about major axis

In all the three cases i.e. the R R manipulator (figure 5.1), a body with two arms undergoing planar motion (figure 5.4), and the spinning satellite (figure 5.7), the responses got from MATLAB and ROSE are consistent.

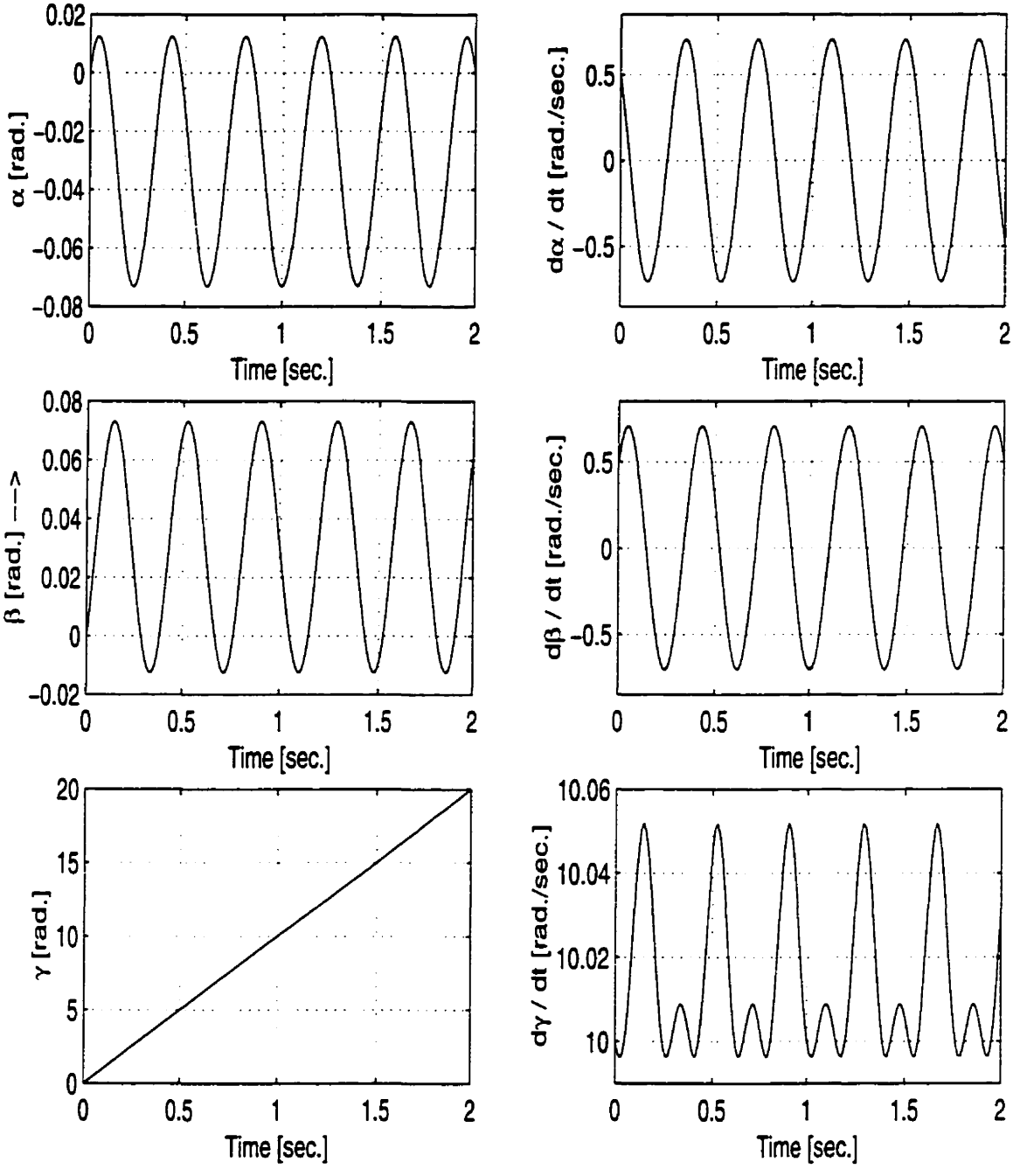

FIGURE 5.8. Variation of attitude and attitude rates of a spinning satellite using MATLAB

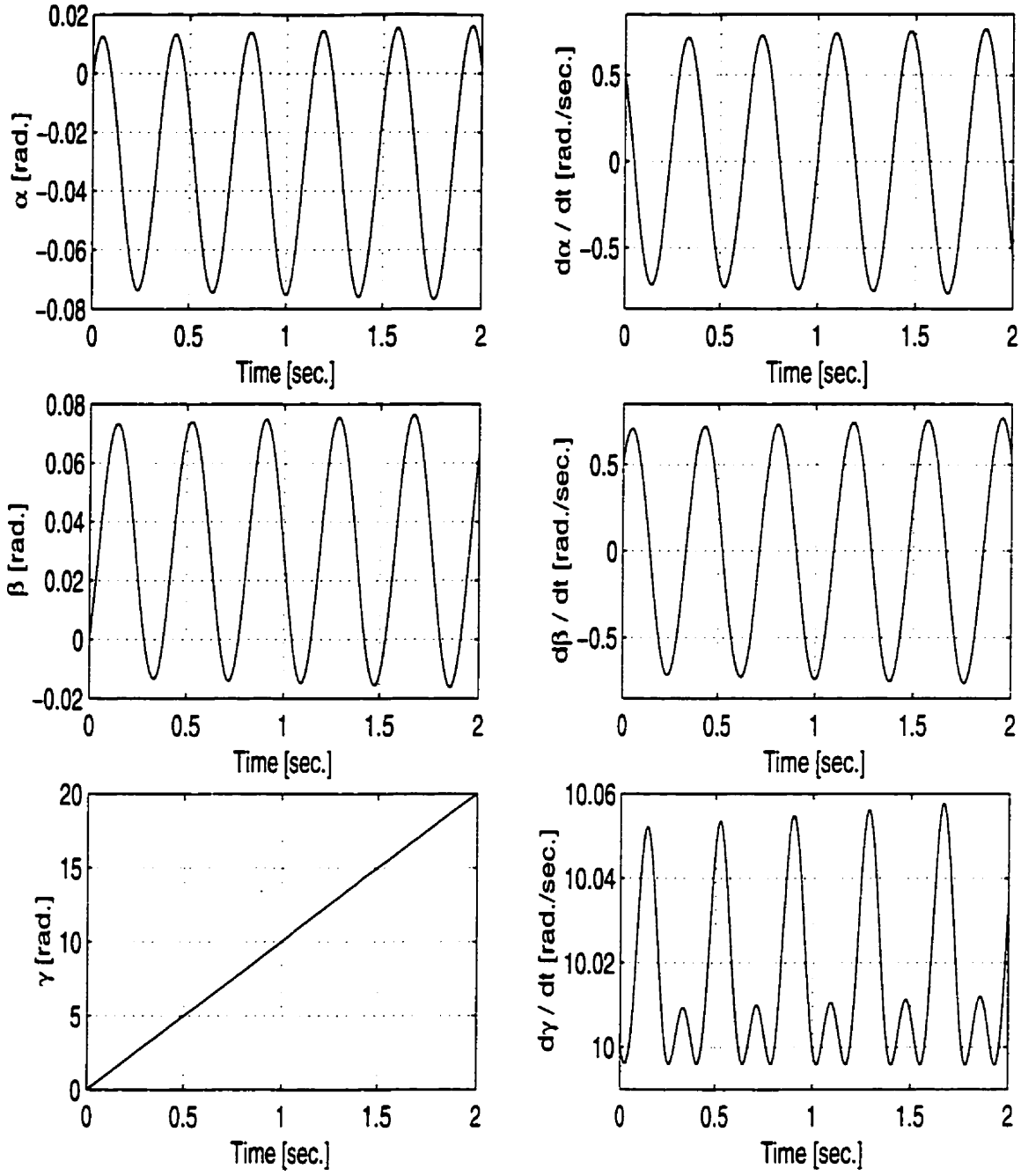

FIGURE 5.9. Variation of attitude and attitude rates of a spinning satellite using ROSE

2. Validation of the Objects using Slew Maneuver : Cassini Spacecraft

The Cassini spacecraft was launched on October 15, 1997 and after an interplanetary cruise of more than seven years, it will arrive at Saturn in February, 2005. Slew maneuvers were done on the Cassini spacecraft, using reaction wheels, on the seventy-fifth day of the year 2000 i.e. March 15, 2000. The maneuvers consisted of slews about the Y-axis, followed by a slew about the X-axis, another slew about the Y-axis, a slew about the Z-axis, and finally a very small slew about the Y-axis. The duration of these slew maneuvers was for a total period of approximately 7000 seconds. Telemetry data were available for the entire duration of the slews, at a frequency of once every four seconds (**Wertz et al.**, *2001*). The slew velocities of the Cassini spacecraft obtained via telemetry are plotted in figure 5.10. The actual time history of the spin rates of the reaction wheels during the slew maneuver are shown in figures 5.11, 5.12, and 5.13. The intention of conducting these slew maneuvers was the inflight estimation of the inertia tensor of the Cassini spacecraft using the spin rates of the reaction wheels.

In order to corroborate the accuracy of the designed objects, the reaction wheels were given time histories, similar to the variation in spin rates of the reaction wheels located in the Cassini spacecraft. The aim of this validation test was to replicate the first slew maneuver about the Y-axis. The time histories that were given as inputs to the reaction wheels for a period of 1400 seconds are shown in figure 5.14. This test was done for a period of 1400 seconds instead of the total period of 7000 seconds, due to the fact that the time involved in simulating 7000 seconds in ROSE would be extremely lengthy and might also result in data storage issues on the computer. As shown in figure 5.15, the spacecraft undergoes an approximate slew of -2.7×10^{-3} *rad./sec.* about the Y-axis, which is the desired result. The angular velocity of the spacecraft about the Y-axis (ω_y) follows the correct trend of rising to an approximately

constant slew rate about the Y-axis and then going back to zero at the end of the slew maneuver. During the slew maneuver ω_x and ω_z are zero. There are small differences between the actual slew velocity of the Cassini spacecraft and the generated simulation result due to the approximations made while prescribing the time histories to the reaction wheels.

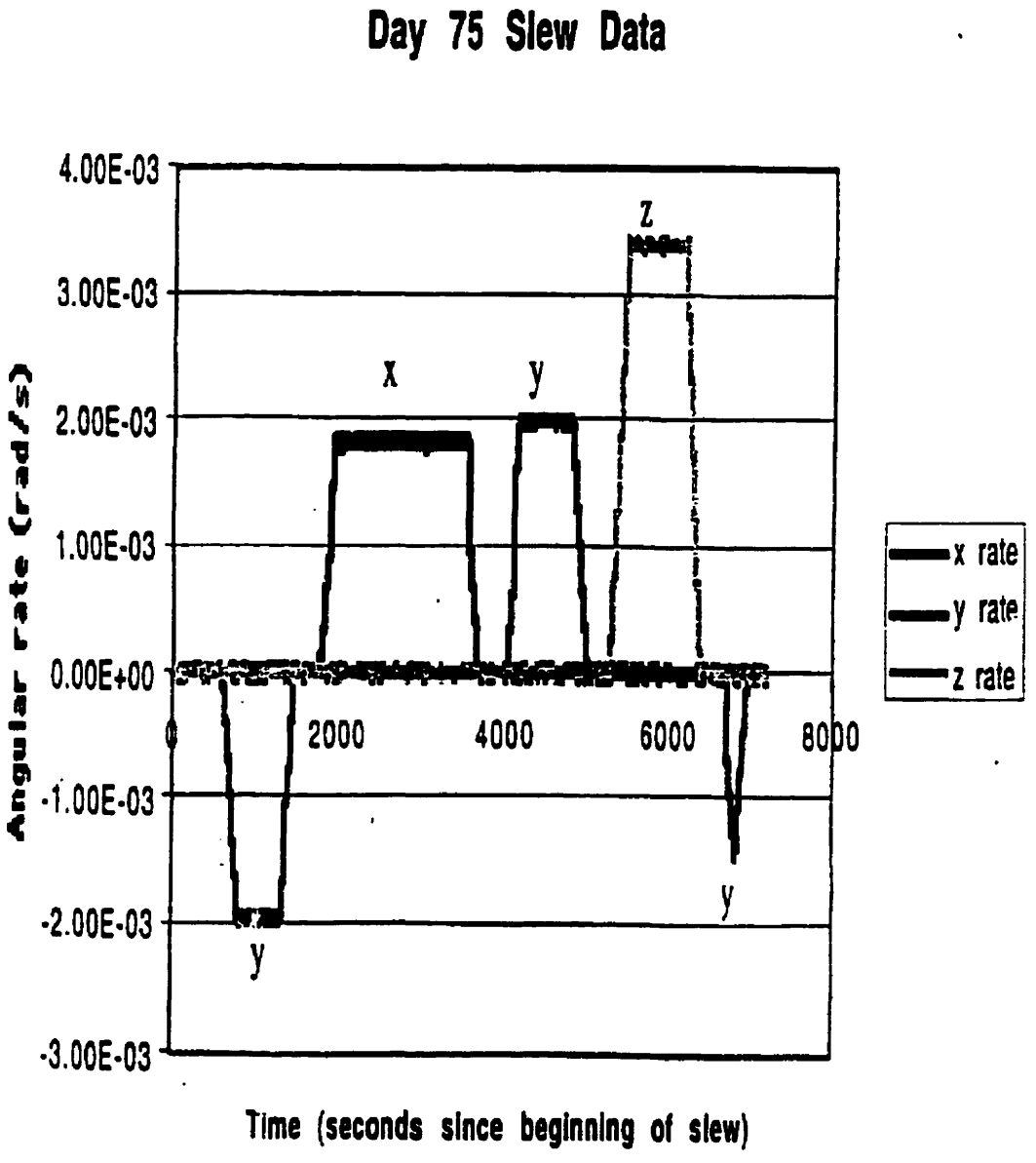

FIGURE 5.10. Slew velocity of the Cassini spacecraft via telemetry data

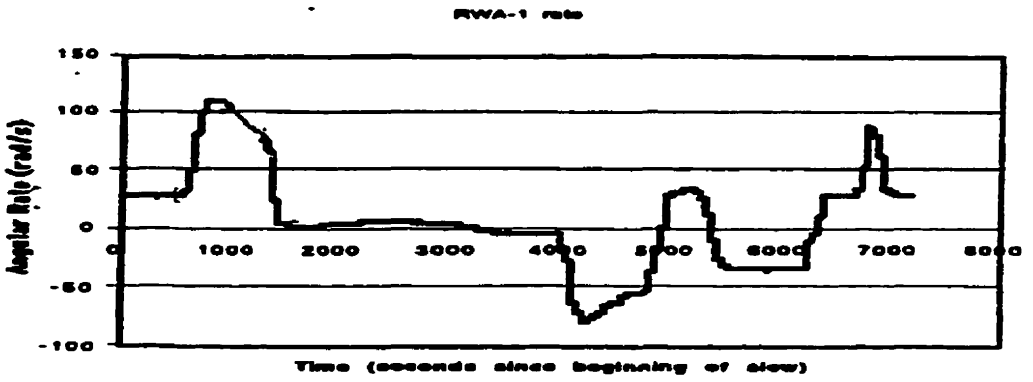

FIGURE 5.11. Variation in spin rate of the reaction wheel 1 with time

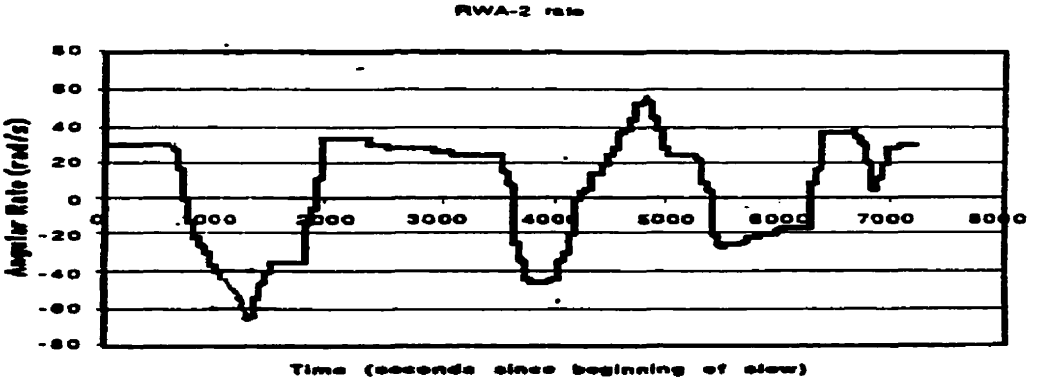

FIGURE 5.12. Variation in spin rate of the reaction wheel 2 with time

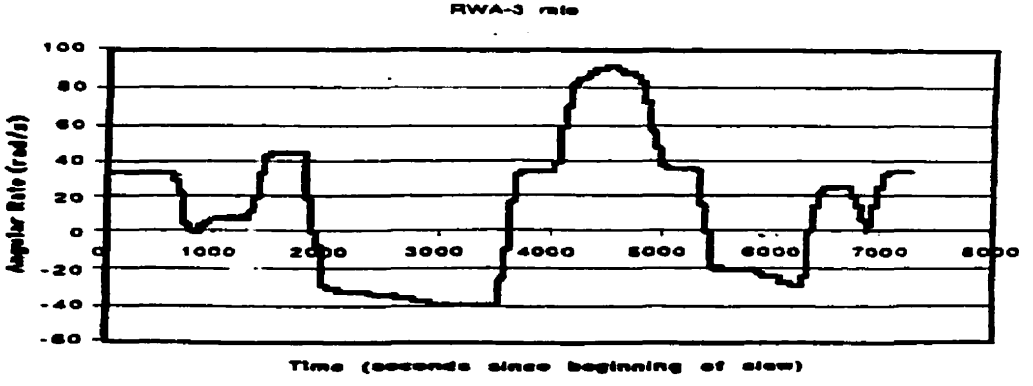

FIGURE 5.13. Variation of spin rate of the reaction wheel 3 with time

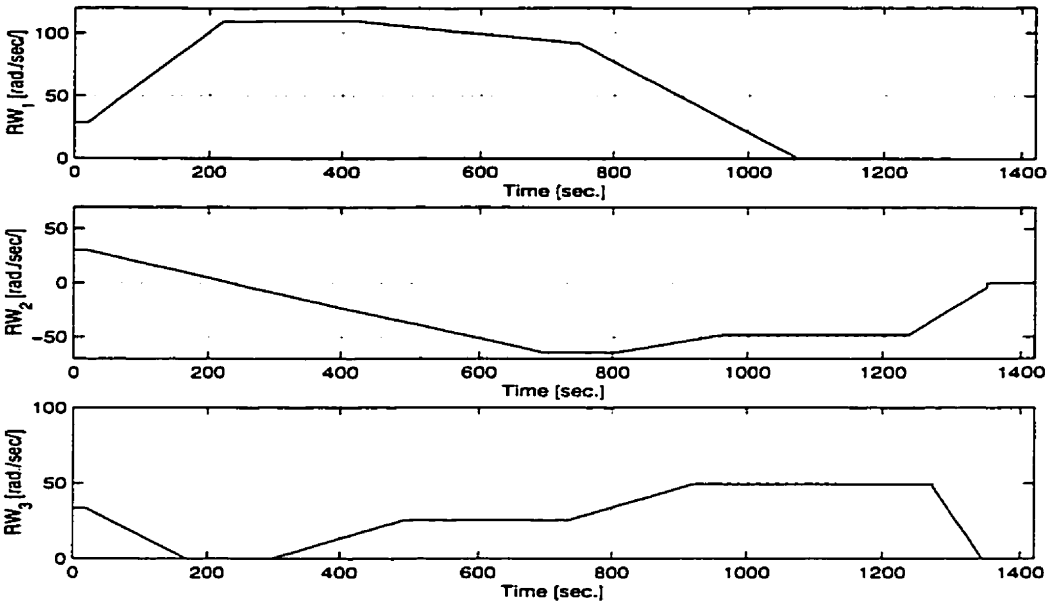

FIGURE 5.14. Time histories of the reaction wheels during the slew maneuver

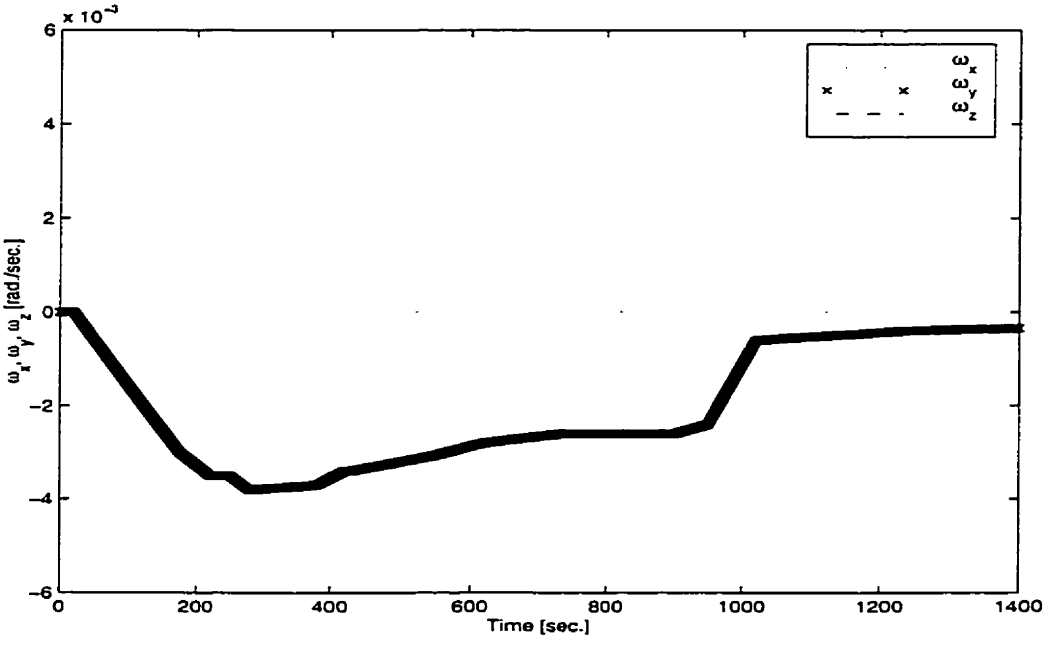

FIGURE 5.15. Slew velocity of the Cassini spacecraft

3. Slew Maneuvers and Reorientation : Cassini Spacecraft

As mentioned in the previous section, the Cassini spacecraft is an interplanetary probe on its way to Saturn. This section presents simulation results obtained by conducting slew and reorientation maneuvers on the model of the Cassini spacecraft.

When a spacecraft is slewed about an axis using reaction wheels, the spin rates of the wheels vary. Since the magnitude of the external torques exerted on the spacecraft about all the axes is negligible, the total angular momentum vector of the spacecraft is conserved throughout the slew maneuver. This total angular momentum vector has two components, one from the spacecraft angular velocity and one from the angular velocity of the reaction wheels. The conservation of the angular momentum allows the total angular momentum evaluated at the initial time (prior to the beginning of the slew) to be set equal to the total angular momentum evaluated throughout the slew. This equality enables the derivation of an equation for each time step throughout the slew, with the only unknown being the angular velocity vector of the reaction wheels. Angular momentum at the beginning of the slew maneuver expressed in the inertial coordinate frame is given by,

$$\mathbf{h}(0) = \mathbf{R}(0)\left[\mathbf{I}_{SC}\,\boldsymbol{\omega}_{SC}(0) + \sum_{i=1}^{3} \mathbf{R}_{w_i}\,\mathbf{I}_{w_i}\left\{\mathbf{R}_{w_i}^{T}\,\boldsymbol{\omega}_{SC}(0) + \boldsymbol{\omega}_{w_i}(0)\right\}\right] \tag{5.1}$$

where,

- $\mathbf{R}(0)$ is the rotation matrix that represents the orientation of the body coordinate frame with respect to the inertial coordinate frame, just prior to the begining of the slew maneuver.
- $\mathbf{I}_{SC}$ is the inertia tensor of the Cassini spacecraft.

$$\mathbf{I}_{SC} = \begin{bmatrix} 8810.8 & -136.8 & 115.3 \\ -136.8 & 8157.3 & 156.4 \\ 115.3 & 156.4 & 4721.8 \end{bmatrix} kg.m.^2 \tag{5.2}$$

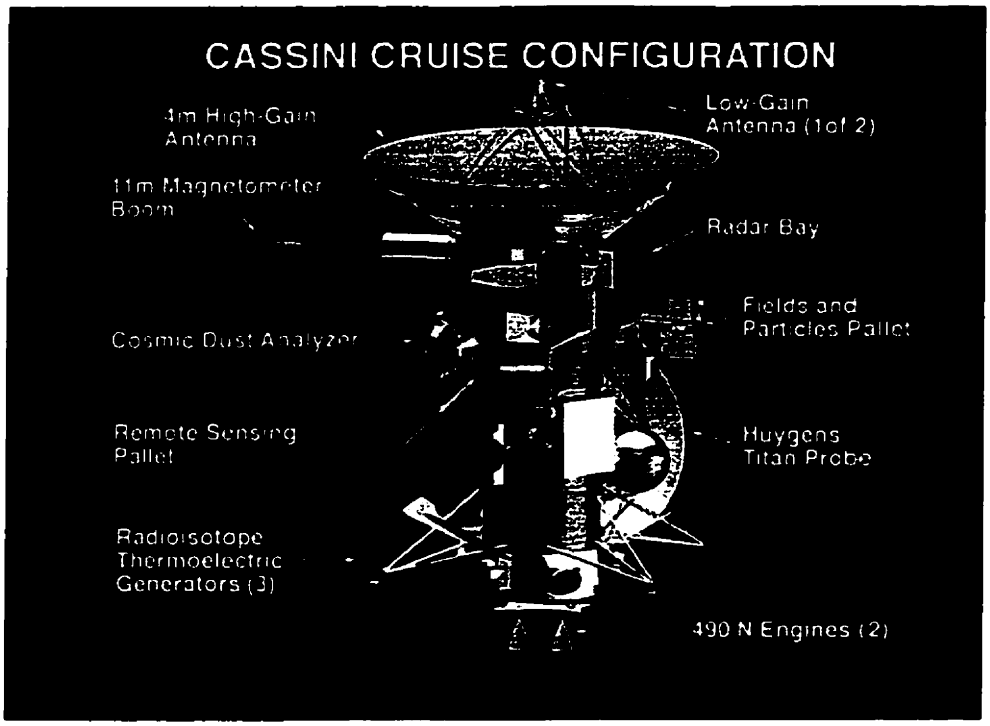

FIGURE 5.16. The Cassini spacecraft (courtesy:*Jet Propulsion Laboratory Photo gallery*)

- $\omega_{SC}(0)$ is the angular velocity of the spacecraft just prior to the begining of the slew maneuver.
- $\mathbf{R}_{w_i}$, $i = 1, 2, 3$ are the matrices defining the orientation of the reaction wheels with respect to the body coordinate frame. The elements of the matrices $\mathbf{R}_{w_i}$, $i = 1, 2, 3$ are all zero, except a column vector which represents the directional cosines relating the frame of the reaction wheel to the body frame of the spacecraft. The orientation of the three reaction wheels relative to the body coordinate frame is determined by the transformation matrix $\mathbf{T}$, such that,

$$\mathbf{T} = \sum_{i=1}^{3} \mathbf{R}_{w_i} \tag{5.3}$$

where $\mathbf{T}$ for the Cassini spacecraft is given as,

$$\mathbf{T} = \begin{bmatrix} 0 & -\frac{1}{\sqrt{2}} & \frac{1}{\sqrt{2}} \\ \sqrt{\frac{2}{3}} & -\frac{1}{\sqrt{6}} & -\frac{1}{\sqrt{6}} \\ \frac{1}{\sqrt{3}} & \frac{1}{\sqrt{3}} & \frac{1}{\sqrt{3}} \end{bmatrix} \tag{5.4}$$

- $\mathbf{I}_{w_i}$, $i = 1, 2, 3$ are the inertia matrices of the each of the reaction wheels expressed in the wheel frame. And,

$$\begin{aligned} \mathbf{I}_w &= \sum_{i=1}^{3} \mathbf{I}_{w_i} \\ &= \begin{bmatrix} I_{w_1} & 0 & 0 \\ 0 & I_{w_2} & 0 \\ 0 & 0 & I_{w_3} \end{bmatrix} \end{aligned} \tag{5.5}$$

  In the above expression, I_{w_1}, I_{w_2}, and I_{w_3} are the moments of inertia about the axis of rotation for the reaction wheels 1, 2, and 3, respectively.

- $\boldsymbol{\omega}_{w_i}(0)$ $i = 1, 2, 3$ are the angular velocities of each of the reaction wheels relative to the spacecraft, just prior to the starting of the slew maneuver. Also,

$$\boldsymbol{\omega}_w = \begin{Bmatrix} \boldsymbol{\omega}_{w_1} \\ \boldsymbol{\omega}_{w_2} \\ \boldsymbol{\omega}_{w_3} \end{Bmatrix} \tag{5.6}$$

and,

$$\mathbf{I}_T = \mathbf{I}_{SC} + \sum_{i=1}^{3} \mathbf{R}_{w_i} \mathbf{I}_{w_i} \mathbf{R}_{w_i}^T \tag{5.7}$$

Using the expressions in equations (5.3), (5.5), (5.6), and (5.7) and applying them to equation (5.1),

$$\dot{\bar{\mathbf{h}}}(0) = \mathbf{R}(0) \left[\bar{\mathbf{I}}_T \boldsymbol{\omega}_{SC}(0) + \mathbf{T} \mathbf{I}_w \boldsymbol{\omega}_w(0) \right] \tag{5.8}$$

Similar to equation (5.8), the angular momentum during the slew maneuver is deduced as,

$$\mathbf{h}(t) = \mathbf{R}(t)\left[\mathbf{I}_T \boldsymbol{\omega}_{SC}(t) + \mathbf{T}\,\mathbf{I}_w \boldsymbol{\omega}_w(t)\right] \tag{5.9}$$

As stated earlier the angular momentum in the inertial frame is constant when there are no external torques acting on the spacecraft. Thus,

$$\mathbf{h}(0) = \mathbf{h}(t) \tag{5.10}$$

Using equations (5.8), (5.9), (5.10), and solving for $\boldsymbol{\omega}_w(t)$,

$$\mathbf{T}\,\mathbf{I}_w \boldsymbol{\omega}_w(t) = \mathbf{R}^T(t)\,\mathbf{R}(0)\left[\mathbf{I}_T \boldsymbol{\omega}_{SC}(0) + \mathbf{T}\,\mathbf{I}_w \boldsymbol{\omega}_w(0)\right] - \mathbf{I}_T \boldsymbol{\omega}_{SC}(t) \tag{5.11}$$

Just prior to the beginning of the slew at time $t = 0$, the angular velocity of the spacecraft $\boldsymbol{\omega}_{SC}(0)$ is approximately zero and $\mathbf{R}(0)$ is an identity matrix. Moreover $\boldsymbol{\omega}_{SC}(t)$ is the desired slew velocity, which is predefined and so the only unknown in equation (5.11) are the velocities of the reaction wheels $\boldsymbol{\omega}_w(t)$. Hence,

$$\boldsymbol{\omega}_w(t) = (\mathbf{T}\,\mathbf{I}_w)^{-1}\left[\mathbf{R}^T(t)\,\mathbf{T}\,\mathbf{I}_w \boldsymbol{\omega}_w(0) - \mathbf{I}_T \boldsymbol{\omega}_{SC}(t)\right] \tag{5.12}$$

Equation (5.12) is applied recursively in order to obtain the angular velocities of the wheels during the entire slew maneuver.

The first simulation involved a reorientation maneuver done on the spacecraft. The spacecraft was reoriented from $\theta_1 = \theta_2 = \theta_3 = 0$ initially to the final orientation of $\theta_1 = \theta_2 = 0$ and $\theta_3 = \frac{\pi}{2}$, as shown in figure 5.17. The prescribed angular velocity of the spacecraft is shown in figure 5.18 and the corresponding spin rates of the reaction wheels are shown in figure 5.19.

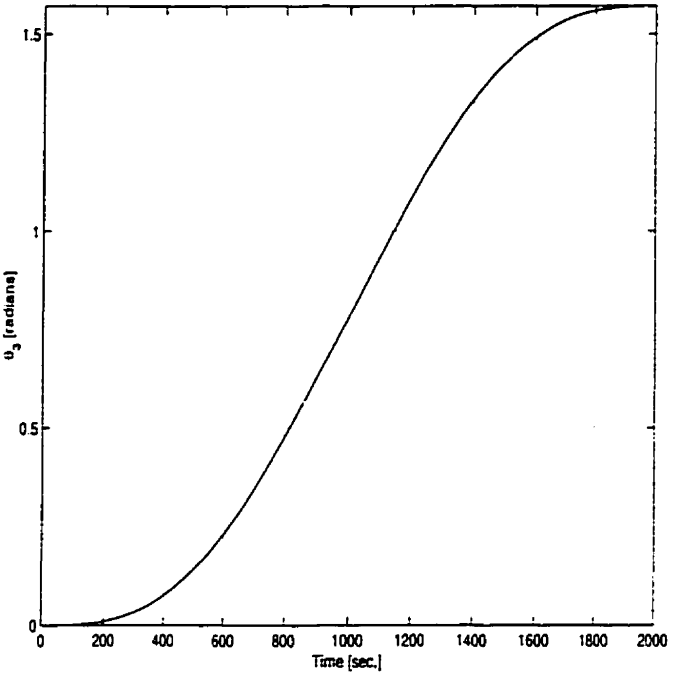

FIGURE 5.17. Change in orientation of the Cassini spacecraft due to the maneuver

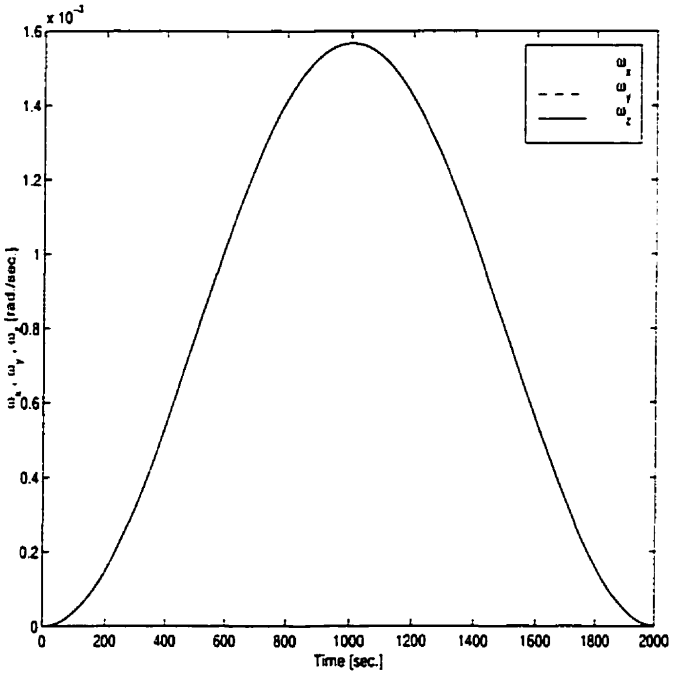

FIGURE 5.18. Angular velocity of the during the re-orientation maneuver

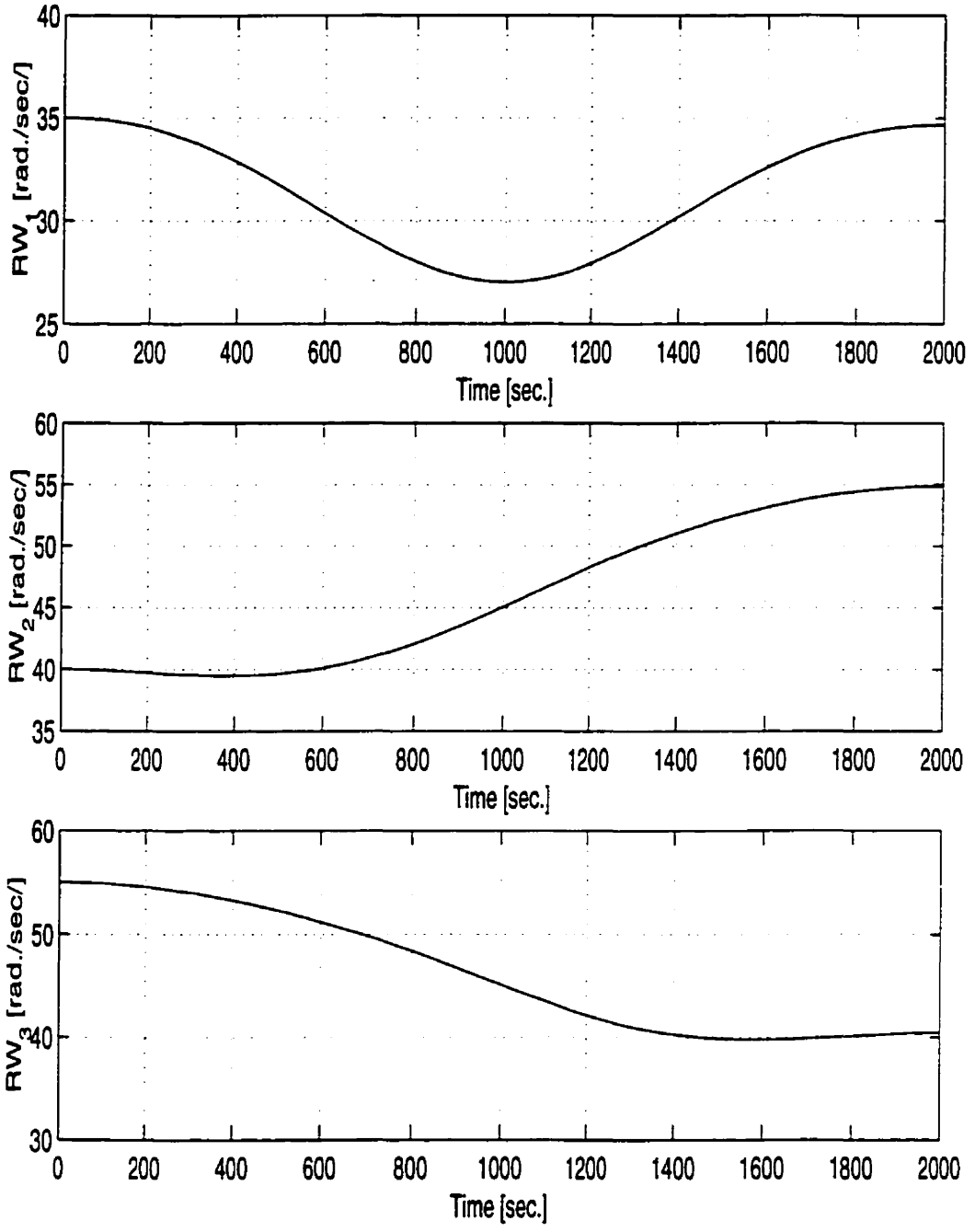

FIGURE 5.19. Angular velocity of the reaction wheels mounted on the Cassini spacecraft during reorientation maneuver

The next simulation on the model of the Cassini spacecraft involved sequential slewing. In this simulation, the angular velocity (slew velocity) of the spacecraft was prescribed, as shown in table 5.4. The slew velocities of the Cassini spacecraft are plotted in figure 5.20. In order to maintain the prescribed slew velocity of the spacecraft, the reaction wheels have to change their spin rate. This change in the spin rates of the reaction wheels has been plotted in figure 5.21. The variation in the spin rates of the reaction wheels is governed by the equation 5.12, which was derived earlier.

No.	**Slew Axis**	**Slew Velocity** (*rad./sec.*)
1.	Y-Axis	0.04
2.	Z-Axis	-0.08
3.	X-Axis	0.07
4.	Z-Axis	-0.03

TABLE 5.4. Slew velocities of the Cassini spacecraft

The reorientation and slew maneuver simulations were conducted to highlight the versatility of the designed objects, wherein the angular velocity of the motherbody could be specified and the reaction wheels would maintain that angular velocity/slew velocity of the motherbody.

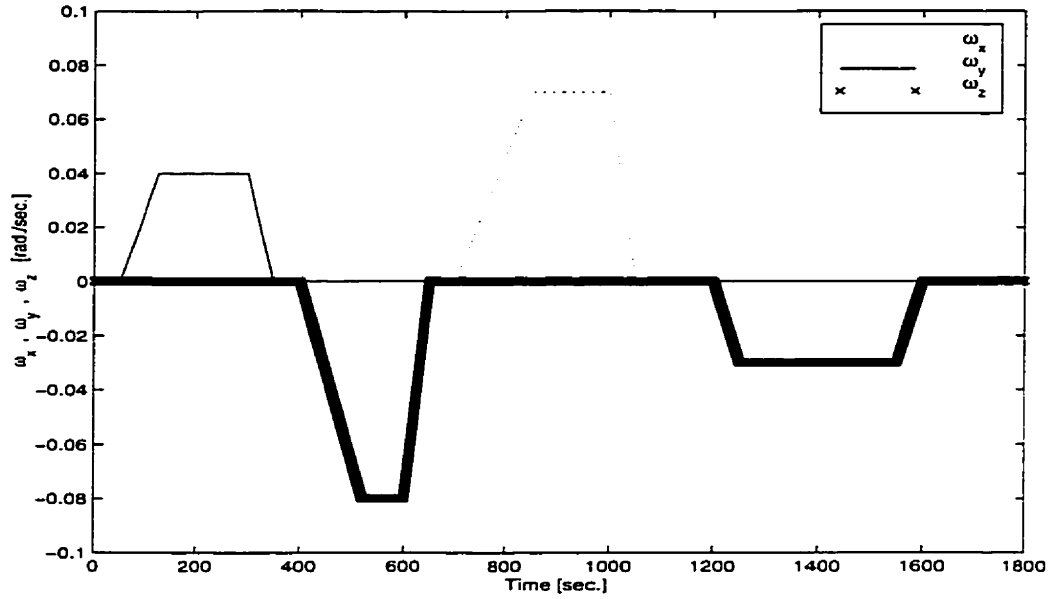

FIGURE 5.20. Slew Velocity of the Cassini spacecraft

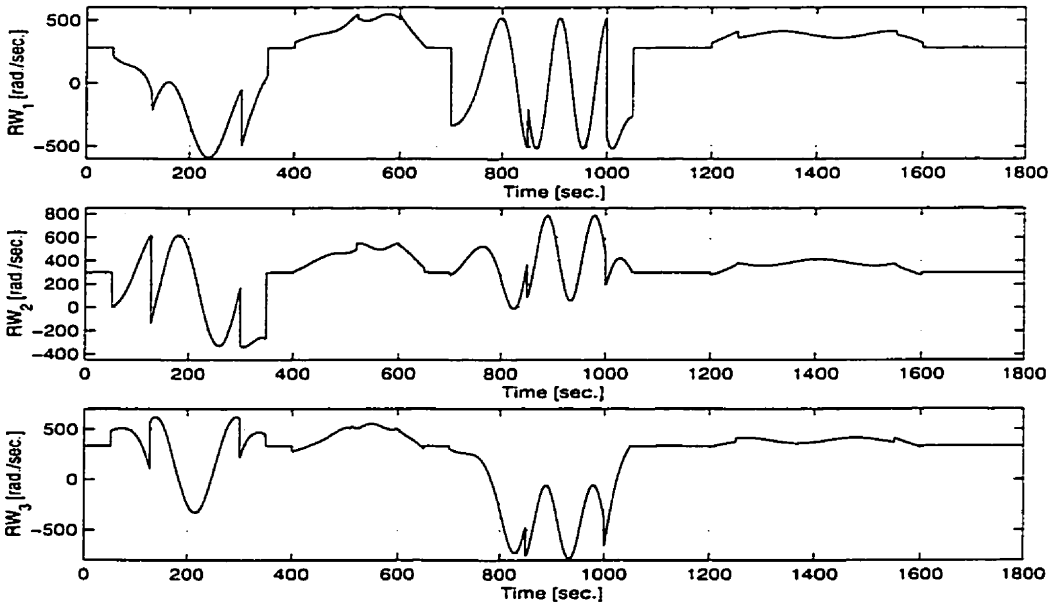

FIGURE 5.21. Time histories of the Reaction Wheels mounted on the Cassini spacecraft during slew maneuvers.

4. Multibody Space Systems

The main goal of the simulations presented in this section was to demonstrate the functionality of the designed objects. The designed objects have been connected to simulate the dynamical response of typical multibody space systems, with one reaction wheel spinning at a high constant spin rate. These multibody space systems include two or more manipulator arms. Initially the uncontrolled motion of the motherbody with the appendages was simulated and then a reaction wheel rotating at a high nominal angular velocity, about the body-fixed axis of the motherbody, was used to restrict the attitude drift of the motherbody.

4.1. Satellite with 2 Arms : Reaction Wheel about Z-Axis. Figure 5.22 depicts a motherbody mounted with two manipulator arms. One of the manipulator joints was supplied with a torque as shown in figure 5.23, about the X-axis, and given by the relation $\tau_{ARM_{1_x}} = \left\{0.002\,t - 0.016\,\sin\left(\frac{2\pi t}{45}\right)\right\}$. The other joint was supplied with a torque as shown in figure 5.24, about the Y-axis, and given by $\tau_{ARM_{2_y}} = \left\{0.01\,t - 0.08\,\sin\left(\frac{2\pi t}{45}\right)\right\}$. The physical data for the multibody system are given in table 5.5. The reaction wheel was mounted along the body-fixed Z-axis of the spacecraft and was spinning at 400 *rad./sec.*. The mass and size of the wheel are negligible compared to those of the spacecraft.

Body	**Mass**$(kg.)$	$\mathbf{I}_{xx}(kg.m.^2)$	$\mathbf{I}_{yy}(kg.m.^2)$	$\mathbf{I}_{zz}(kg.m.^2)$
Satellite	200.0	12.5	12.5	50.0
Arm 1	10	0.4	0.4	0.8
Arm 2	10	0.4	0.4	0.8

TABLE 5.5. Data for motherbody mounted with two manipulators

The attitude and attitude rates of the motherbody with and without the reaction wheel are depicted in figures 5.25 and 5.26, respectively. It is seen that the attitude drift of the motherbody is completely arrested due to the spinning reaction wheel. As seen from figure 5.25(a), without spin stabilization, α begins to grow at 17.9 seconds and reaches a maximum of -6.14 radians and the disturbances in β begins at 17.9

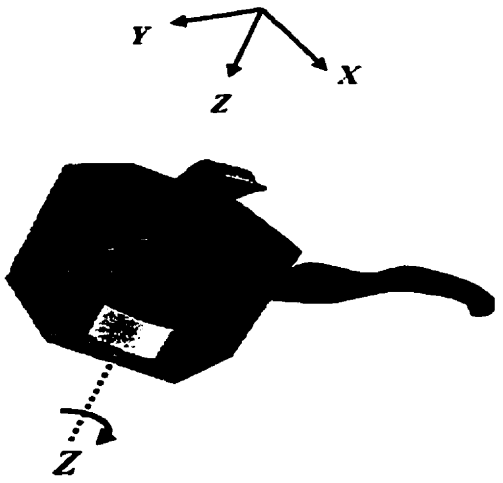

FIGURE 5.22. Motherbody with reaction wheel spinning about the Z-axis

seconds and goes to a high of 1.17 radians. The variations in γ begins at 21.8 seconds and reaches a maximum of -2.6 radians. Figure 5.26(a) depicts the variation in the attitude rates without spin stabilization. $\dot{\alpha}$ begins to oscillate at 21.4 seconds and reaches a maximum of -2.23 *rad./sec.* and the disturbances in $\dot{\beta}$ begins at 17.1 seconds and goes to a high of -0.77 *rad./sec.*. The variations in $\dot{\gamma}$ begins at 25.0 seconds and reaches a maximum of 2.1 *rad./sec.*

Due to the presence of the spinning reaction wheel, as seen in figure 5.25(b), the maximum magnitude of the perturbations in α is 0.02 radians, while for β the maximum magnitude is 0.007 radians, and the perturbations in γ reaches a maximum value of 0.008 radians. Figure 5.26(b) depicts the variation in the attitude rates with time, as the reaction wheel spins at a constant spin rate. The maximum magnitude of the perturbations in $\dot{\alpha}$ is 0.26 *rad./sec.*, while for $\dot{\beta}$ the maximum magnitude is 0.09 *rad./sec.*, and the perturbations in $\dot{\gamma}$ also reaches a maximum value of 0.09 *rad./sec.*

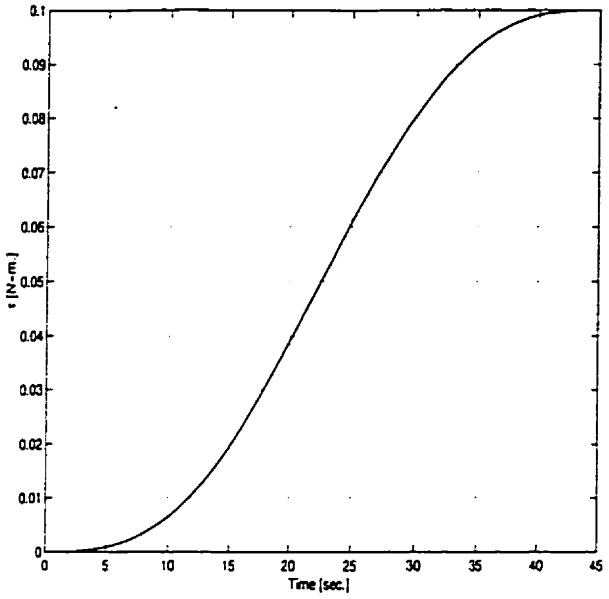

FIGURE 5.23. Joint Torque to the arm applied about the X-axis

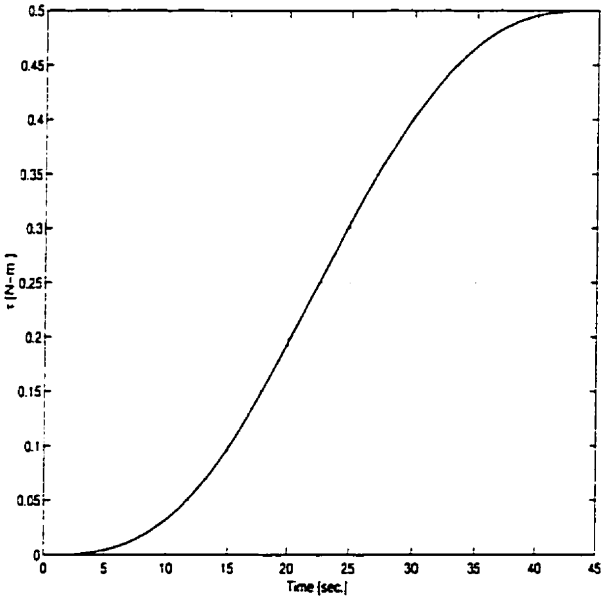

FIGURE 5.24. Joint Torque to the arm applied about the Y-axis

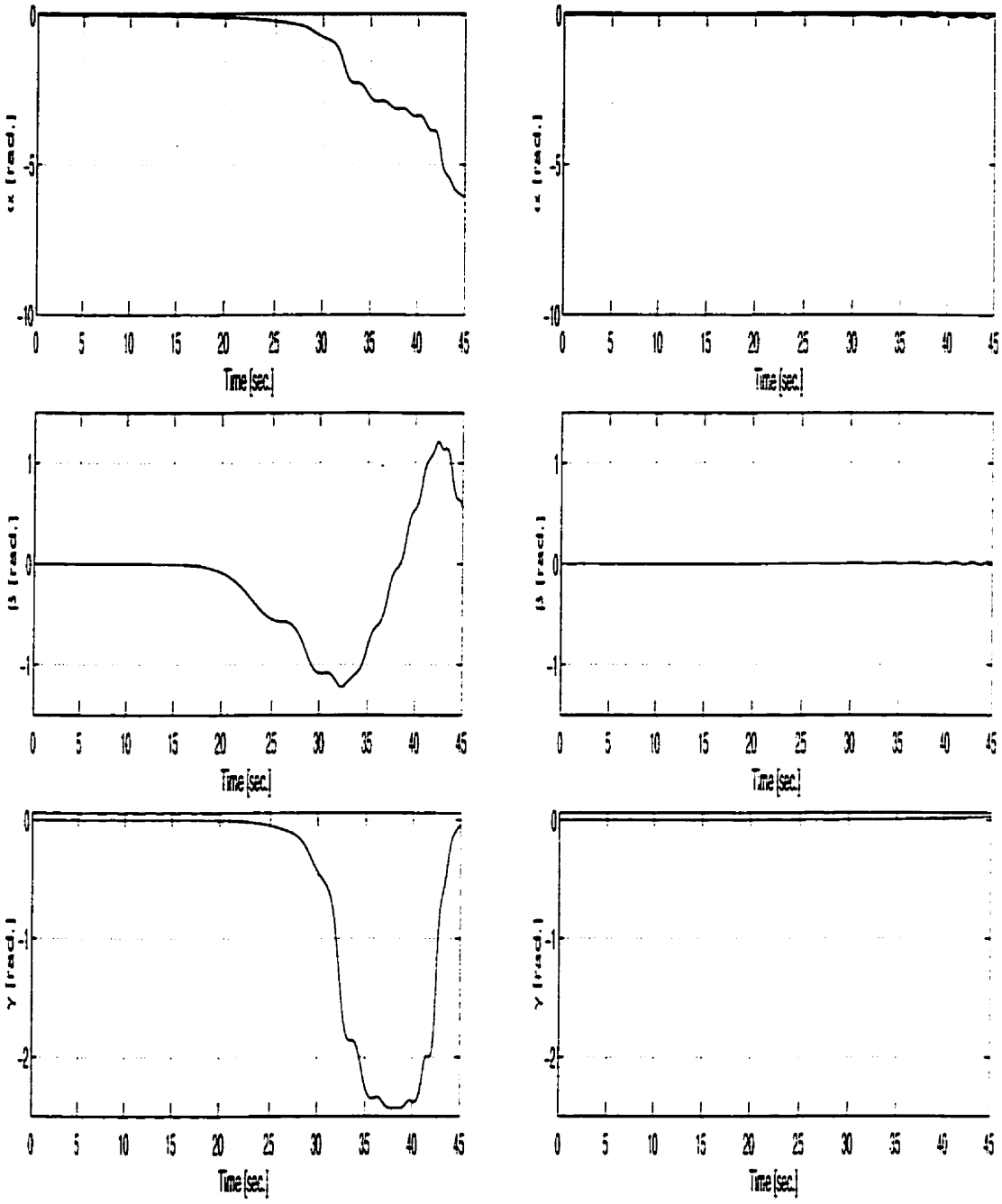

(a) (b)

FIGURE 5.25. Comparison of the variation in the attitude of the motherbody (a) Without spin stabilization (b) With wheel spinning about the Z-axis

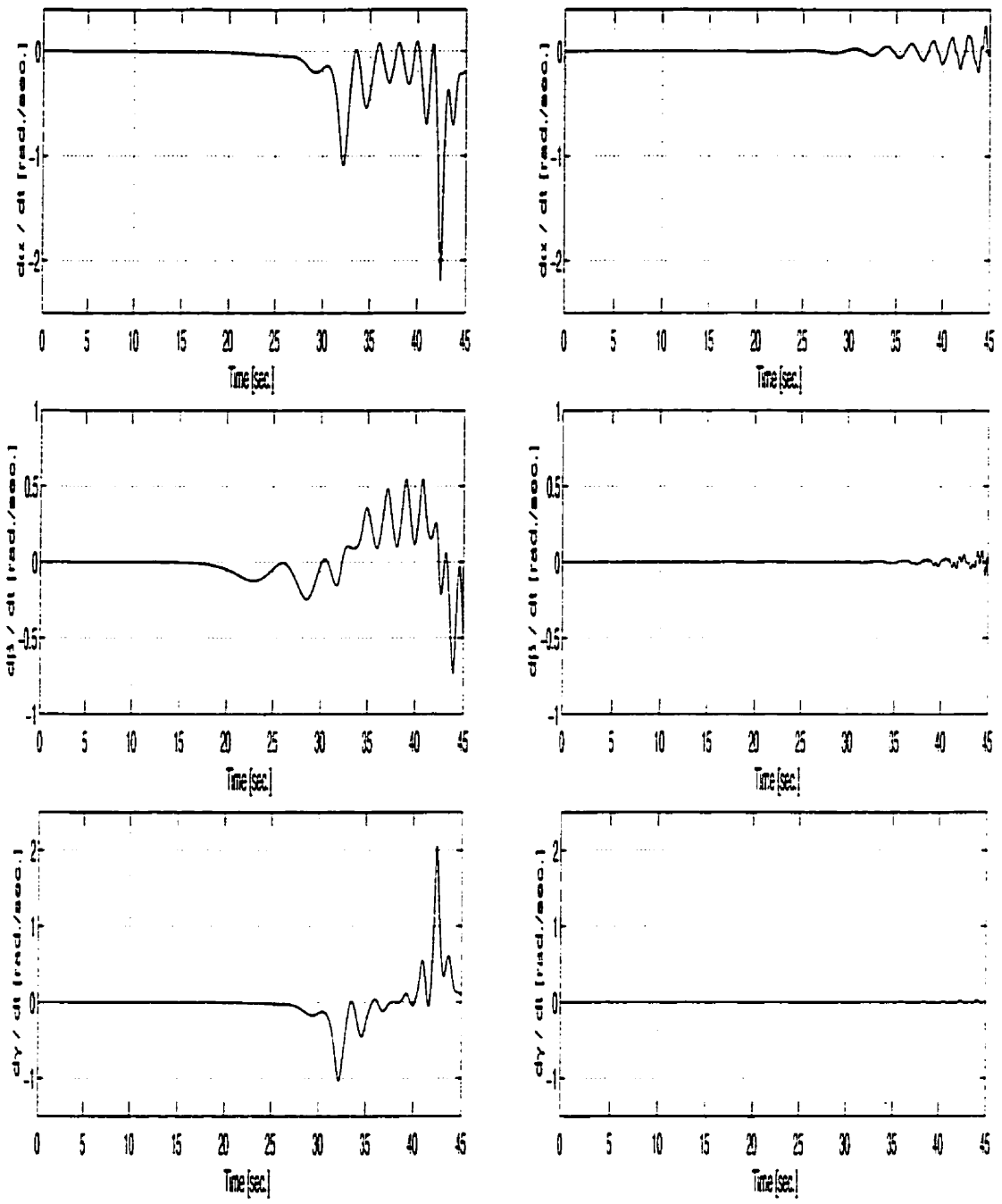

FIGURE 5.26. Comparison of the variation in rates of change in the attitude of the motherbody (a) Without spin stabilization (b) With wheel spinning about the Z-axis

4.2. Motherbody with Multiple Appendages : Reaction Wheel about the Y-Axis. Figure 5.27 shows a motherbody mounted with three sets of appendages. This example represents the fact that the dynamics of a complex multibody system (7 bodies, in this example) can be simulated using the designed objects. The reaction wheel was spinning at a constant speed of 250 *rad./sec.*, about the body-fixed Y-axis. The torque applied to the each of the joints is shown in figure 5.28, and is given by $\tau = 0.001\left\{1.0 - \cos\left(\frac{2\pi t}{30}\right)\right\}$. The joint torque was about the X-axis for the first joint and about the Z-axis for the second joint, for each of the arms. As shown in figures 5.29 and 5.30, due to the presence of the reaction wheel spinning about the body-fixed Y-axis , the variations in attitude and attitude rates about the X and Z axes have been arrested. As seen figure 5.29(a), the maximum variation in α and γ are -0.037 radians and -0.025 radians, respectively, while from figure 5.30(a), the maximum variation in $\dot{\alpha}$ and $\dot{\gamma}$ are 11.17 *rad./sec.* and 7.59 *rad./sec.*, respectively. Due to the presence of the reaction wheel spinning at 250 *rad./sec.* , there are no noticeable variations in α, γ, $\dot{\alpha}$, and $\dot{\gamma}$, but β and $\dot{\beta}$ about the Y-axis remain unchanged.

Body	**Mass**$(kg.)$	$\mathbf{I}_{xx}(kg.m.^2)$	$\mathbf{I}_{yy}(kg.m.^2)$	$\mathbf{I}_{zz}(kg.m.^2)$
Satellite	500.0	125.0	125.0	250.0
Arm 1 to 3 *Link 1*	20	3.3	3.3	6.7
Arm 1 to 3 *Link 2*	10	0.8	0.4	0.4

TABLE 5.6. Data for motherbody with multiple appendages

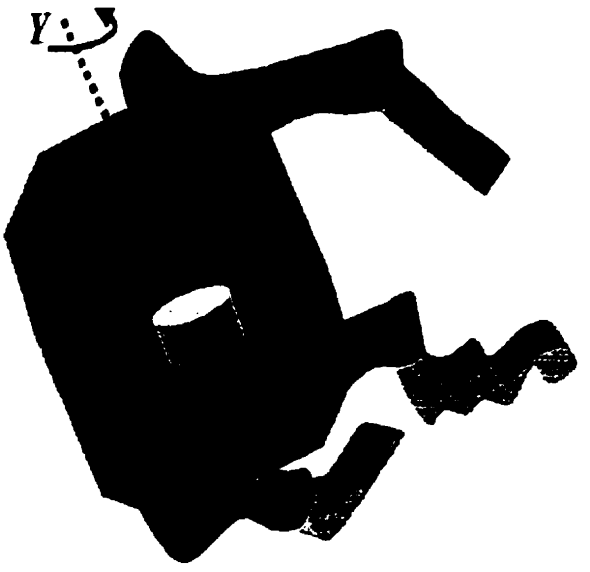

FIGURE 5.27. Multibody space system with reaction wheel spinning about the Y-axis

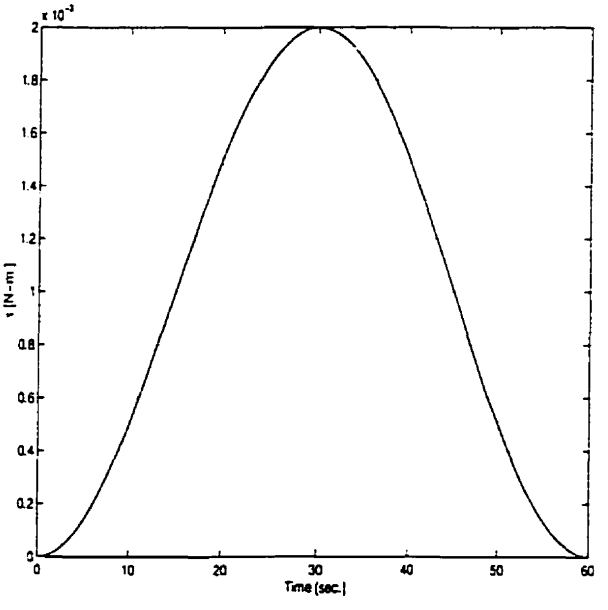

FIGURE 5.28. Joint Torque applied to the arms

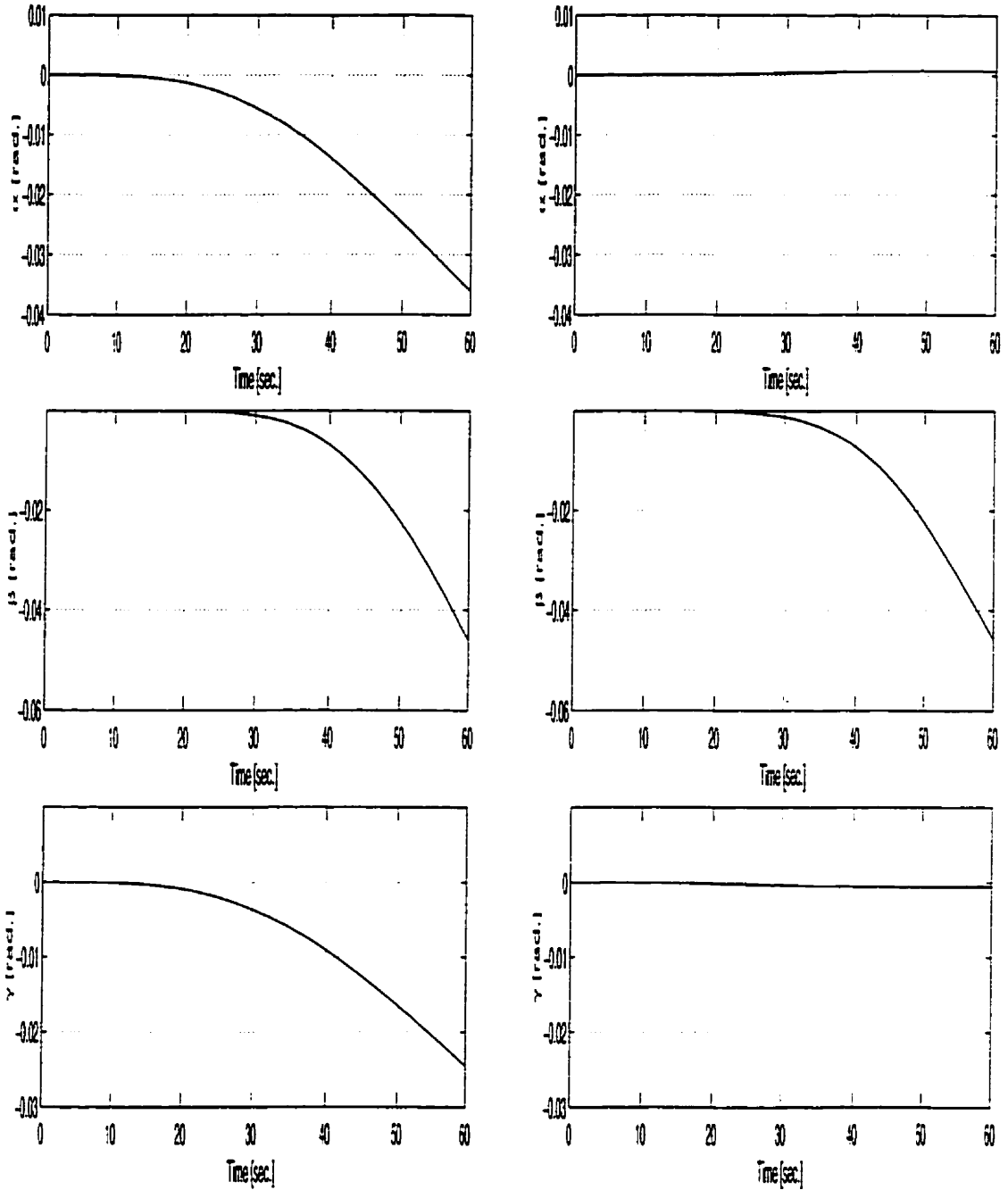

(a) (b)

FIGURE 5.29. Comparison of the variation in the attitude of the motherbody (a) Without spin stabilization (b) With wheel spinning about the Y-axis

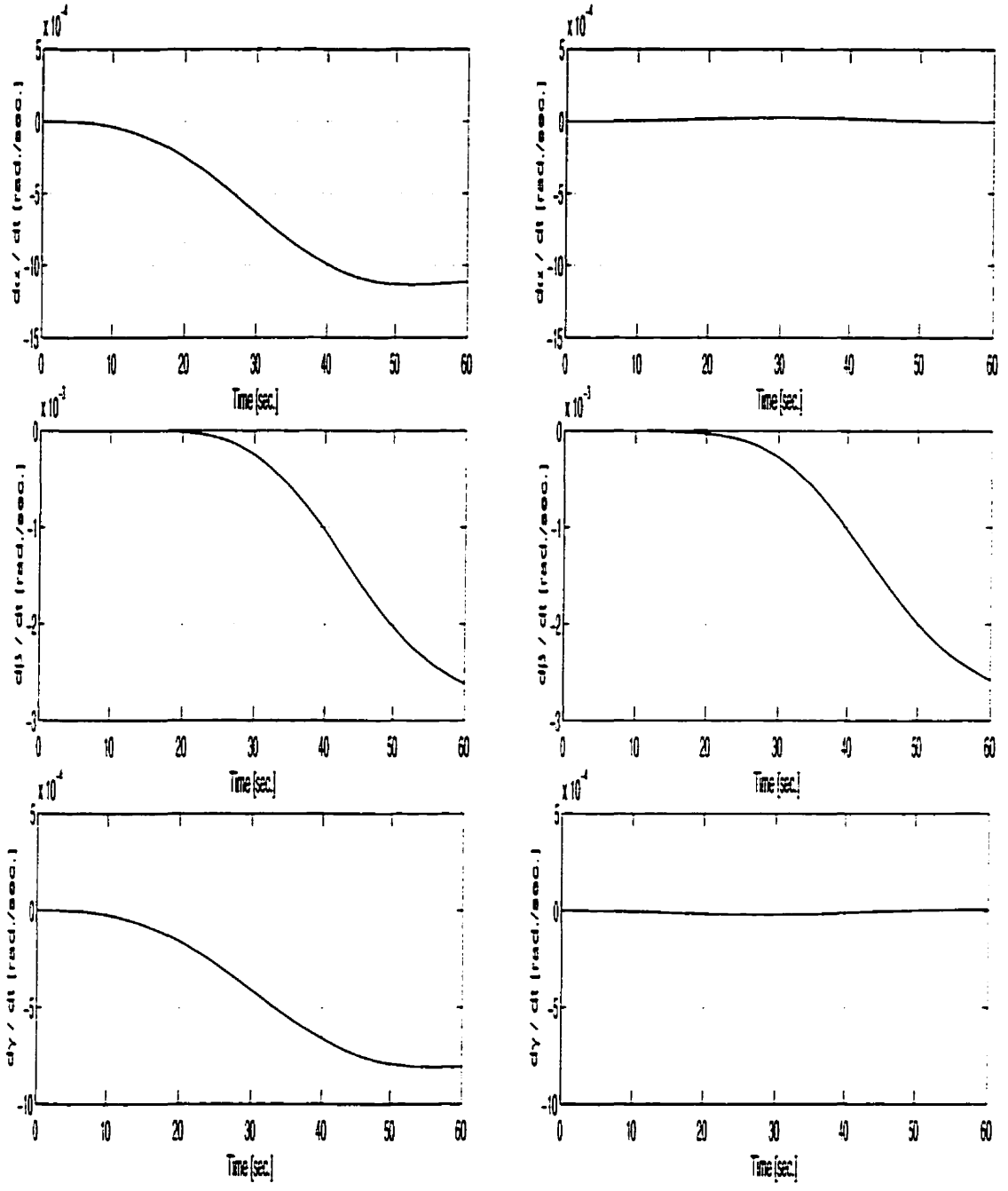

(a) (b)

FIGURE 5.30. Comparison of the variation in rates of change of the attitude of the motherbody (a) Without spin stabilization (b) With wheel spinning about the Y-axis

5. Attitude Control

Since attitude control of the spacecraft or satellite is of prime concern, reaction wheels are used as attitude control devices. Reaction wheels are referred to as momentum transfer devices. They compensate for the change in angular momentum of the system, when external torques are applied to the system and as a result, it is possible to maintain a constant angular momentum. The reaction wheels compensate for the change in angular momentum by varying its spin rate. In this section, the spin rate of the reaction wheels have been considered to be functions of the body quaternion of the motherbody. The objects have been designed such that spin rate of the reaction wheel can be in the form of a P.I.D. control law.

5.1. Attitude Control of the Clementine Spacecraft. Clementine, the Deep Space Program Science Experiment spacecraft, was launched in January 1994 to map the surface of the moon (**DeLaHunt et al.**, *1995*). The spacecraft characteristics (deployed and wet configuration) are provided in table 5.7. The attitude control system requirements and constraints led to the need for small lightweight reaction wheels for the three-axis precision control system. The total mass of the three reaction wheels was 8.4 kg. The wheels were mounted so that their axes were mutually orthogonal.

Mass $(kg.)$	$\mathbf{I}_{xx}$ $(kg.m.^2)$	$\mathbf{I}_{yy}$ $(kg.m.^2)$	$\mathbf{I}_{zz}$ $(kg.m.^2)$
456.0	93.0	80.0	107.0

TABLE 5.7. Characteristics of the Clementine spacecraft

In the simulation presented here, the spacecraft was subjected to small initial perturbation of 0.02 *rad./sec.*, about all the three axes. The P.I. control law supplied to the wheels is given in equation (5.13). Each element of the 3 × 1 vector ω_{wheel}

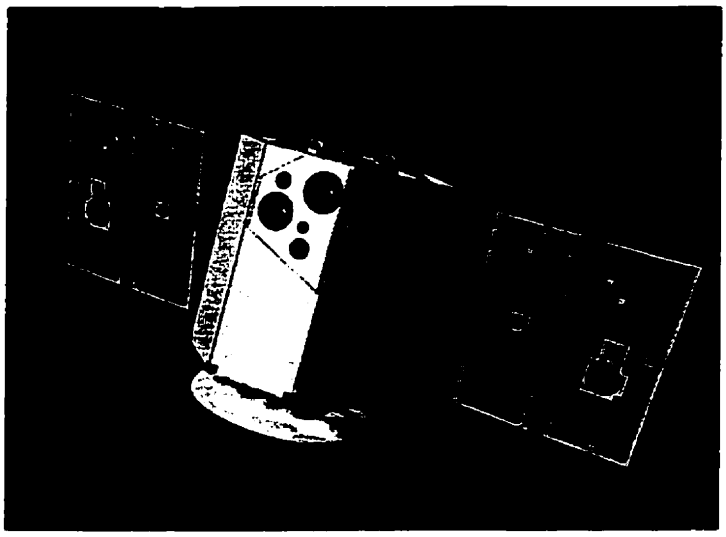

FIGURE 5.31. The Clementine spacecraft

represents the spin rate of one reaction wheel.

$$\omega_{wheel} = -\begin{bmatrix} 65 & 0 & 0 & 0 \\ 0 & 65 & 0 & 0 \\ 0 & 0 & 65 & 0 \end{bmatrix} \hat{\mathbf{q}} - \begin{bmatrix} 55 & 0 & 0 & 0 \\ 0 & 55 & 0 & 0 \\ 0 & 0 & 55 & 0 \end{bmatrix} \int \hat{\mathbf{q}}\, dt \qquad (5.13)$$

The uncontrolled attitude and attitude rates of the spacecraft are shown in figures 5.32(a) and 5.33(a), respectively, while the controlled variations in the attitude and attitude rates are shown in figures 5.32(b) and 5.33(b), respectively. The salient features, that can be inferred from figure 5.32(b), have been tabulated in table 5.8.

Attitude	Overshoot (radians)	Peak Time (seconds)	Settling Time (seconds)
$Attitude_X$	0.024	2.5	30.0
$Attitude_Y$	0.022	2.5	27.0
$Attitude_Z$	0.027	2.5	37.0

TABLE 5.8. Attitude characteristics due to P.I. control

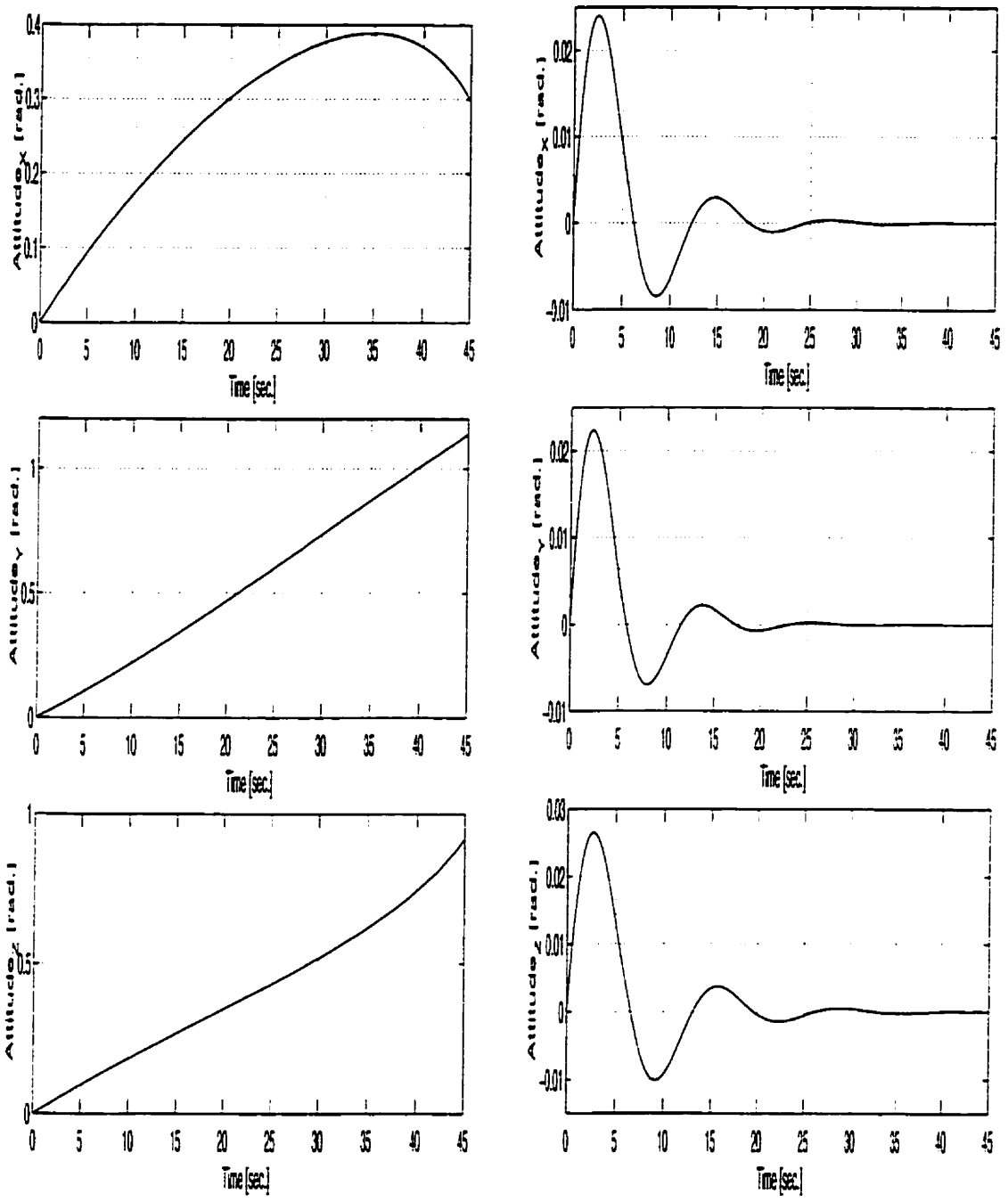

FIGURE 5.32. Variation in the attitude of the Clementine spacecraft (a) Uncontrolled (b) P.I. control applied to the reaction wheels

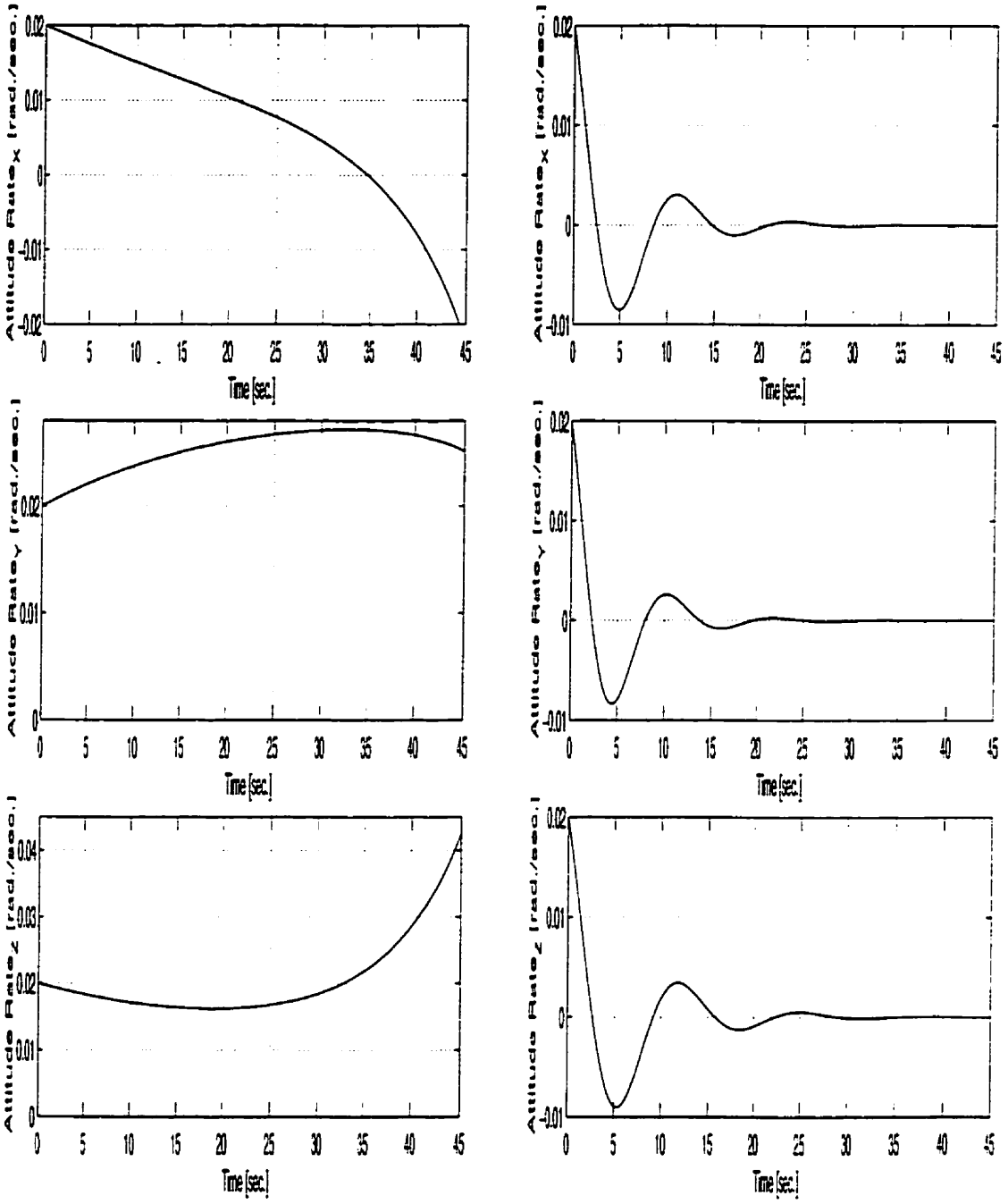

FIGURE 5.33. Variation in the attitude rates of the Clementine spacecraft (a) Uncontrolled (b) P.I. control applied to the reaction wheels

5.2. Attitude Control of a Spacecraft Carrying Two Manipulators. Figure 5.34 shows a motherbody mounted with two appendages. The joint torque was applied about the Z-axis to these appendages and is shown in figure 5.35. The physical data for the spacecraft and the appendages are given in table 5.9. Initially

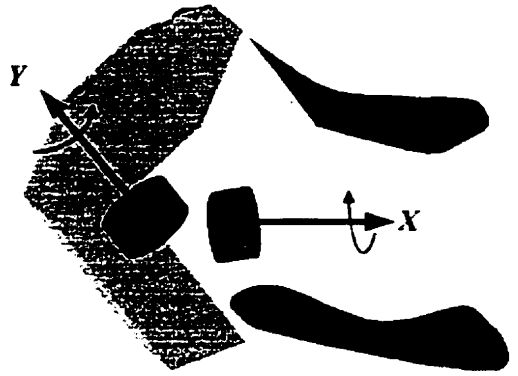

FIGURE 5.34. Motherbody with reaction wheels about the X and Y axes

Body	Mass$(kg.)$	$\mathbf{I}_{xx}(kg.m.^2)$	$\mathbf{I}_{yy}(kg.m.^2)$	$\mathbf{I}_{zz}(kg.m.^2)$
Satellite	200.0	12.5	12.5	50.0
Arm 1	10	0.4	0.4	0.8
Arm 2	10	0.4	0.4	0.8

TABLE 5.9. Data for motherbody and two appendages

the uncontrolled attitude angles are plotted, as shown in figure 5.36. *line (a)*. Figure 5.36, *line (b)*, considers two reaction wheels spinning at a constant spin rate of 300 *rad./sec.*, about the X and Y axes. It is seen that the variations in γ are arrested, but the perturbations in α and β are still present. From figure 5.36, *line (b)*, it can be noted that when there are two reaction wheels spinning at a constant rate, the maximum variation in α and β is 0.0282 radians and -0.0055 radians, respectively.

Figure 5.36, *line (c)*, depicts the changes in the attitude angles when a P.I.D. control is applied to the reaction wheel spinning about the body-fixed Z-axis. The

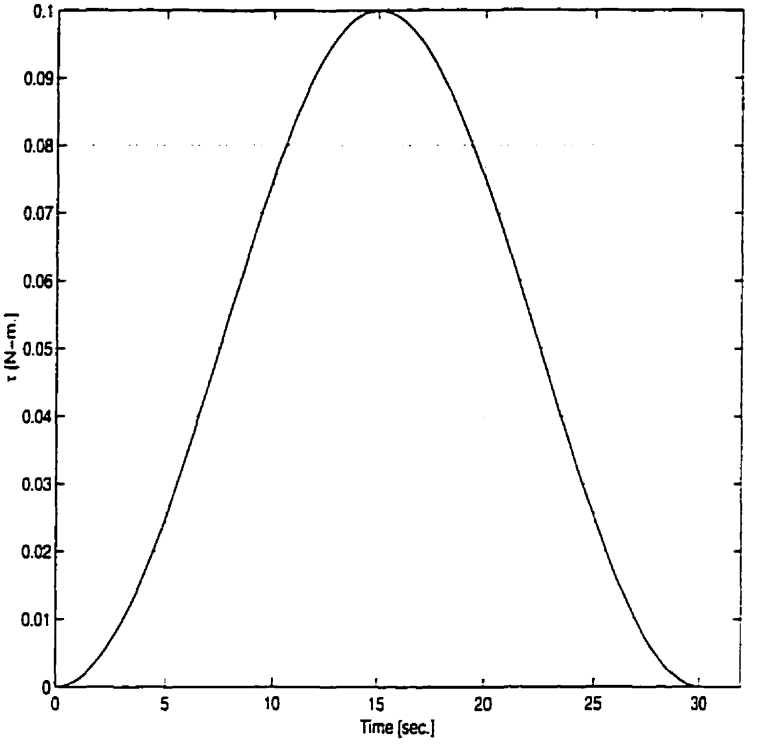

FIGURE 5.35. Joint torque to the arms applied about the Z-axis

P.I.D. control law is given by,

$$\begin{aligned} \omega_{wheel} &= \begin{bmatrix} 0 & 0 & 45.0 & 50.0 \end{bmatrix} \hat{\mathbf{q}} - \begin{bmatrix} 0 & 0 & 20.0 & 45.0 \end{bmatrix} \int \hat{\mathbf{q}}\, dt \\ &\quad + \begin{bmatrix} 0 & 0 & 350.0 & 350.0 \end{bmatrix} \dot{\hat{\mathbf{q}}} \end{aligned} \tag{5.14}$$

It is seen that the variations in γ, can be damped out with this P.I.D. control. Due to the application of this P.I.D. control law to the reaction wheel, the overshoot of γ is 1.87 radians at 2.56 seconds and at 6.03 seconds, γ starts to oscillate. At 30.0 seconds. γ has a value of 0.18 radians. Moreover, the variations in α and β are completely arrested due to the application of this P.I.D. control law to the reaction wheel.

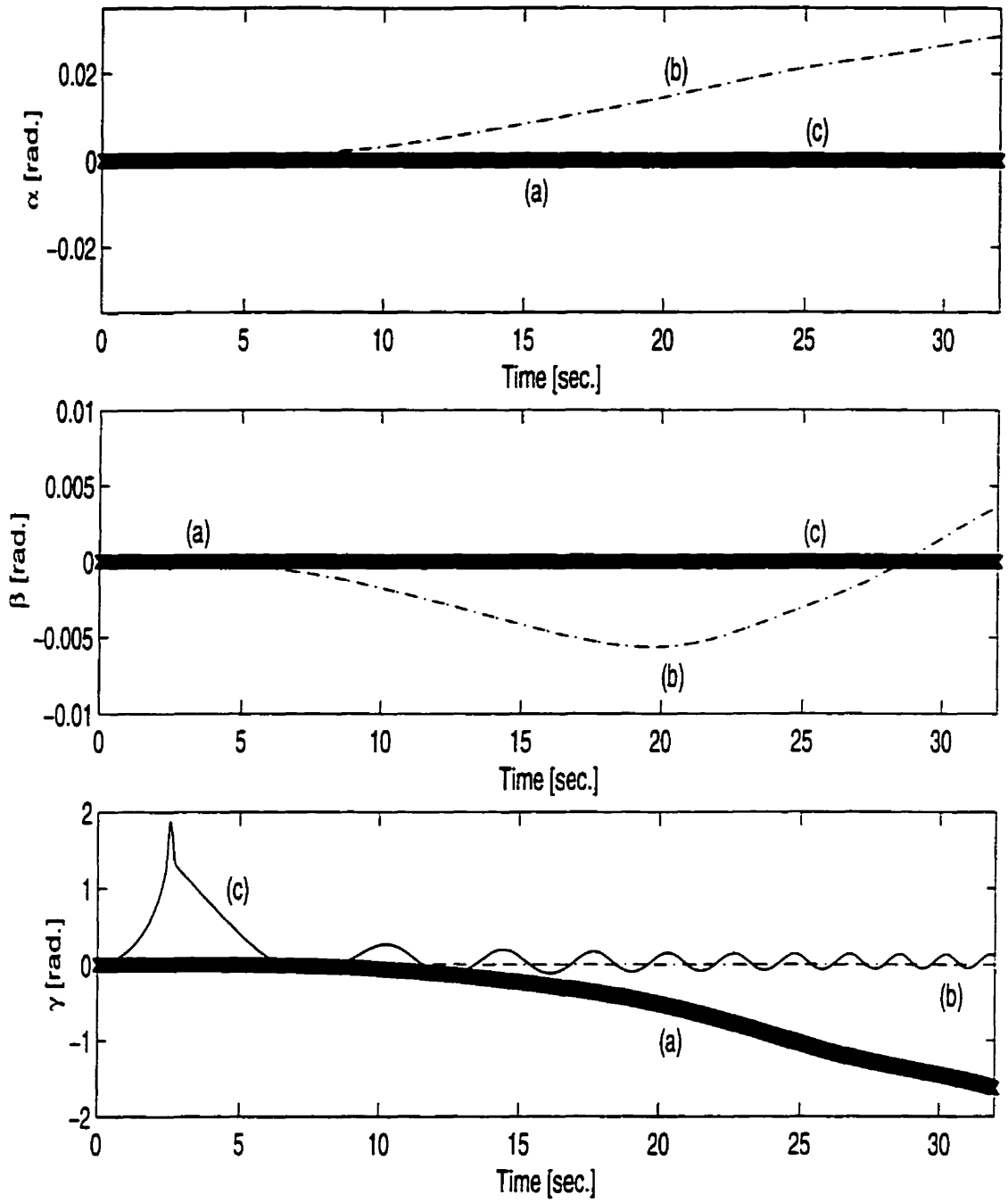

FIGURE 5.36. Variation in attitude of the spacecraft (a) Uncontrolled (b) Reaction wheels spinning at contant speed about the X and Y axes (c) P.I.D. control applied to reaction wheel spining about the Z-axis

CHAPTER 6

Conclusion

As space technology and its commercialization expands, the use of in-orbit multibody space systems will be more prevalent. They will serve multi-faceted purposes. The dynamic modeling of such multibody space systems is known to be complicated. Only recently have researchers shifted focus from the customary and prevalent procedure-oriented approach of modeling and simulating complex multibody systems to the more accurate, versatile, and user friendly object-oriented approach.

The attitude stabilization and control of a spacecraft that carries multiple appendages or robotic manipulators are quite important. The orientation of the motherbody needs to be maintained, since it is necessary to preserve communication link with the Earth stations and also to accomplish the mission objectives of the spacecraft. Reaction wheels are one of the most common and efficient methods of maintaining the attitude of the spacecraft.

In this thesis, three reaction wheels, each spinning about a fixed axis and located in the spacecraft, are considered for the attitude control and stabilization of the motherbody. The development of objects that could enable simulation of a spacecraft containing reaction wheels has not been done prior to this work. Hence, the essence of this research was to develop a dynamics formalism which embraced the

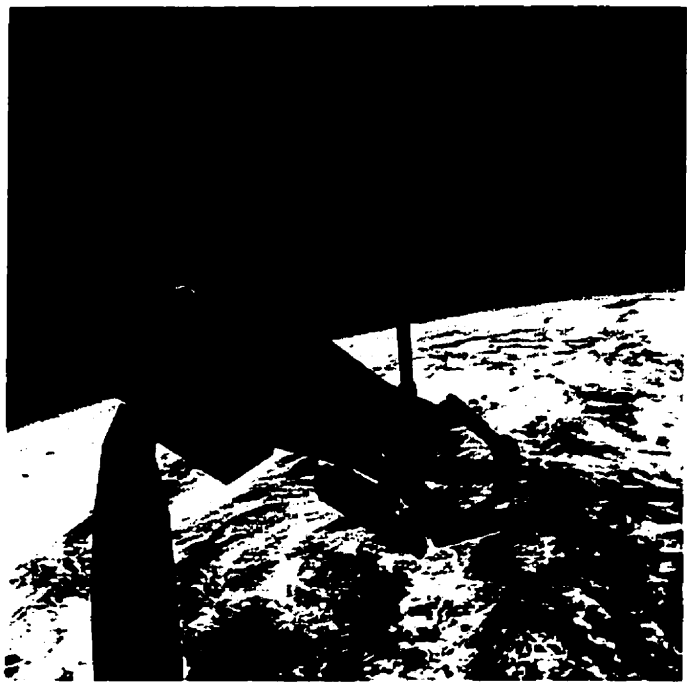

FIGURE 6.1. Artist's impression of the next generation of space robots (courtesy:*NASA Photo gallery*)

object-oriented concepts and addressed the dynamic simulation of a spacecraft with reaction wheels. This involved the modeling, designing, and coding of objects that would simulate the dynamic response of a complex multibody space system, with the motherbody containing reaction wheels.

The first step in this research project was to devise a mathematical model for the system under consideration. In order to frame the mathematical model of the system, the underlying kinematic relationships were first formulated. A variation of the Lagrangian dynamics and the principle of Natural Orthogonal Complement, in order to eliminate the kinematic constraints, were used to derive the dynamic equations of motion of the spacecraft coupled with the reaction wheels. Such a formulation technique has been proven to be computationally more efficient for complex multibody systems. The multibody system could be in the form of a spacecraft with multiple appendages, in an open chain configuration. The objects that simulate the dynamic

response of the motherbody containing reaction wheels have been designed, so as to be part of a standard multibody system software package used in ROSE (Real-time Object-oriented Software Environment).

In order to ascertain the functionality and precision of the proposed objects, several validation tests were conducted. These representative examples verified the definitiveness of the designed objects by comparing the simulated responses with the results derived using standard procedure. The rigid body systems considered for validation included a R R manipulator, a body with two arms undergoing planar motion, and a satellite spinning about its major axis, while undergoing 3 D motion. The dynamic equations of motion for the mentioned rigid body systems were known and then coded in MATLAB. The dynamic responses obtained from both MATLAB and ROSE were close.

Further validation of the designed objects was done by simulating a slew maneuver on the Cassini spacecraft, in order to verify the accuracy of the coded objects. In this test, the inputs to the reaction wheels were time varying spin rates, which were got from actual telemetry data aboard the Cassini spacecraft. By providing these time varying spin rates to the reaction wheels, it was possible to slew the spacecraft about the required axis, at the prescribed rate. The results obtained were similar to those available from the actual spacecraft.

In order to highlight the adaptability and functionality of the coded objects, the next set of simulations conducted considered the motherbody containing a reaction wheel. The motherbody and reaction wheel were part of a representative multibody space system, having two or more connected appendages. Initial simulation results considered the absence of the reaction wheel in the multibody space system. There were variations in the attitude of the motherbody, due to the application of time

varying joint torques to the connected appendages. Then the reaction wheel was considered spinning at a high constant nominal spin rate, about the body-fixed axis of the motherbody. It was shown that the variations in the attitude of the motherbody could be arrested about at least one of its axes, due to the reaction wheel spinning at a high spin rate.

It was also demonstrated that the variations in the attitude of the motherbody could be damped out by providing appropriate control gains to the reaction wheels located in the motherbody. The control law provided to the reaction wheels were in the form of a P.I.D. control law, wherein the spin rate of the reaction wheels were functions of the body quaternion of the motherbody. The Clementine spacecraft, which had three reaction wheels, was considered as an example. The application of a P.I. control law to the reaction wheels of the Clementine spacecraft resulted in the controlled and damped out variations of the spacecraft attitude. It was also shown for a representative multibody space system, that the motherbody's attitude is better controlled by a P.I.D. control law, applied to the reaction wheel, as opposed to reaction wheels spinning at a constant high spin rate.

1. Recommendations for Future Work

In this thesis, the objects were designed to simulate a spacecraft containing three reaction wheels, which was part of an effort to develop a multibody space system software package. The objects were designed so as to integrate and assimilate with the existing objects. Future work could look into the prospect of fully developing this software package by designing objects that could simulate the various complex aspects and functionalities of the dynamics and control of a multibody space system.

- In this thesis, the bodies connected to the motherbody were considered rigid. Future research could consider the dynamic interaction between flexible appendages mounted on the motherbody and could explore the use of reaction wheels, in order to maintain the attitude of the spacecraft.

- Single gimbal or double gimbal control moment gyros are also bias momentum transfer devices that can be used to control the attitude of the spacecraft. Efforts could me made to develop objects that would simulate a spacecraft or satellite containing such variable speed control moment gyros.
- Emphasis could be laid on the control aspect of the reaction/momentum wheels. More robust control techniques could be applied to the wheels in order to guarantee greater stability and better attitude control of the system. Studies could be done on choosing gains required for stability of the system. The possibility of using adaptive control techniques and optimization principle for formulating the control laws to be fed to the reaction wheels, could be explored.
- In the present work, open kinematic chains had been considered. Research could be done and objects could be designed to simulate closed kinematic chains.

REFERENCES

Amirouche F., 1992, *Computational Methods in Multi-body Dynamics*, Prentice Hall.

Angeles A. and Lee S., 1989, "The Modeling of Holonomic Mechanical Systems using a Natural Orthogonal Complement", *Transactions of the C.S.M.E.*, Vol.13, No.4, pp.81-88.

Anantharaman M., 1996, "Flexible Multibody Dynamics-An Object-Oriented Approach", *Nonlinear Dynamics*, Vol.9, pp.205-221.

Booch G., 1994, *Object-Oriented Analysis and Design with Applications*, Benjamin-Cummings Publishing.

Chobotov V. A., 1991, *Spacecraft Attitude Dynamics and Control*, Krieger Publishing Company.

Craig J. J., 1998, *Introduction to Robotics: Mechanics and Control*, Second Edition, Addison-Wesley Publishing Company, Inc.

Cyril X., Angeles J., and Misra A. K., 1991, "Dynamcis of Flexible Multi-body Mechanical Systems", *Transactions of the C.S.M.E.*, Vol.15, No.3, pp.235-255.

David L., 1995, "Robots for all Reasons", *Aerospace America*, Vol.33, No.9, pp.30-35.

DeLaHunt P., Gates S., and Levenson M., 1995, " Clementine Attitude Determination and Control System", *Journal of Spacecraft and Rockets*, Vol.32, No.6, pp.1054-1059.

Hughes P. C., 1986, *Spacecraft Attitude Dynamics*, John Wiley and Sons, Inc.

Jaar G. J., 1993, "Dynamics and Control of a Spacecraft-Mounted Robot Capturing a Spinning Satellite", M.Eng. Thesis, *Department of Mechanical Engineering, McGill University*, Montreal.

Kecskeméthy A., 1995, "Object-oriented Modeling of Mechanical Systems", *Kinematics and Dynamics of Multibody Systems*, edited by J. Angeles and A. Kecskemethy, Chap. 6, Springer-Verlag, pp.217-276.

Kilston, S. and Friedman, E.,2000. "Space - How Far We Have Come, How Far There Is To Go", *Proceedings of the IEEE*, Vol.88, No.3, pp.429-438.

Lückel J., Junker F., and Toepper S., 1993, "Block-Oriented Modeling of Rigid Multibody Systems with regard to Subsystem Techniques", *Advanced Multibody System Dynamics*, Kluwer Academic Publishing, pp.49-66

Min B., Misra A. K., Cyril X., Modi V. J., and de Silva C. W., 1999, "Object-Oriented Modeling of the Dynamics of Flexible Multibody Systems", *AAS/AIAA Astrodynamics Specialist Conference*, Paper AAS 99-454.

Min B., Misra A. K., Cyril X., Modi V. J., and de Silva, C. W., 2000, "Simulation of the Dynamics of Space Systems using Object-Oriented Modeling", *AIAA Modeling and Simulation Technologies, Conference and Exhibit*, AIAA 2000-4177.

Mitsushige O., 1996, "Coordinated Control of Spacecraft Attitude and its Manipulator", *Proceedings of the 1996 IEEE*, International Conference on Robotics and Automation, Minneapolis, Minnesota, pp.732-738.

Mitsushige, O., 1997, "Motion Control of the Satellite Mounted Robot Arm which assures satellite Attitude Stability", *Acta Astronautica*, Vol.41, No.11, pp.739-750.

Mitsushige O., 2000, "Improvement of the Satellite Attitude Stability by the Sliding Mode Control While a Robot Arm Works on a Satellite", *AAS/AIAA Space Flight Mechanics Meeting*, Paper AAS 00-146.

Modi V. J., 1974, "Attitude Dynamics of Satellites with Flexible Appendages - A Brief Review", *Journal of Spacecraft and Rockets*, Vol.11, No.11, pp.743-751.

Modi V. J. and Ng A. C., 1990, "Dynamics of Systems with Interconnected Flexible Members in the Presence of Thermal Deformations", *Dynamics of Flexible Structures in Space*, edited by Kirk C. L and Junkins J. L., Springer-Verlag, pp.199-213.

Otter M. and Hocke M., 1993, "An Object-Oriented Data Model for Multibody Systems", *Advanced Multibody System Dynamics*, W.Schiehlen(ed.), Kluwer Academic Publishers, pp.19-48.

Sebest R. W., 1989, *Concepts of Programming Languages*, Benjamin-Cummings Publishing Company.

Shabana A. A., 1998, *Dynamics of Multibody Systems*, Cambridge University Press, Second Edition.

Stuelpnagel J., 1964, "On the Parameterization of Three-Dimensional Rotation Group", *SIAM, Rev*, Vol.6, No.4, pp.422-430.

Wallrapp 0., 1993, "Standard Input Data of Flexible Members in Multibody Systems", *Advanced Multibody System Dynamics*, Kluwer Academic Publishers, pp.445-450.

Wertz J. A. and Lee A. Y., 2001, "Inflight Estimation of the Cassini Spacecraft's Inertia Tensor", *AAS/AIAA Space Flight Mechanics Meeting*, Paper AAS-01-179.

Wittenburg J., 1974, "Automatic Construction of Nonlinear Equations of Motion for Systems with Many Degrees of Freedom", Gyrodynamics, P.Y. Willems (ed.), *Springer-Verlag*, Berlin, pp.10-22.

Van Woerkom P. Th. L. M., 1993, "Synthesis and Survey of Control Laws for Large Flexible Spacecraft", *Control-Theory and Advanced Technology*, Vol.9, No.3, pp.639-669.

Van Woerkom P. Th. L. M. and Misra A. K., 1996, "Robotic Manipulators in Space: A Dynamics and Control Perspective", *Acta Astronautica*, Vol.38., Nos.4-8, pp.411-421.

APPENDIX A

Relations Pertaining to the Algebraic Constraint Wrench

The algebraic constraint for body i is given as,

$$\hat{\mathbf{q}}_i^T \hat{\mathbf{q}}_i = \mathbf{q}_i^T \boldsymbol{\Sigma} \mathbf{q}_i = 1 \tag{A.1}$$

where,

$$\boldsymbol{\Sigma} = \begin{bmatrix} \mathbf{0} & \mathbf{0} \\ \mathbf{0} & \mathbf{1} \end{bmatrix} \tag{A.2}$$

Differentiating equation (A.1) with respect to time,

$$2\,\mathbf{q}_i^T \boldsymbol{\Sigma} \dot{\mathbf{q}}_i = 0 \tag{A.3}$$

Now using equation (2.16), the above equation is,

$$\left(2\,\mathbf{q}_i^T \boldsymbol{\Sigma}\right) \boldsymbol{\Lambda}_i \mathbf{v}_i = 0 \tag{A.4}$$

Alternatively,

$$\boldsymbol{\Lambda}_i^T (\boldsymbol{\Sigma} \mathbf{q}_i) = 0 \tag{A.5}$$

The algebraic constraint wrench for body i is given as (**Cyril et al.**, *1991*),

$$\mathbf{w}_i^A = \left(\mathbf{q}_i^T \boldsymbol{\Sigma}\right)^T \lambda = \lambda \boldsymbol{\Sigma} \mathbf{q}_i \tag{A.6}$$

where λ is the Lagrange multiplier and $\mathbf{w}_i^A$ is the algebraic constraint wrench of body i. Thus using equations (A.5) and (A.6),

$$\boldsymbol{\Lambda}_i^T \mathbf{w}_i^A = \mathbf{0} \tag{A.7}$$

APPENDIX B

Relations Used to Simplify the Equation of Motion for Body i

$\dot{\mathbf{L}}_i$ is initialized as a 6×7 matrix for body i and is given as,

$$\dot{\mathbf{L}}_i = \begin{bmatrix} \mathbf{0} & \mathbf{0} \\ \mathbf{0} & \dot{\hat{\mathbf{L}}}_i \end{bmatrix} \tag{B.1}$$

where,

$$\dot{\hat{\mathbf{L}}}_i = 2\left[\dot{r}_{o_i}\mathbf{1} + \dot{\mathbf{r}}_i^{\times} - \dot{\mathbf{r}}_i\right] \tag{B.2}$$

$\dot{\mathbf{A}}_i$ is initialized as a 7×6 matrix for body i and is given as,

$$\dot{\mathbf{A}}_i = \begin{bmatrix} \mathbf{0} & \mathbf{0} \\ \mathbf{0} & \dot{\hat{\mathbf{A}}}_i \end{bmatrix} \tag{B.3}$$

where,

$$\dot{\hat{\mathbf{A}}}_i = \frac{1}{2}\begin{bmatrix} \dot{r}_{o_i}\mathbf{1} - \dot{\mathbf{r}}_i^{\times} \\ -\dot{\mathbf{r}}_i^{T} \end{bmatrix} \tag{B.4}$$

Having defined expressions for $\dot{\mathbf{L}}_i$ and $\dot{\mathbf{\Lambda}}_i$, the following relations are used to simplify the equation of motion, equation (2.36), of the i^{th} body,

$$\Rightarrow \mathbf{L}_i \dot{\mathbf{\Lambda}}_i = -\dot{\mathbf{L}}_i \mathbf{\Lambda}_i \tag{B.5}$$

$$\Rightarrow \dot{\mathbf{I}}_i = \dot{\mathbf{L}}_i^T \mathbf{M}_i \mathbf{L}_i + \mathbf{L}_i^T \dot{\mathbf{M}}_i \mathbf{L}_i + \mathbf{L}_i^T \mathbf{M}_i \dot{\mathbf{L}}_i \tag{B.6}$$

The derivation presented below provides an expression for $\frac{\partial \mathbf{v}_i}{\partial \mathbf{q}_i}$. It can be shown that (**Cyril et al.**, *1991*),

$$\hat{\mathbf{L}}_i \hat{\mathbf{q}}_i = \mathbf{0} \tag{B.7}$$

Thus,

$$\mathbf{L}_i \mathbf{q}_i = \begin{bmatrix} \mathbf{1} & \mathbf{0} \\ \mathbf{0} & \hat{\mathbf{L}}_i \end{bmatrix} \begin{Bmatrix} \dot{\mathbf{p}}_i \\ \hat{\mathbf{q}}_i \end{Bmatrix} = \begin{Bmatrix} \dot{\mathbf{p}}_i \\ \mathbf{0} \end{Bmatrix} \tag{B.8}$$

Alternatively,

$$\mathbf{L}_i \mathbf{q}_i = \begin{bmatrix} \mathbf{1} & \mathbf{0} \\ \mathbf{0} & \mathbf{0} \end{bmatrix} \begin{Bmatrix} \dot{\mathbf{p}}_i \\ \hat{\mathbf{q}}_i \end{Bmatrix} = \mathbf{C}\,\mathbf{q}_i \tag{B.9}$$

where, $\mathbf{C}$ is a constant. Using the relation derived in equation (B.9),

$$\mathbf{L}_i \mathbf{q}_i = \mathbf{C}\,\mathbf{q}_i$$

Thus,

$$\dot{\mathbf{L}}_i \mathbf{q}_i + \mathbf{L}_i \dot{\mathbf{q}}_i = \mathbf{C}\,\dot{\mathbf{q}}_i \tag{B.10}$$

Rearranging terms in the above equation,

$$\mathbf{v}_i = \mathbf{L}_i \dot{\mathbf{q}}_i = -\dot{\mathbf{L}}_i \mathbf{q}_i + \mathbf{C}\,\dot{\mathbf{q}}_i \tag{B.11}$$

Hence,

$$\Rightarrow \frac{\partial \mathbf{v}_i}{\partial \mathbf{q}_i} = -\dot{\mathbf{L}}_i \tag{B.12}$$

Thus, using the relation derived for $\frac{\partial \mathbf{v}_i}{\partial \mathbf{q}_i}$ in equation (B.12), $\frac{\partial}{\partial \mathbf{q}_i}\left(\mathbf{v}_i^T \mathbf{M}_i \mathbf{v}_i\right)$ is evaluated as,

$$\begin{aligned} \Rightarrow \frac{\partial}{\partial \mathbf{q}_i}\left(\mathbf{v}_i^T \mathbf{M}_i \mathbf{v}_i\right) &= 2\left(\frac{\partial \mathbf{v}_i}{\partial \mathbf{q}_i}\right)^T \mathbf{M}_i \mathbf{v}_i + \mathbf{v}_i^T \frac{\partial \mathbf{M}_i}{\partial \mathbf{q}_i} \mathbf{v}_i \\ &= -2\dot{\mathbf{L}}_i^T \mathbf{M}_i \mathbf{v}_i + \mathbf{v}_i^T \frac{\partial \mathbf{M}_i}{\partial \mathbf{q}_i} \mathbf{v}_i \end{aligned} \tag{B.13}$$

APPENDIX C

Kinetic Energy of the Wheel

The mathematical analysis presented here, involves the application of the Euler-Lagrange equation to each of the kinetic energy terms due to the reaction wheel. The foregoing analysis enables the generatation of the inertia and wrench terms of the dynamic equations of motion of a spacecraft containing reaction wheels. As stated previously, the terms with the subscript 'B' are associated with the motherbody. It should be noted that the relations derived earlier, for the i^{th} body, can be applied to the motherbody.

1. TERM 1

The first term in kinetic energy equation (2.51) is,

$$T_1 = \frac{1}{2}\,\mathbf{v}_B^T\,\mathbf{M}_w\,\mathbf{v}_B \tag{C.1}$$

Using equation (2.12), that relates the twist of the motherbody to the time derivative of its pose,

$$\mathbf{v}_B = \mathbf{L}_B\,\dot{\mathbf{q}}_B$$

Substituting the above expression for $\mathbf{v}_B$ in equation (C.1),

$$T_1 = \frac{1}{2}\,\dot{\mathbf{q}}_B^T\,\mathbf{L}_B^T\,\mathbf{M}_w\,\mathbf{L}_B\,\dot{\mathbf{q}}_B \tag{C.2}$$

The following is defined as,

$$\mathbf{\Psi}_w = \mathbf{L}_B^T \mathbf{M}_w \mathbf{L}_B \tag{C.3}$$

Substituting equation (C.3) in equation (C.2),

$$T_1 = \frac{1}{2} \dot{\mathbf{q}}_B^T \mathbf{\Psi}_w \dot{\mathbf{q}}_B \tag{C.4}$$

Now evaluating each term of Euler-Lagrange equation (2.30),

$$\frac{\partial T_1}{\partial \dot{\mathbf{q}}_B} = \left(\frac{1}{2} \mathbf{\Psi}_w \dot{\mathbf{q}}_B \right) + \left(\frac{1}{2} \dot{\mathbf{q}}_B^T \mathbf{\Psi}_w \right)^T \tag{C.5}$$

The above expression is rewritten as,

$$\frac{\partial T_1}{\partial \dot{\mathbf{q}}_B} = \mathbf{\Psi}_w \dot{\mathbf{q}}_B \tag{C.6}$$

Also,

$$\frac{\partial T_1}{\partial \mathbf{q}_B} = \frac{1}{2} \left(\frac{\partial \mathbf{v}_B}{\partial \mathbf{q}_B} \right)^T \mathbf{M}_w \mathbf{v}_B + \frac{1}{2} \left(\frac{\partial \mathbf{v}_B}{\partial \mathbf{q}_B} \right)^T \left(\mathbf{v}_B^T \mathbf{M}_w \right)^T + \frac{1}{2} \mathbf{v}_B^T \frac{\partial \mathbf{M}_w}{\partial \mathbf{q}_B} \mathbf{v}_B \tag{C.7}$$

which is rewritten as,

$$\frac{\partial T_1}{\partial \mathbf{q}_B} = \left(\frac{\partial \mathbf{v}_B}{\partial \mathbf{q}_B} \right)^T \mathbf{M}_w \mathbf{v}_B + \frac{1}{2} \mathbf{v}_B^T \frac{\partial \mathbf{M}_w}{\partial \mathbf{q}_B} \mathbf{v}_B \tag{C.8}$$

But, from equation (B.12), which is rewritten below,

$$\left(\frac{\partial \mathbf{v}_B}{\partial \mathbf{q}_B} \right)^T = -\dot{\mathbf{L}}_B$$

The expression for $\frac{\partial T_1}{\partial \mathbf{q}_B}$ is now rewritten as,

$$\frac{\partial T_1}{\partial \mathbf{q}_B} = -\dot{\mathbf{L}}_B \mathbf{M}_w \mathbf{v}_B + \frac{1}{2} \mathbf{v}_B^T \frac{\partial \mathbf{M}_w}{\partial \mathbf{q}_B} \mathbf{v}_B \tag{C.9}$$

Taking the time derivative of equation (C.6),

$$\frac{d}{dt} \left(\frac{\partial T_1}{\partial \dot{\mathbf{q}}_B} \right) = \dot{\mathbf{\Psi}}_w \dot{\mathbf{q}}_B + \mathbf{\Psi}_w \ddot{\mathbf{q}}_B \tag{C.10}$$

Taking the time derivative of the equation (2.16), which is rewritten below, the relation obtained is,

$$\dot{\mathbf{q}}_B = \mathbf{\Lambda}_B \mathbf{v}_B$$

$$\ddot{\mathbf{q}}_B = \dot{\mathbf{\Lambda}}_B \mathbf{v}_B + \mathbf{\Lambda}_B \dot{\mathbf{v}}_B \tag{C.11}$$

and, taking the time derivative of equation (C.3),

$$\dot{\Psi}_w = \dot{\mathbf{L}}_B^T \mathbf{M}_w \mathbf{L}_B + \mathbf{L}_B^T \dot{\mathbf{M}}_w \mathbf{L}_B + \mathbf{L}_B^T \mathbf{M}_w \dot{\mathbf{L}}_B \tag{C.12}$$

Substituting equations (C.11) and (C.12) into equation (C.10),

$$\begin{aligned} \frac{d}{dt}\left(\frac{\partial T_1}{\partial \dot{\mathbf{q}}_B}\right) &= \dot{\mathbf{L}}_B^T \mathbf{M}_w \mathbf{L}_B \mathbf{\Lambda}_B \mathbf{v}_B + \mathbf{L}_B^T \mathbf{M}_w \mathbf{L}_B \dot{\mathbf{\Lambda}}_B \mathbf{v}_B + \mathbf{L}_B^T \mathbf{M}_w \mathbf{L}_B \mathbf{\Lambda}_B \dot{\mathbf{v}}_B \\ &\quad + \mathbf{L}_B^T \dot{\mathbf{M}}_w \mathbf{L}_B \mathbf{\Lambda}_B \mathbf{v}_B + \mathbf{L}_B^T \mathbf{M}_w \dot{\mathbf{L}}_B \mathbf{\Lambda}_B \mathbf{v}_B \end{aligned} \tag{C.13}$$

The terms $\frac{\partial T_1}{\partial \mathbf{q}_B}$ and $\frac{d}{dt}\left(\frac{\partial T_1}{\partial \dot{\mathbf{q}}_B}\right)$ derived in equations (C.9) and (C.13), respectively, are used while applying the Euler-Lagrange equation to term 1 (T_1). Using equations (2.20), (B.5), (C.9), (C.13), pre-multiplying by $\mathbf{\Lambda}_B^T$ in order to eliminate the algebraic constraint, and finally applying the Euler-Lagrange equation (2.30) on term 1 (T_1).

$$\begin{aligned} \mathbf{\Lambda}_B^T \left[\frac{d}{dt}\left(\frac{\partial T_1}{\partial \dot{\mathbf{q}}_B}\right) - \frac{\partial T_1}{\partial \mathbf{q}_B}\right] &= \mathbf{\Lambda}_B^T \dot{\mathbf{L}}_B^T \mathbf{M}_w \mathbf{v}_B - \mathbf{M}_w \dot{\mathbf{L}}_B \mathbf{\Lambda}_B \mathbf{v}_B \\ &\quad + \mathbf{M}_w \dot{\mathbf{v}}_B + \mathbf{\Lambda}_B^T \dot{\mathbf{L}}_B^T \mathbf{M}_w \mathbf{v}_B + \dot{\mathbf{M}}_w \mathbf{v}_B + \mathbf{M}_w \dot{\mathbf{L}}_B \mathbf{\Lambda}_B \mathbf{v}_B \\ &\quad - \frac{1}{2} \mathbf{\Lambda}_B^T \left(\mathbf{v}_B^T \frac{\partial \mathbf{M}_w}{\partial \mathbf{q}_B} \mathbf{v}_B\right) \end{aligned} \tag{C.14}$$

Alternatively,

$$\begin{aligned} \mathbf{\Lambda}_B^T \left[\frac{d}{dt}\left(\frac{\partial T_1}{\partial \dot{\mathbf{q}}_B}\right) - \frac{\partial T_1}{\partial \mathbf{q}_B}\right] &= 2\,\mathbf{\Lambda}_B^T \dot{\mathbf{L}}_B^T \mathbf{M}_w \mathbf{v}_B + \mathbf{M}_w \dot{\mathbf{v}}_B + \dot{\mathbf{M}}_w \mathbf{v}_B \\ &\quad - \frac{1}{2} \mathbf{\Lambda}_B^T \left(\mathbf{v}_B^T \frac{\partial \mathbf{M}_w}{\partial \mathbf{q}_B} \mathbf{v}_B\right) \end{aligned} \tag{C.15}$$

2. TERM 2

The second term in kinetic energy equation (2.51) is,

$$T_2 = \mathbf{v}_B^T \mathbf{M}_w \, {}^B\mathbf{v}_w \tag{C.16}$$

Substituting equation (2.12) in equation (C.16),

$$T_2 = \dot{\mathbf{q}}_B^T \mathbf{L}_B^T \mathbf{M}_w \, {}^B\mathbf{v}_w \tag{C.17}$$

Now evaluating each term of the Euler-Lagrange equation (2.30),

$$\frac{\partial T_2}{\partial \dot{\mathbf{q}}_B} = \mathbf{L}_B^T \mathbf{M}_w \, {}^B\mathbf{v}_w + \left(\frac{\partial {}^B\mathbf{v}_w}{\partial \dot{\mathbf{q}}_B} \right)^T \mathbf{M}_w \mathbf{L}_B \dot{\mathbf{q}}_B \tag{C.18}$$

and,

$$\begin{aligned} \frac{d}{dt}\left(\frac{\partial T_2}{\partial \dot{\mathbf{q}}_B} \right) &= \dot{\mathbf{L}}_B^T \mathbf{M}_w \, {}^B\mathbf{v}_w + \mathbf{L}_B^T \dot{\mathbf{M}}_w \, {}^B\mathbf{v}_w + \mathbf{L}_B^T \mathbf{M}_w \frac{d \, {}^B\mathbf{v}_w}{dt} \\ &+ \frac{d}{dt}\left(\frac{\partial {}^B\mathbf{v}_w}{\partial \dot{\mathbf{q}}_B} \right)^T \mathbf{M}_w \mathbf{L}_B \dot{\mathbf{q}}_B + \left(\frac{\partial {}^B\mathbf{v}_w}{\partial \dot{\mathbf{q}}_B} \right)^T \dot{\mathbf{M}}_w \mathbf{L}_B \dot{\mathbf{q}}_B \\ &+ \left(\frac{\partial {}^B\mathbf{v}_w}{\partial \dot{\mathbf{q}}_B} \right)^T \mathbf{M}_w \dot{\mathbf{L}}_B \dot{\mathbf{q}}_B + \left(\frac{\partial {}^B\mathbf{v}_w}{\partial \dot{\mathbf{q}}_B} \right)^T \mathbf{M}_w \mathbf{L}_B \ddot{\mathbf{q}}_B \end{aligned} \tag{C.19}$$

Using the expression for $\ddot{\mathbf{q}}_B$, derived in equation (C.11) and rewritten below,

$$\ddot{\mathbf{q}}_B = \dot{\mathbf{\Lambda}}_B \mathbf{v}_B + \mathbf{\Lambda}_B \dot{\mathbf{v}}_B$$

Substituting the expression for $\ddot{\mathbf{q}}_B$ in equation (C.19), and using the relations derived in equations (2.16) and (B.5),

$$\begin{aligned}\frac{d}{dt}\left(\frac{\partial T_2}{\partial \dot{\mathbf{q}}_B}\right) &= \dot{\mathbf{L}}_B^T \mathbf{M}_w {}^B\mathbf{v}_w + \mathbf{L}_B^T \dot{\mathbf{M}}_w {}^B\mathbf{v}_w + \mathbf{L}_B^T \mathbf{M}_w \frac{d\,{}^B\mathbf{v}_w}{dt} \\ &+ \frac{d}{dt}\left(\frac{\partial {}^B\mathbf{v}_w}{\partial \dot{\mathbf{q}}_B}\right)^T \mathbf{M}_w \mathbf{v}_B + \left(\frac{\partial {}^B\mathbf{v}_w}{\partial \dot{\mathbf{q}}_B}\right)^T \dot{\mathbf{M}}_w \mathbf{v}_B \\ &+ \left(\frac{\partial {}^B\mathbf{v}_w}{\partial \dot{\mathbf{q}}_B}\right)^T \mathbf{M}_w \dot{\mathbf{L}}_B \mathbf{\Lambda}_B \mathbf{v}_B - \left(\frac{\partial {}^B\mathbf{v}_w}{\partial \dot{\mathbf{q}}_B}\right)^T \mathbf{M}_w \dot{\mathbf{L}}_B \mathbf{\Lambda}_B \mathbf{v}_B \\ &+ \left(\frac{\partial {}^B\mathbf{v}_w}{\partial \dot{\mathbf{q}}_B}\right)^T \mathbf{M}_w \dot{\mathbf{v}}_B \end{aligned} \tag{C.20}$$

The expression for $\frac{\partial T_2}{\partial \mathbf{q}_B}$ is derived below, which is also used in the Euler-Lagrange equation (2.30).

$$\frac{\partial T_2}{\partial \mathbf{q}_B} = \left(\frac{\partial \mathbf{v}_B}{\partial \mathbf{q}_B}\right)^T \mathbf{M}_w {}^B\mathbf{v}_w + \left(\frac{\partial {}^B\mathbf{v}_w}{\partial \mathbf{q}_B}\right)^T \mathbf{M}_w \mathbf{v}_B + \mathbf{v}_B^T \frac{\partial \mathbf{M}_w}{\partial \mathbf{q}_B} {}^B\mathbf{v}_w \tag{C.21}$$

The terms $\frac{d}{dt}\left(\frac{\partial T_2}{\partial \dot{\mathbf{q}}_B}\right)$ and $\frac{\partial T_2}{\partial \mathbf{q}_B}$ derived in equations (C.20) and (C.21), respectively, are used while applying the Euler-Lagrange equation to term 2 (T_2). Using expressions derived in equations (2.20), (C.20), (C.21), and as stated earlier, pre-multiplying by $\mathbf{\Lambda}_B^T$ in order to eliminate the algebraic constraint, and finally applying the Euler-Lagrange equation (2.30) on term 2 (T_2),

$$\begin{aligned}\mathbf{\Lambda}_B^T \left[\frac{d}{dt}\left(\frac{\partial T_2}{\partial \dot{\mathbf{q}}_B}\right) - \frac{\partial T_2}{\partial \mathbf{q}_B}\right] &= \mathbf{\Lambda}_B^T \dot{\mathbf{L}}_B^T \mathbf{M}_w {}^B\mathbf{v}_w + \dot{\mathbf{M}}_w {}^B\mathbf{v}_w + \mathbf{M}_w \frac{d^B\mathbf{v}_w}{dt} \\ &+ \mathbf{\Lambda}_B^T \frac{d}{dt}\left(\frac{\partial {}^B\mathbf{v}_w}{\partial \dot{\mathbf{q}}_B}\right)^T \mathbf{M}_w \mathbf{v}_B + \mathbf{\Lambda}_B^T \left(\frac{\partial {}^B\mathbf{v}_w}{\partial \dot{\mathbf{q}}_B}\right)^T \dot{\mathbf{M}}_w \mathbf{v}_B + \mathbf{\Lambda}_B^T \left(\frac{\partial {}^B\mathbf{v}_w}{\partial \dot{\mathbf{q}}_B}\right)^T \mathbf{M}_w \dot{\mathbf{v}}_B \\ &+ \mathbf{\Lambda}_B^T \dot{\mathbf{L}}_B^T \mathbf{M}_w {}^B\mathbf{v}_w - \mathbf{\Lambda}_B^T \left(\frac{\partial {}^B\mathbf{v}_w}{\partial \mathbf{q}_B}\right)^T \mathbf{M}_w \mathbf{v}_B - \mathbf{\Lambda}_B^T \left(\mathbf{v}_B^T \frac{\partial \mathbf{M}_w}{\partial \mathbf{q}_B} {}^B\mathbf{v}_w\right) \end{aligned} \tag{C.22}$$

Alternatively,

$$\Lambda_B^T \left[\frac{d}{dt}\left(\frac{\partial T_2}{\partial \dot{\mathbf{q}}_B}\right) - \frac{\partial T_2}{\partial \mathbf{q}_B}\right] = 2\,\Lambda_B^T \dot{\mathbf{L}}_B^T \mathbf{M}_w\, {}^B\mathbf{v}_w + \dot{\mathbf{M}}_w\, {}^B\mathbf{v}_w + \mathbf{M}_w \frac{d\,{}^B\mathbf{v}_w}{dt}$$
$$+ \Lambda_B^T \frac{d}{dt}\left(\frac{\partial {}^B\mathbf{v}_w}{\partial \dot{\mathbf{q}}_B}\right)^T \mathbf{M}_w \mathbf{v}_B + \Lambda_B^T \left(\frac{\partial {}^B\mathbf{v}_w}{\partial \dot{\mathbf{q}}_B}\right)^T \dot{\mathbf{M}}_w \mathbf{v}_B + \Lambda_B^T \left(\frac{\partial {}^B\mathbf{v}_w}{\partial \dot{\mathbf{q}}_B}\right)^T \mathbf{M}_w \dot{\mathbf{v}}_B$$
$$- \Lambda_B^T \left(\frac{\partial {}^B\mathbf{v}_w}{\partial \mathbf{q}_B}\right)^T \mathbf{M}_w \mathbf{v}_B - \Lambda_B^T \left(\mathbf{v}_B^T \frac{\partial \mathbf{M}_w}{\partial \mathbf{q}_B}\, {}^B\mathbf{v}_w\right) \tag{C.23}$$

3. TERM 3

The third term in kinetic energy equation (2.51) is,

$$T_3 = \frac{1}{2}\, {}^B\mathbf{v}_w^T \mathbf{M}_w\, {}^B\mathbf{v}_w \tag{C.24}$$

As done previously, each term of the Euler-Lagrange equation (2.30) is evaluated, wherein the kinetic energy is given above, in equation (C.24). The expressions derived for $\frac{d}{dt}\left(\frac{\partial T_3}{\partial \dot{\mathbf{q}}_B}\right)$ and $\frac{\partial T_3}{\partial \mathbf{q}_B}$ are given below:

$$\frac{\partial T_3}{\partial \dot{\mathbf{q}}_B} = \frac{1}{2}\left(\frac{\partial {}^B\mathbf{v}_w}{\partial \dot{\mathbf{q}}_B}\right)^T \mathbf{M}_w\, {}^B\mathbf{v}_w + \frac{1}{2}\left(\frac{\partial {}^B\mathbf{v}_w}{\partial \dot{\mathbf{q}}_B}\right)^T \left({}^B\mathbf{v}_w^T \mathbf{M}_w\right)^T$$
$$= \left(\frac{\partial {}^B\mathbf{v}_w}{\partial \dot{\mathbf{q}}_B}\right)^T \mathbf{M}_w\, {}^B\mathbf{v}_w \tag{C.25}$$

Taking the time derivative of equation (C.25),

$$\frac{d}{dt}\left(\frac{\partial T_3}{\partial \dot{\mathbf{q}}_B}\right) = \frac{d}{dt}\left(\frac{\partial {}^B\mathbf{v}_w}{\partial \dot{\mathbf{q}}_B}\right)^T \mathbf{M}_w\, {}^B\mathbf{v}_w + \left(\frac{\partial {}^B\mathbf{v}_w}{\partial \dot{\mathbf{q}}_B}\right)^T \dot{\mathbf{M}}_w\, {}^B\mathbf{v}_w$$
$$+ \left(\frac{\partial {}^B\mathbf{v}_w}{\partial \dot{\mathbf{q}}_B}\right)^T \mathbf{M}_w \frac{d\,{}^B\mathbf{v}_w}{dt} \tag{C.26}$$

and now, evaluating $\frac{\partial T_3}{\partial \mathbf{q}_B}$,

$$\frac{\partial T_3}{\partial \mathbf{q}_B} = \left(\frac{\partial {}^B\mathbf{v}_w}{\partial \mathbf{q}_B}\right)^T \mathbf{M}_w\, {}^B\mathbf{v}_w + \frac{1}{2}\, {}^B\mathbf{v}_w^T \frac{\partial \mathbf{M}_w}{\partial \mathbf{q}_B}\, {}^B\mathbf{v}_w \tag{C.27}$$

The terms $\frac{d}{dt}\left(\frac{\partial T_3}{\partial \dot{\mathbf{q}}_B}\right)$ and $\frac{\partial T_3}{\partial \mathbf{q}_B}$ derived in equations (C.26) and (C.27), respectively, are used while applying the Euler-Lagrange equation to term 3 (T_3). Using expressions

derived in equations (C.26), (C.27), pre-multiplying by $\mathbf{\Lambda}_B^T$, and finally applying the Euler-Lagrange equation(2.30) on term 3 (T_3),

$$\begin{aligned}\mathbf{\Lambda}_B^T \quad \left[\frac{d}{dt}\left(\frac{\partial T_3}{\partial \dot{\mathbf{q}}_B}\right) - \frac{\partial T_3}{\partial \mathbf{q}_B}\right] &= \mathbf{\Lambda}_B^T \left[\frac{d}{dt}\left(\frac{\partial {}^B\mathbf{v}_w}{\partial \dot{\mathbf{q}}_B}\right)^T \mathbf{M}_w \, {}^B\mathbf{v}_w\right] \\ &+ \mathbf{\Lambda}_B^T \left[\left(\frac{\partial {}^B\mathbf{v}_w}{\partial \dot{\mathbf{q}}_B}\right)^T \dot{\mathbf{M}}_w \, {}^B\mathbf{v}_w\right] + \mathbf{\Lambda}_B^T \left[\left(\frac{\partial {}^B\mathbf{v}_w}{\partial \dot{\mathbf{q}}_B}\right)^T \mathbf{M}_w \frac{d\,{}^B\mathbf{v}_w}{dt}\right] \\ &- \mathbf{\Lambda}_B^T \left[\left(\frac{\partial {}^B\mathbf{v}_w}{\partial \mathbf{q}_B}\right)^T \mathbf{M}_w \, {}^B\mathbf{v}_w\right] - \frac{1}{2}\mathbf{\Lambda}_B^T \left[{}^B\mathbf{v}_w^T \frac{\partial \mathbf{M}_w}{\partial \mathbf{q}_B} \, {}^B\mathbf{v}_w\right] \end{aligned} \tag{C.28}$$

The reaction wheels are located at a fixed orientation with respect to the body reference frame of the spacecraft, hence,

$$\frac{\partial \mathbf{M}_w}{\partial \mathbf{q}_B} = \mathbf{0} \tag{C.29}$$

and,

$$\dot{\mathbf{M}}_w = \mathbf{0} \tag{C.30}$$

Thus, adding expressions obtained from equations (C.15), (C.23), and (C.28), and using the relations stated in equations (C.29) and (C.30),

$$\begin{aligned}\mathbf{\Lambda}_B^T \quad \left[\frac{d}{dt}\left(\frac{\partial T_w}{\partial \dot{\mathbf{q}}_B}\right) - \frac{\partial T_w}{\partial \mathbf{q}_B}\right] &= 2\,\mathbf{\Lambda}_B^T \dot{\mathbf{L}}_B^T \mathbf{M}_w \mathbf{v}_B + \mathbf{M}_w \dot{\mathbf{v}}_B - \mathbf{\Lambda}_B^T \left(\frac{\partial {}^B\mathbf{v}_w}{\partial \mathbf{q}_B}\right)^T \mathbf{M}_w \mathbf{v}_B \\ &+ 2\,\mathbf{\Lambda}_B^T \dot{\mathbf{L}}_B^T \mathbf{M}_w \, {}^B\mathbf{v}_w + \mathbf{M}_w \frac{d\,{}^B\mathbf{v}_w}{dt} + \mathbf{\Lambda}_B^T \frac{d}{dt}\left(\frac{\partial {}^B\mathbf{v}_w}{\partial \dot{\mathbf{q}}_B}\right)^T \mathbf{M}_w \mathbf{v}_B \\ &+ \mathbf{\Lambda}_B^T \left(\frac{\partial {}^B\mathbf{v}_w}{\partial \dot{\mathbf{q}}_B}\right)^T \mathbf{M}_w \dot{\mathbf{v}}_B + \mathbf{\Lambda}_B^T \left[\frac{d}{dt}\left(\frac{\partial {}^B\mathbf{v}_w}{\partial \dot{\mathbf{q}}_B}\right)^T \mathbf{M}_w \, {}^B\mathbf{v}_w\right] \\ &+ \mathbf{\Lambda}_B^T \left[\left(\frac{\partial {}^B\mathbf{v}_w}{\partial \dot{\mathbf{q}}_B}\right)^T \mathbf{M}_w \frac{d\,{}^B\mathbf{v}_w}{dt}\right] - \mathbf{\Lambda}_B^T \left[\left(\frac{\partial {}^B\mathbf{v}_w}{\partial \mathbf{q}_B}\right)^T \mathbf{M}_w \, {}^B\mathbf{v}_w\right] \end{aligned} \tag{C.31}$$

Now the inertia and wrench terms in equation (C.31) are separated and rewritten as,

$$\begin{aligned}
\mathbf{M}_w \dot{\mathbf{v}}_B \quad & + \boldsymbol{\Lambda}_B^T \left(\frac{\partial^B \mathbf{v}_w}{\partial \dot{\mathbf{q}}_B} \right)^T \mathbf{M}_w \dot{\mathbf{v}}_B = -2 \boldsymbol{\Lambda}_B^T \dot{\mathbf{L}}_B^T \mathbf{M}_w \mathbf{v}_B - \boldsymbol{\Lambda}_B^T \frac{d}{dt} \left(\frac{\partial^B \mathbf{v}_w}{\partial \dot{\mathbf{q}}_B} \right)^T \mathbf{M}_w \mathbf{v}_B \\
& + \boldsymbol{\Lambda}_B^T \left(\frac{\partial^B \mathbf{v}_w}{\partial \mathbf{q}_B} \right)^T \mathbf{M}_w \mathbf{v}_B - 2 \boldsymbol{\Lambda}_B^T \dot{\mathbf{L}}_B^T \mathbf{M}_w {}^B\mathbf{v}_w - \mathbf{M}_w \frac{d\, {}^B\mathbf{v}_w}{dt} \\
& - \boldsymbol{\Lambda}_B^T \left[\frac{d}{dt} \left(\frac{\partial^B \mathbf{v}_w}{\partial \dot{\mathbf{q}}_B} \right)^T \mathbf{M}_w {}^B\mathbf{v}_w \right] - \boldsymbol{\Lambda}_B^T \left[\left(\frac{\partial^B \mathbf{v}_w}{\partial \dot{\mathbf{q}}_B} \right)^T \mathbf{M}_w \frac{d\, {}^B\mathbf{v}_w}{dt} \right] \\
& + \boldsymbol{\Lambda}_B^T \left[\left(\frac{\partial^B \mathbf{v}_w}{\partial \mathbf{q}_B} \right)^T \mathbf{M}_w {}^B\mathbf{v}_w \right] \qquad \text{(C.32)}
\end{aligned}$$

APPENDIX D

System Wrench Terms

There are analogous terms appearing in the system wrench of the i^{th} body and in the wrench terms due to the reaction wheel. In the treatment given below, the subscript used is i, which represents the i^{th} body of the multibody system, but this methodology has also been extended to similar terms appearing in the wrench due to the reaction wheel. The system wrench for the i^{th} body, from equation (2.39), is rewritten below for convenience as,

$$\boldsymbol{\phi}_i^S = -\dot{\mathbf{M}}_i\,\mathbf{v}_i - 2\,\boldsymbol{\Lambda}_i^T\,\dot{\mathbf{L}}_i^T\,\mathbf{M}_i\,\mathbf{v}_i + \frac{1}{2}\,\boldsymbol{\Lambda}_i^T\left(\mathbf{v}_i^T\,\frac{\partial \mathbf{M}_i}{\partial \mathbf{q}_i}\,\mathbf{v}_i\right) \tag{D.1}$$

Now terms $-2\,\boldsymbol{\Lambda}_i^T\,\dot{\mathbf{L}}_i^T\,\mathbf{M}_i\,\mathbf{v}_i$ and $\frac{1}{2}\,\boldsymbol{\Lambda}_i^T\left(\mathbf{v}_i^T\,\frac{\partial \mathbf{M}_i}{\partial \mathbf{q}_i}\,\mathbf{v}_i\right)$ of the above equation are further simplified to ease the process of coding the system wrench. Each of the terms in equation (D.1) is a 6−dimensional vector.

- ***Term 1***

$$\begin{aligned} -2\,\boldsymbol{\Lambda}_i^T\,\dot{\mathbf{L}}_i^T\,\mathbf{M}_i\,\mathbf{v}_i &= -2\begin{bmatrix} \mathbf{1} & \mathbf{0} \\ \mathbf{0} & \hat{\boldsymbol{\Lambda}}_i^T \end{bmatrix} + \begin{bmatrix} \mathbf{0} & \mathbf{0} \\ \mathbf{0} & \dot{\hat{\mathbf{L}}}_i^T \end{bmatrix} \mathbf{M}_i\,\mathbf{v}_i \\ &= \begin{Bmatrix} \mathbf{0} \\ -2\,\hat{\boldsymbol{\Lambda}}_i^T\,\dot{\hat{\mathbf{L}}}_i^T\,\left(\mathbf{M}_i^{rd}\,\dot{\mathbf{p}}_i + \mathbf{M}_i^{rr}\,\boldsymbol{\omega}_i\right) \end{Bmatrix} \end{aligned} \tag{D.2}$$

• *Term 2*

$$\frac{1}{2}\mathbf{\Lambda}_i^T\left(\mathbf{v}_i^T\frac{\partial \mathbf{M}_i}{\partial \mathbf{q}_i}\mathbf{v}_i\right) = \frac{1}{2}\begin{bmatrix}\mathbf{1} & \mathbf{0}\\ \mathbf{0} & \hat{\mathbf{\Lambda}}_i^T\end{bmatrix}\begin{Bmatrix}\mathbf{0}\\ \left(\mathbf{v}_i^T\frac{\partial \mathbf{M}_i}{\partial \hat{\mathbf{q}}_i}\mathbf{v}_i\right)\end{Bmatrix} = \begin{Bmatrix}\mathbf{0}\\ \frac{1}{2}\hat{\mathbf{\Lambda}}_i^T\left(\mathbf{v}_i^T\frac{\partial \mathbf{M}_i}{\partial \hat{\mathbf{q}}_i}\mathbf{v}_i\right)\end{Bmatrix} \tag{D.3}$$

The derivation given below was used in deriving equation (D.3) and in evaluating the term $\mathbf{v}_i^T\frac{\partial \mathbf{M}_i}{\partial \mathbf{q}_i}\mathbf{v}_i$, which is a $7-$ dimensional vector,

$$\mathbf{v}_i^T\frac{\partial \mathbf{M}_i}{\partial \mathbf{q}_i}\mathbf{v}_i = \left\{\mathbf{v}_i^T\frac{\partial \mathbf{M}_i}{\partial \mathbf{q}_{i_{(j)}}}\mathbf{v}_i\right\}_{j=1}^{7} = \begin{Bmatrix}\mathbf{v}_i^T\frac{\partial \mathbf{M}_i}{\partial \mathbf{p}_i}\mathbf{v}_i\\ \mathbf{v}_i^T\frac{\partial \mathbf{M}_i}{\partial \hat{\mathbf{q}}_i}\mathbf{v}_i\end{Bmatrix} = \begin{Bmatrix}\mathbf{0}\\ \mathbf{v}_i^T\frac{\partial \mathbf{M}_i}{\partial \hat{\mathbf{q}}_i}\mathbf{v}_i\end{Bmatrix} \tag{D.4}$$

The following relationship can be noted,

$$\Rightarrow \mathbf{v}_i^T\mathbf{M}_i\mathbf{v}_i = \begin{Bmatrix}\dot{\mathbf{p}}_i^T & \boldsymbol{\omega}_i^T\end{Bmatrix}\begin{bmatrix}\mathbf{M}_i^{dd} & \mathbf{M}_i^{dr}\\ \mathbf{M}_i^{rd} & \mathbf{M}_i^{rr}\end{bmatrix}\begin{Bmatrix}\dot{\mathbf{p}}_i\\ \boldsymbol{\omega}_i\end{Bmatrix} \tag{D.5}$$

From the above equation, it can be inferred that,

$$\Rightarrow \left(\mathbf{v}_i^T\frac{\partial \mathbf{M}_i}{\partial \hat{\mathbf{q}}_i}\mathbf{v}_i\right) = \left(\dot{\mathbf{p}}_i^T\frac{\partial \mathbf{M}_i^{dd}}{\partial \hat{\mathbf{q}}_i}\dot{\mathbf{p}}_i\right) + \left(\boldsymbol{\omega}_i^T\frac{\partial \mathbf{M}_i^{rr}}{\partial \hat{\mathbf{q}}_i}\boldsymbol{\omega}_i\right) + 2\left(\dot{\mathbf{p}}_i^T\frac{\partial \mathbf{M}_i^{dr}}{\partial \hat{\mathbf{q}}_i}\boldsymbol{\omega}_i\right)$$
$$= \left(\boldsymbol{\omega}_i^T\frac{\partial \mathbf{M}_i^{rr}}{\partial \hat{\mathbf{q}}_i}\boldsymbol{\omega}_i\right) + 2\left(\dot{\mathbf{p}}_i^T\frac{\partial \mathbf{M}_i^{dr}}{\partial \hat{\mathbf{q}}_i}\boldsymbol{\omega}_i\right) \tag{D.6}$$

The simplification of the terms of equation (D.6) is treated in a more rigorous manner by expressing $\mathbf{v}_i^T\frac{\partial \mathbf{M}_i}{\partial \hat{\mathbf{q}}_i}\mathbf{v}_i$ in the form $\mathbf{a}^T\frac{\partial \mathbf{M}}{\partial \hat{\mathbf{q}}}\mathbf{b}$ (*Note*: The subscript i, representing the i^{th} body, has been neglected in the following derivation). If $\mathbf{R}$ is the rotation matrix,

defined by the Euler Parameter $\left\{ \begin{array}{c} \mathbf{r} \\ r_o \end{array} \right\}$ and $\mathbf{R}$ is given by,

$$\mathbf{R} = \left(2r_o^2 - 1\right)\mathbf{1} + 2\,\mathbf{r}\,\mathbf{r}^T + 2r_o\,\mathbf{r}^{\times} \tag{D.7}$$

Further if we define, $\mathbf{W}$ is a constant reference Matrix, then let,

$$\mathbf{M} = \mathbf{R}\,\mathbf{W}\,\mathbf{R}^T \tag{D.8}$$

and,

$$\mathbf{W} = \mathbf{R}^T\,\mathbf{M}\,\mathbf{R} \tag{D.9}$$

Let $\mathbf{c} = \mathbf{R}^T\,\mathbf{b}$, and using equations (D.7), (D.8), and (D.9) we get.

$$\begin{aligned}
\left(\mathbf{a}^T \frac{\partial \mathbf{M}}{\partial \hat{\mathbf{q}}}\,\mathbf{b}\right) &= \frac{\partial}{\partial \hat{\mathbf{q}}}\left(\mathbf{a}^T\,\mathbf{R}\,\mathbf{W}\,\mathbf{R}^T\,\mathbf{b}\right) \\
&= \frac{\partial}{\partial \hat{\mathbf{q}}}\left(\mathbf{a}^T\,\mathbf{R}\,\mathbf{W}\,\mathbf{c}\right) \\
&= \frac{\partial}{\partial \hat{\mathbf{q}}}\left(\left(2r_o^2 - 1\right)\mathbf{a}^T\,\mathbf{W}\,\mathbf{c} + 2\,\mathbf{a}^T\,\mathbf{r}\,\mathbf{r}^T\,\mathbf{W}\,\mathbf{c} + 2r_o\,\mathbf{a}^T\,\mathbf{r}^{\times}\,\mathbf{W}\,\mathbf{c}\right) \\
&= \frac{\partial}{\partial \left\{ \begin{array}{c} \mathbf{r} \\ r_o \end{array} \right\}}\left(\left(2r_o^2 - 1\right)\mathbf{a}^T\,\mathbf{W}\,\mathbf{c} + 2\left(\mathbf{r}^T\,\mathbf{a}\right)\left(\mathbf{r}^T\,\mathbf{W}\,\mathbf{c}\right) - 2r_o\mathbf{r}^T\,\mathbf{a}^{\times}\,\mathbf{W}\,\mathbf{c}\right) \\
&= \left\{ \begin{array}{c} 2\left(\mathbf{r}^T\,\mathbf{W}\,\mathbf{c}\right)\mathbf{a} + 2\left(\mathbf{r}^T\,\mathbf{a}\right)\mathbf{W}\,\mathbf{c} - 2r_o\,\mathbf{a}^{\times}\,\mathbf{W}\,\mathbf{c} \\ 4r_o\,\mathbf{a}^T\,\mathbf{W}\,\mathbf{c} - 2\mathbf{r}^T\,\mathbf{a}^{\times}\,\mathbf{W}\,\mathbf{c} \end{array} \right\} \\
&= \left\{ \begin{array}{c} 2\left(\mathbf{r}^T\,\mathbf{R}^T\,\mathbf{M}\,\mathbf{c}\right)\mathbf{a} + 2\left(\mathbf{r}^T\,\mathbf{a}\right)\mathbf{R}^T\,\mathbf{M}\,\mathbf{c} - 2r_o\,\mathbf{a}^{\times}\,\mathbf{R}^T\,\mathbf{M}\,\mathbf{c} \\ 4r_o\,\mathbf{a}^T\,\mathbf{R}^T\,\mathbf{M}\,\mathbf{c} - 2\mathbf{r}^T\,\mathbf{a}^{\times}\,\mathbf{R}^T\,\mathbf{M}\,\mathbf{c} \end{array} \right\}
\end{aligned} \tag{D.10}$$

Now using the relations in equations (D.7), (D.8), (D.9), and (D.10) and substituting them into $\left(\mathbf{a}^T \frac{\partial \mathbf{M}}{\partial \hat{\mathbf{q}}} \mathbf{b}\right)$,

$$
\begin{aligned}
\left(\mathbf{a}^T \frac{\partial \mathbf{M}}{\partial \hat{\mathbf{q}}} \mathbf{b}\right) &= \frac{\partial}{\partial \hat{\mathbf{q}}} \left(\mathbf{a}^T \mathbf{R} \mathbf{W} \mathbf{R}^T \mathbf{b}\right) \\
&= \frac{\partial}{\partial \hat{\mathbf{q}}} \left(\mathbf{b}^T \mathbf{R} \mathbf{W}^T \mathbf{R}^T \mathbf{a}\right) \\
&= \left\{ \begin{array}{c} 2\left(\mathbf{r}^T \mathbf{W} \mathbf{R}^T \mathbf{b}\right) \mathbf{a} + 2\left(\mathbf{r}^T \mathbf{a}\right) \mathbf{W} \mathbf{R}^T \mathbf{b} - 2 r_o \mathbf{a}^{\times} \mathbf{W} \mathbf{R}^T \mathbf{b} \\ +2\left(\mathbf{r}^T \mathbf{W}^T \mathbf{R}^T \mathbf{a}\right) \mathbf{b} + 2\left(\mathbf{r}^T \mathbf{b}\right) \mathbf{W}^T \mathbf{R}^T \mathbf{a} - 2 r_o \mathbf{b}^{\times} \mathbf{W}^T \mathbf{R}^T \mathbf{a} \\ 4 r_o \mathbf{a}^T \mathbf{W} \mathbf{R}^T \mathbf{b} - 2 \mathbf{r}^T \mathbf{a}^{\times} \mathbf{W} \mathbf{R}^T \mathbf{b} + 4 r_o \mathbf{b}^T \mathbf{W}^T \mathbf{R}^T \mathbf{a} - 2 \mathbf{r}^T \mathbf{b}^{\times} \mathbf{W}^T \mathbf{R}^T \mathbf{a} \end{array} \right\} \\
&= \left\{ \begin{array}{l} \left\{ \begin{array}{c} 2\left(\mathbf{r}^T \mathbf{R}^T \mathbf{M} \mathbf{b}\right) \mathbf{a} + 2\left(\mathbf{r}^T \mathbf{a}\right) \mathbf{R}^T \mathbf{M} \mathbf{b} \\ -2 r_o \mathbf{a}^{\times} \mathbf{R}^T \mathbf{M} \mathbf{b} + 2\left(\mathbf{r}^T \mathbf{R}^T \mathbf{M}^T \mathbf{a}\right) \mathbf{b} \\ +2\left(\mathbf{r}^T \mathbf{b}\right) \mathbf{R}^T \mathbf{M}^T \mathbf{a} - 2 r_o \mathbf{b}^{\times} \mathbf{R}^T \mathbf{M}^T \mathbf{a} \end{array} \right\} \Rightarrow 3 \times 1 \\ \left(\begin{array}{c} 4 r_o \mathbf{a}^T \mathbf{R}^T \mathbf{M} \mathbf{b} - 2 \mathbf{r}^T \mathbf{a}^{\times} \mathbf{R}^T \mathbf{M} \mathbf{b} \\ +4 r_o \mathbf{b}^T \mathbf{R}^T \mathbf{M}^T \mathbf{a} - 2 \mathbf{r}^T \mathbf{b}^{\times} \mathbf{R}^T \mathbf{M}^T \mathbf{a} \end{array} \right) \Rightarrow 1 \times 1 \end{array} \right\}
\end{aligned}
\tag{D.11}
$$

The above is a 4−dimensional vector.

Document Log:

Manuscript Version 1 — June, 2001

Typeset by $\mathcal{AMS}$-LaTeX — 16 September 2001

SARTHAK MISRA

CENTRE FOR INTELLIGENT MACHINES, MCGILL UNIVERSITY, 3480 UNIVERSITY ST., MONTRÉAL (QUÉBEC) H3A 2A7, CANADA, *Tel.* : (514) 398-1059

E-mail address: sarthak@cim.mcgill.ca

Typeset by $\mathcal{AMS}$-LaTeX